IMPACT OF ENGINE OIL CONTAMINATION IN DIESEL AND HVO ON PARTICULATE MATTER'S MICRO- AND NANOSTRUCTURE USING ELECTRON MICROSCOPY IMAGE ANALYSIS

PHYO ZIN KO KO

A THESIS REPORT SUBMITTED IN PARTIAL FULFILLMENT
OF THE REQUIREMENTS FOR THE DEGREE OF
MASTER OF ENGINEERING IN AUTOMOTIVE ENGINEERING
INTERNATIONAL COLLEGE
KING MONGKUT'S INSTITUTE OF TECHNOLOGY LADKRABANG
ACADEMIC YEAR 2018

KMITL-2018-IC-M-004-009

IMPACT OF ENGINE OIL CONTAMINATION IN DIESEL AND HVO ON PARTICULATE MATTER'S MICRO- AND NANOSTRUCTURE USING ELECTRON MICROSCOPY IMAGE ANALYSIS

PHYO ZIN KO KO

A THESIS REPORT SUBMITTED IN PARTIAL FULFILLMENT

OF THE REQUIREMENTS FOR THE DEGREE OF

MASTER OF ENGINEERING IN AUTOMOTIVE ENGINEERING

INTERNATIONAL COLLEGE

KING MONGKUT'S INSTITUTE OF TECHNOLOGY LADKRABANG

ACADEMIC YEAR 2018

KMITL-2018-IC-M-004-009

THESIS TITLE	Impact of Engine Oil Contamination in Diesel and HVO on Particulate Matter's Micro- and Nanostructure using Electron Microscopy Image Analysis
STUDENT NAME	Mr. Phyo Zin Ko Ko
STUDENT ID	60610031
DEGREE	Master of Engineering
PROGRAM	Automotive Engineering
ADVISOR	Asst. Prof. Dr. Preechar Karin
CO-ADVISOR	Dr. Nuwong Chollacoop
CO-ADVISOR	Prof. Dr. Katsunori Hanamura

ABSTRACT

Combustion and particulate emission characteristics of synthetic biodiesel: hydrotreated vegetable oil (HVO) were compared with conventional diesel fuel combustion. Combustion pressure, brake specific fuel consumption, engine performance, heat release rates and thermal efficiency of HVO combustion were successfully investigated. Compared to conventional diesel, HVO is a synthetic paraffinic fuel with higher cetane index and lower fuel density that might achieve more complete combustion and resulting less smoke intensity. Fuel vaporization of HVO was better than diesel leading to greater fuel atomization which could significantly reduce the heat release rates. Physicochemical characterization of particulate matter influenced by engine oil additives from engine combustion of diesel and HVO were successfully investigated using electron microscopy, electron dispersive x-ray spectroscopy and thermogravimetric analysis (TGA). The agglomerate structure of diesel PM, HVO PM and diesel blending lubricant PM are similar in micro- scales. However, nanostructure of soot is composed of curve line crystallites while the metal oxide ash nanostructure was found out lattice fringes composed of parallel straight-line hatch patterns. The oxidation kinetics of fuel blending lubricant PMs are higher than pure fuel PMs due to catalytic effect of metal oxide ash on soot oxidation kinetics.

Keywords: HVO, Particulate Matter, Metal Oxide Ash, Electron Microscopy, TGA

ACKNOWLEDGEMENTS

First of all, I would like to thank to my parents, the ones who understood, sacrificed and allowed me to get a chance of postgraduate study.

I would like to dedicate all of my success to my thesis's main advisor, Asst. Prof. Dr. Preechar Karin who supported me in either academic guidelines to accomplish this thesis or many opportunities and greatest helps of all time. Thank you very much for each and everything, Professor.

As being co-advisors, Prof. Dr. Katsunori Hanamura from Tokyo Institute of Technology, Japan and Dr. Nuwong Chollacoop from National Science and Technology Development Agency (NSTDA), Thailand, thank you very much for advising me to achieve a good research direction along this academic year.

I would like to express my sincerely gratitude to International College, King Mongkut's Institute of Technology Ladkrabang for offering not only full scholarship but also research budgets. I also would like to thank to Bangchak Corporation (BCP) which sponsored designed lubricants to conduct this research.

Thanks a lot to Ms. Wannipha, Ms. Palm and Ms. Minn who kindly helped me whenever official documents were needed. And also, thanks a lot to seniors from KMITL Automotive laboratory; Mr. Ake, Mr. Ton, Mr. Park, Mr. Nick and Mr. Toey who shared their knowledges for experimental works and technical analysis. Finally, I would like to thank to my brotherhood seniors, Mr. Boom and Mr. Bank who were working, making funs and cheering together with me along this moment of study.

Koko
April 29, 2019

TABLE OF CONTENTS

Chapters **Page**

LIST OF TABLES

Tables **Page**

LIST OF FIGURES

Figures **Page**

CHAPTER 1

INTRODUCTION

1.1 Research Background

Among internal combustion engines that are used in automotive vehicles, diesel engine has higher thermal efficiency due to its attaining higher compression ratio. On the other hand, diesel engines trail black smokes containing much amount of particulate matter (PM) which are derived from incomplete combustion around single fuel droplets during spraying the fuel inside the engine cylinder. Diesel particulate matters are harmful to human health and must be removed owing to increasingly stringent emission regulations. As shown in figure 2.1, particulate matter are composed of solid fraction (soot and ash), soluble organic fraction (SOF) and volatile organic matters (VOF) which are composed of sulfates and nitrates organic compounds. Each PM morphology and chemical composition are commonly varied by the engine operating conditions, fuel properties and types of lubricating oil used [1, 2].

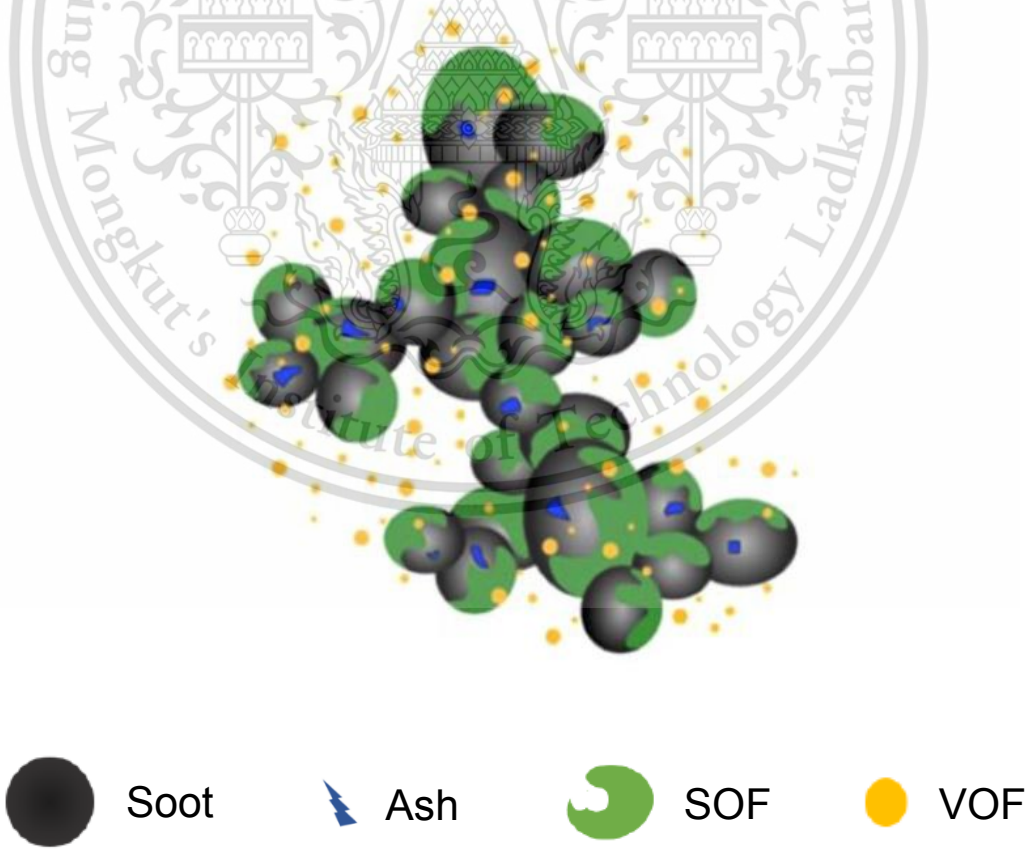

Figure 1.1 Composition of Diesel Particulate Matter [1].

Regarding to decrease the consumption of fossil diesel and reduce the particulate emission, a synthetic biodiesel: hydrotreated vegetable oil (HVO) is presented as a second generation of biodiesel which is the absence of oxygenated molecules. Combustion characteristics, thermal efficiency and smoke intensity of HVO were significant advantages compared to conventional diesel.

Among aftertreatment emission control systems, diesel particulate filer (DPF) is one of most effective ways to trap the particulate matter emitted from the exhaust gas. A conventional DPF is composed of honeycomb shape rectangular channels (containing inlet and outlet channels) which is made up of silicon carbide or cordierite ceramic materials. Exhaust gas with particulate matters enter into the inlet channels and passing through the channel wall then exit to the atmosphere through the outlet channels. When the exhaust gas passing through the channel wall, PM must be trapped and accumulated at the wall surface. The trapped PMs have to be removed from DPF by using regeneration process. Regeneration process is a chemical oxidation process which can burn the soot into carbon dioxide. Although regeneration process can burn the soot effectively, unburnt metal oxide ashes are still available inside the inlet channels while engine's PMs are composed of soot and ash as a solid fraction. In fact, ash is incombustible material. These metal oxide ashes are originated from engine oil's additives, engine wear and fuel trace metals. However, it is mainly originated from engine oil's additives.

1.2 Objectives

1) To investigate the combustion characteristics and particulate emission of synthetic biodiesel: Hydrotreated Vegetable Oil (HVO)

2) To analyze the physicochemical characteristics of diesel particulate matters focusing on metal oxide ashes which are mainly derived from engine oil's additives

1.3 Scope of Works

In the first part of thesis, combustion characteristics such as combustion pressure analysis, brake specific fuel consumption, engine performance, heat release rates and thermal efficiency of Hydrotreated Vegetable Oil (HVO) were investigated by referencing with the characteristics of conventional diesel. Soot quantity were also measured by using opacity smoke meter. Physical characterization as well as morphology and analysis of single primary particle nanostructure of particulate matter emitted from HVO fuel combustion were compared with diesel particulate matter using electron microscopy. Thermogravimetric analysis of both PMs were investigated to analyze the influence of metal oxide ash on soot oxidation kinetics.

Secondly, impact of contamination of engine oil additives on particulate emission were investigated not only on physical characterization but also chemical composition by using electron microscopy and electron dispersive x-ray spectroscopy. To investigate the influence of metal oxide ash which are derived from unburned engine oil additives, isothermal thermogravimetric analysis was used under pure air atmospheric condition.

CHAPTER 2

LITERATURE REVIEWS

2.1 Particulate Matter Emitted from Diesel Engine

Diesel engines trail black smokes containing much amount of particulate matter (PM) which are the result of incomplete combustion around fuel rich zone where fuel is injected from the nozzle. Diesel particulate matters are harmful to the human health and it can cause lung cancer, asthma and so on. Owing to strictly legislation on emission regulations of automotive vehicles, PM must be removed. Alternative fuels as well as biofuels are present in order to reduce the consumption of fossil diesel and reduce the particulate emission. Physical characteristics and chemical composition of PM emitted from internal combustion engines are mainly dependent upon engine operating conditions, fuels and types of lubricating oil used.

2.1.1 Composition of particulate matter

Composition of particulate matters emitted from automotive vehicles can be divided into (2) parts; solid and soluble organic fraction. Soot (formed by incomplete combustion of unburned hydrocarbon) and ash fraction (derived from lubricant additives engine wear and fuel trace metals) are regarded as solid fraction of PM.

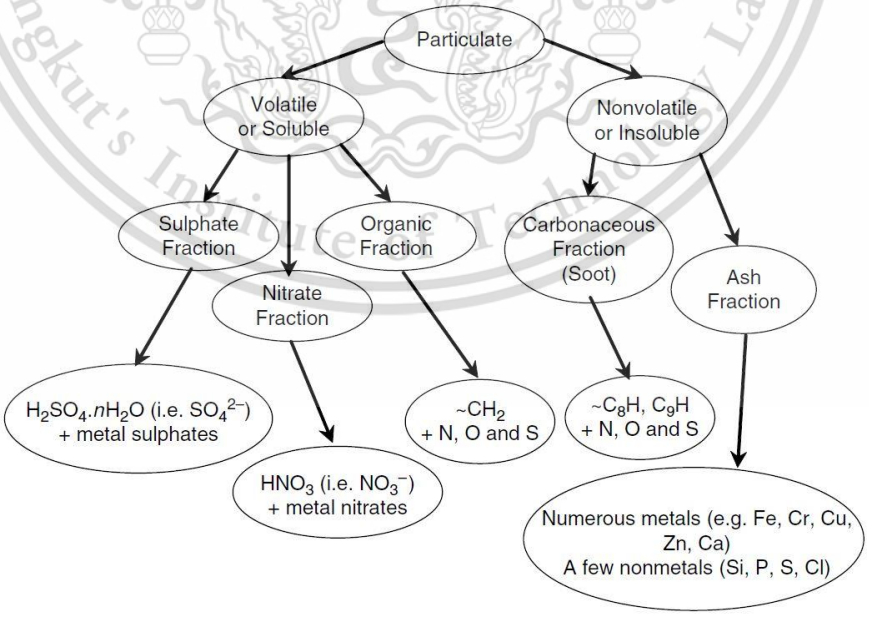

Figure 2.1 Conceptual model of particulate composition, terminating in five distinct groups or fractions: sulphates, nitrates, organics, carbonaceous and ash [1].

Soluble organic fraction is composed of sulphate, nitrate and organic compounds which are mainly originated from the acidic composition fuel and lubricant as shown in figure 2.1. As soluble organic fraction, sulphate and organic compounds are originated from fuel and lubricant. Carbonaceous fraction (soot) mainly comes from unburned hydrocarbon of fuel while the ash fraction is mainly derived from metallic engine oil additives, material disintegration such as engine wear and a very few amounts is derived from aerosol particles [1].

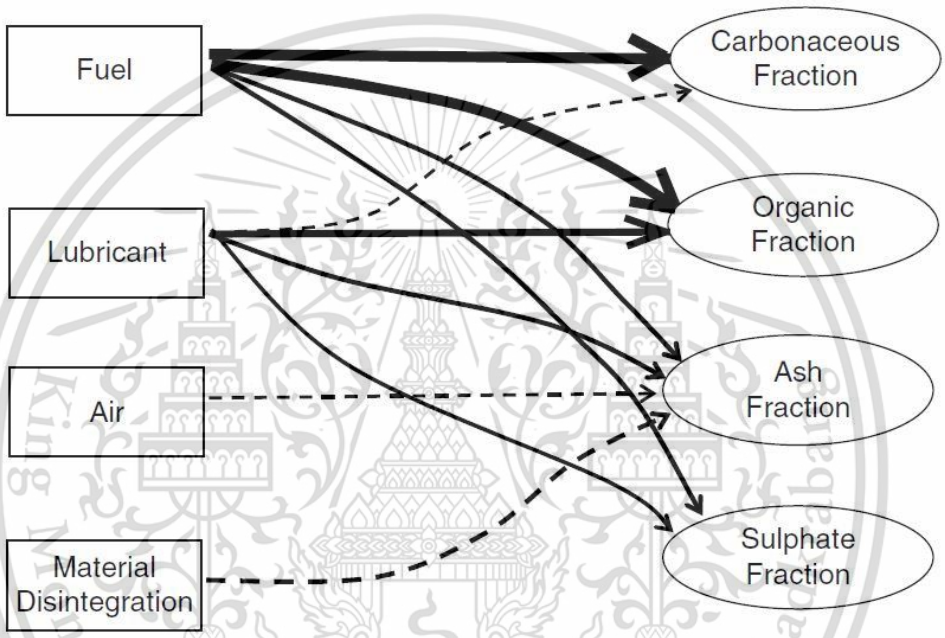

Figure 2.2 Origination of solid fraction (soot, ash) and soluble organic fraction (sulphate, nitrate compounds) [1].

2.1.2 Initial diesel soot formation

John E. Dec [2] proposed a conceptual model using laser-sheet imaging which identifies the specific areas (i.e. rich vapor-fuel/air mixture, fuel-rich premixed flame, initial soot formation and so on) during the fuel mixing controlled phase as described in figure 2.3. A mixture of fuel vapor and air is formed at the downstream of fuel jet from the nozzle. Initial soot formation is occurred at the fuel-rich premixed flame where this zone has a high concentration of soot precursors [1, 2].

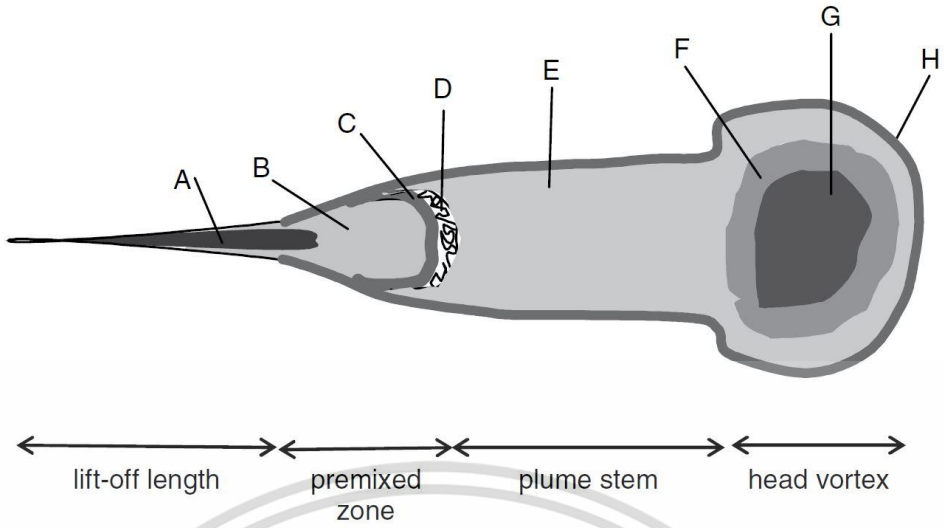

Figure 2.3 Conceptual model of combustion during the mixing-controlled phase: A, liquid fuel; B, mixture of fuel vapor and air; C, fuel-rich premixed flame; D, initial soot formation; E, F, G, in order of increasing soot concentration; H, diffusion-flame [1].

2.1.3 Soot agglomerated particles formation process

Figure 4.24 demonstrates the process of agglomerated structure of soot from the liquid (or) vapor phase fuel hydrocarbons comparts pyrolysis, nucleation, coalescence and agglomeration process. In pyrolysis process, molecular structure of fuel are changed by the presence of high temperature resulting as soot precursors. These gas-phase species of soot precursors are transformed into solid-phase soot particle in nucleation process. Surface growth process is followed by nucleation process to achieve more concentration of solid-phase soot particles resulting as single primary particle of soot. Single primary particle of soot is sizing in the range of 10 – 60 nm [3]. Theses primary particle of soot are agglomerated to become soot agglomerated particles.

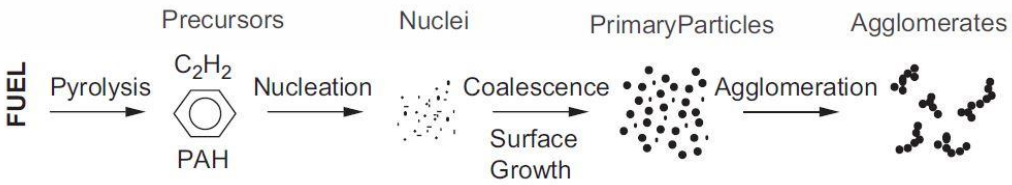

Figure 2.4 Schematic diagram of the steps in the soot formation process [3].

2.2 Engine Operating Parameters Effecting on Particulate Matter

Physical and chemical properties of particulate matter emitted from internal combustion engines is varied by engine operating conditions, fuels and types of lubricating oil used. Many literatures have investigated the effects of engine operating parameters on morphology, particle size distribution and oxidation kinetics of diesel particulate matters. When the engine load is increased, particle size ranges were increased. Smaller particles sizing in the range of 40 – 50 nm were found out under no load condition while 60 – 70 nm particles were found out under engine full load condition as shown in figure 2.5. Due to higher engine load condition, combustion chamber temperature and amount of injected fuel is higher. This effect might promote initial soot formation and also accelerate the agglomeration process [4, 5]. Moreover, lower engine speed produce larger particle size with slightly aggregate structure. The impact of engine load at constant engine speed is more prominent than various engine speed. The oxidation kinetics of diesel PMs emitted from higher engine speed with lower engine load was faster than the PM emitted from lower engine speed with higher engine load condition as described in table 2.1 [6].

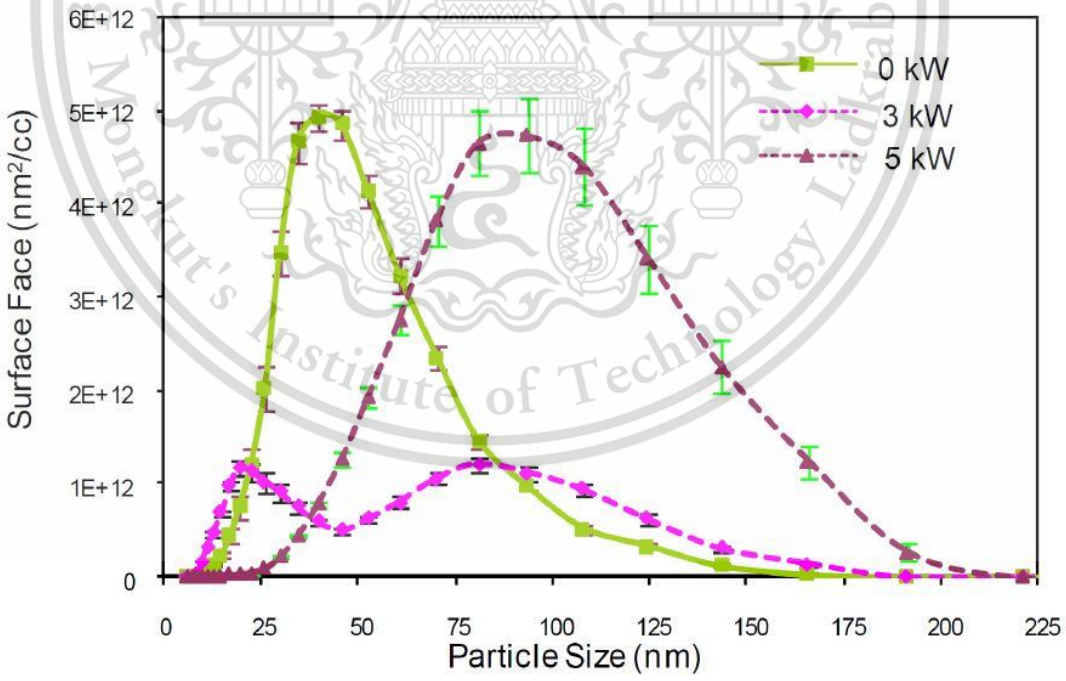

Figure 2.5 Particle surface area and size distribution from a diesel engine at different engine loads [4].

Table 2.1 Factors affecting on diesel particulate matters [6].

Test mode	speed (rpm)	Torque (Nm)	D_p(sd) (nm)	L_a (sd) (nm)	T_f (sd) (nm)	D_s (sd) (nm)	Volatiles (%)	T_i (°C)	E (kJ/mol)	A (S^{-1})
1	1280	216	26.08 (2.50)	0.754 (0.0637)	1.226 (0.0521)	0.387 (0.011)	14.3±0.72	537.7	110.6±1.51	8.97×10^4
2	2560	216	23.87 (2.29)	0.747 (0.0409)	1.215 (0.0589)	0.382 (0.010)	17.8±0.98	533.6	114.2±1.54	1.84×10^5
3	1920	224	24.46 (1.97)	0.749 (0.0873)	1.237 (0.0705)	0.383 (0.011)	17.0±0.85	528.9	107.0±1.28	6.36×10^4
4	1920	112	21.30 (1.91)	0.731 (0.0213)	1.317 (0.0296)	0.375 (0.008)	47.9±2.54	508.5	90.6±1.78	8.12×10^3
5	1920	56	20.52 (2.13)	0.707 (0.0212)	1.391 (0.0413)	0.373 (0.015)	58.5±2.63	485.8	77.8±2.09	1.50×10^3

2.3 Alternative Fuels

Fossil diesel is produced from fractional distillation process of petroleum (or) crude oil. Diesel engines are more efficient than gasoline engines. In fact, diesel requires less refining than gasoline resulting cheaper alternative. However, fossil diesel combustion produces particulate matter (PM) emission from incomplete combustion and depletion (limited availability) are the major downsides of diesel fuel.

Regarding to reducing particulate emission and fossil diesel consumption, biodiesel stands for the renewable form of energy. Due to attaining higher cetane number, biodiesel can be used in compression ignition engine without engine modification. Biodiesel or fatty acid methyl/ethyl ester (FAME/FAEE) is derived from vegetable oil or animal fat through transesterification process. As a modern biodiesel manufacturing process, partially hydrotreated to FAME (H-FAME) can obtain a high-quality biodiesel. In this process, the conventional biodiesel (FAME) was hydrogenated by hydrogen and a catalyst at low temperature and pressure. The purpose of H-FAME process is to reduce the number of double bonds/unsaturated fatty acids and transformed to be monounsaturated FAME. Some researchers have been reported that high quality biodiesel (H-FAME) also has satisfactory properties such as reducing CO, HC, NOx and soot, less fuel consumption and oxidation stability was significantly improved as a blending percentage of 10% (B10).

Unlike first generation biodiesel, hydrotreated vegetable oil; HVO (second generation biodiesel) is produced from hydrotreating of vegetable oils as well as suitable waste and residue fat fractions. In this process, hydrogen is used to remove oxygen from the triglyceride vegetable oil molecules and to split the triglyceride into three separate chains, thus creating hydrocarbons which are like existing diesel fuel components. Moreover, the different manufacturing process from biodiesel is that HVO is free of aromatics made by Fishcher Tropsch synthesis after gasification process.

Therefore, HVO is represented as second generation biodiesel (or) synthetic biodiesel with the absence of oxygen molecules.

2.4 Particulate Matters Emitted from Biodiesel Combustion

As a pre-treatment for reducing particulate emission and saving fossil diesel consumption, switching to biodiesel usage is a good option. In general, biodiesel is produced from palm oil, sugar cane, molasses and so on. Ethanol can also be produced from sugarcane, molasses and cassava roots. Diesel blending biodiesel fuel stands for an effective way to be either saving fossil diesel consumption or attaining less particulate emission from the automotive vehicles (E.g. Thailand use diesel vs biodiesel blending fuel with a proportion of 7% biodiesel blended fuel as conventional diesel for domestic application in 2019).

2.4.1 Effect of Biodiesel on Combustion Characteristics

One of the main prominent characteristics of biodiesel combustion can be regarded as less soot contamination from vehicle emission. J. Boonsakda et al. [7] investigated the effect of biodiesel blended fuel combustion on particulate matter quantity and nanostructure analysis by blending biodiesel proportion as 20%, 40%, 60% and 80% compared to conventional diesel B7 and also with B100. Less soot contamination was found out by increasing the blending proportion of biodiesel as shown in figures 2.6.

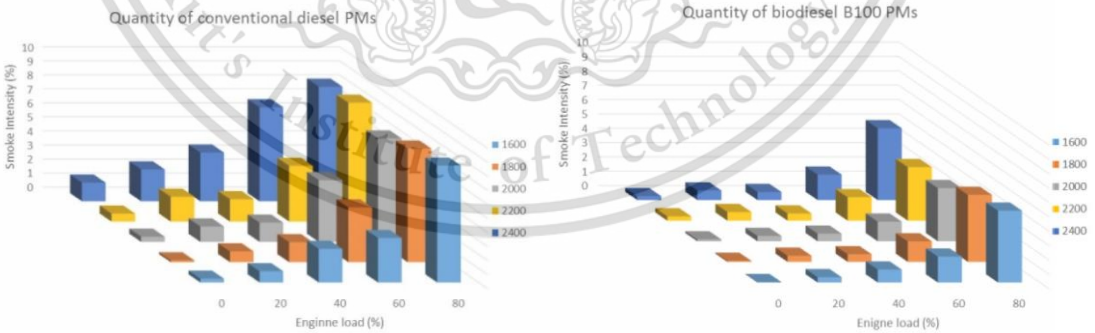

(a) Smoke intensity of B7 (b) Smoke intensity of B100

Figures 2.6 Soot contamination percentage of diesel blending biodiesel in proportion of (a) conventional diesel B7 and (b) 100% Biodiesel B100 [7].

P. Karin et al. [8, 9] investigated the oxidation kinetics of biodiesel particulate matters compared to diesel PMs using isothermal thermogravimetric analysis (TGA) under pure air atmospheric condition. Biodiesel PM were easier to oxidize than diesel PM due to presence of oxygenated molecules inside biodiesel PMs as shown in figure 2.7. Faster oxidation kinetics of biodiesel need lower activation energy and the author concluded with the calculation of apparent activation energy (E_a) as shown in table 2.2. Activation energy between carbon verses oxygen molecules during TGA of diesel PM and biodiesel PM were 124 kJ/mol and 121 kJ/mol respectively.

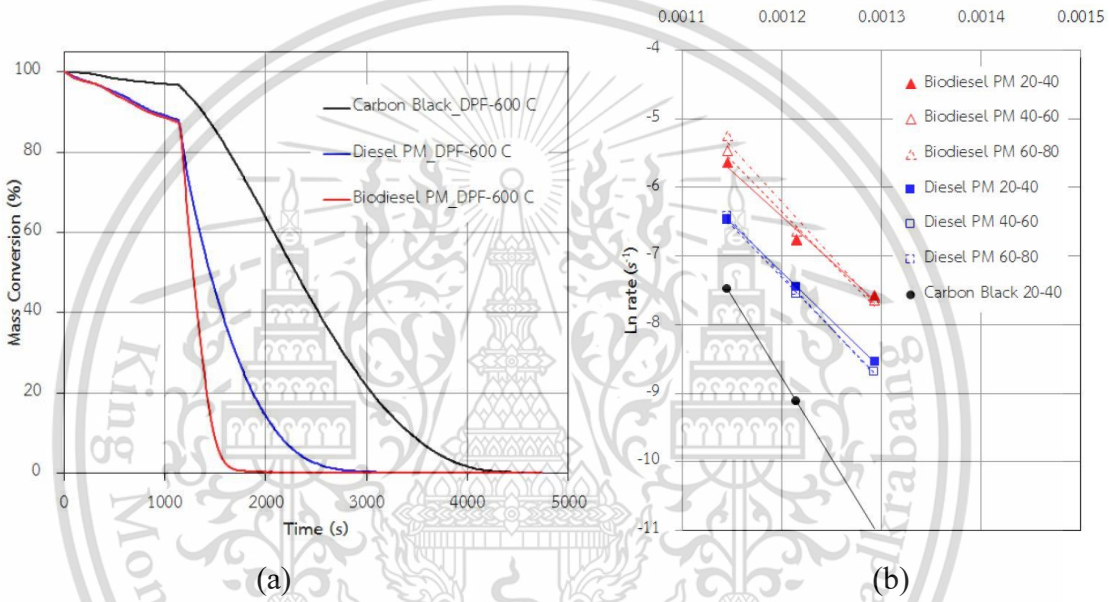

Figures 2.7 (a) Isothermal thermogravimetric analysis of carbon black, diesel PM and biodiesel PM under pure air atmosphere showing faster oxidation kinetics of biodiesel PM and (b) Arrhenius plot of diesel and biodiesel engine's PMs compared with carbon black [8].

Table 2.2 Apparent activation energy (Ea) of engine's PMs [8].

	Apparent Activation Energy *Ea* (kJ/mole)
PMs Oxidize with DPF Powder	
PMs Burned Fraction	
Biodiesel Engine's PMs	121±11
Biodiesel 20-40% burned	109
Biodiesel 40-60% burned	121
Biodiesel 60-80% burned	131
Diesel Engine's PMs	124±7
Diesel 20-40% burned	117
Diesel 40-60% burned	124
Diesel 60-80% burned	130
Pure PMs Oxidize without DPF Powder	
Biodiesel Engine's PMs	152±5 (Karin *et al.*, 2015)
Diesel Engine's PMs	159±6 (Karin *et al.*, 2015)

2.5 Aftertreatment Technologies for Diesel Particulate Emission

Regarding to strictly legislation of emission regulation on particulate emission (i.e. Euro 5, Euro 6) emitted from automotive vehicles, diesel particulate matter must be removed due to its harmful effects for human health. Among post-treatment (or) aftertreatment technologies for controlling exhaust gas and particulate emission, exhaust gas recirculation (EGR), diesel oxidation catalyst (DOC) and diesel particulate filter (DPF) are commonly used in diesel engines. In this article, fundamentals and working principles of DPF will be mainly discussed.

2.5.1 Operating principle of diesel particulate filter

A diesel particulate filter is composed of honey-comb shape rectangular channels which are made up of cordierite (or) silicon carbide ceramic materials. Exhaust gas containing particulate matters enter into the inlet channel and passing through the channel wall then exit to the atmosphere through the outlet channel [9]. When PM passing through the channel wall, all of PM must be trapped at the surface of inlet channel wall as shown in figures 2.8.

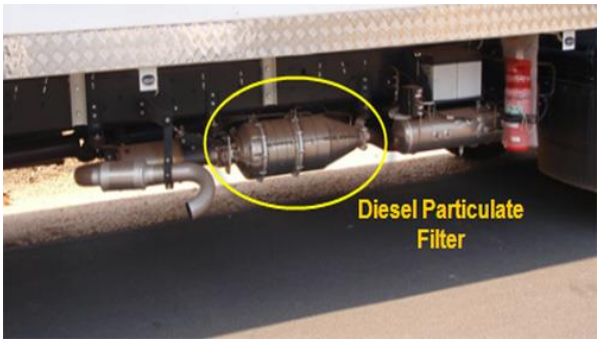

(a)

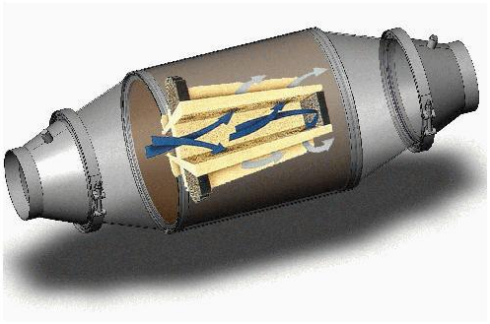

(b)

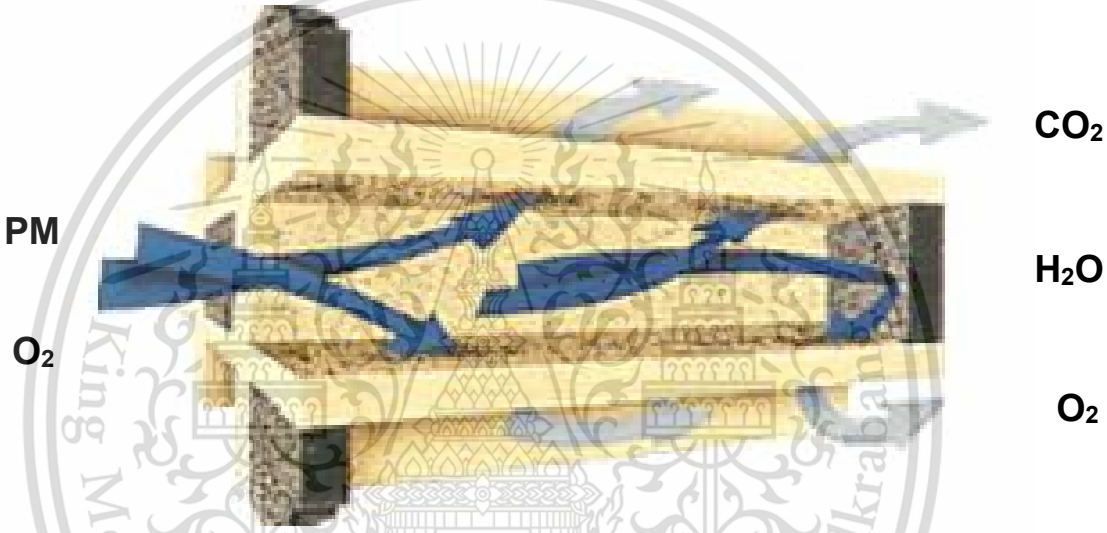

(c)

Figures 2.8 (a) A truck equipped with DPF (b) Inside structure of DPF and (c) Working principle of DPF [10].

2.5.2 Regeneration process in diesel particulate filter

Due to continuous entering of particulate matter into the inlet channels during vehicle running, much PMs are accumulated and trapped inside the inlet channels of diesel particulate filter. The trapped PMs must be removed in order to get effective filtration length for all the time. A chemical oxidation process which can oxidize the trapped soot (carbon) into carbon dioxide is termed as DPF regeneration process. There are two types of regeneration: (i) passive regeneration and (ii) active regeneration. Passive regeneration uses catalyst that is added into diesel fuel as additives or the catalyst is coated on the ceramic filter wall. In fact, the exhaust gas temperature inside DPF will be increased and this effect leads to resulting more soot oxidation as shown in figure 2.9. In active regeneration, engine throttling and burner regeneration are the

popular technologies in order to burn the trapped soot into carbon dioxide effectively. Wider throttling increases combustion temperature resulting in higher exhaust gas temperature. Burner regeneration system is equipped with computer controlled electronic burner and it is fitted at the front of the filter to increase the exhaust gas temperature as shown in figure 2.10. This burner can increase the exhaust gas temperature around 650°C which is the sufficient temperature for burning the trapped soot completely. Active regeneration is designed to initiate when passive regeneration is not enough for certain soot loading condition [10].

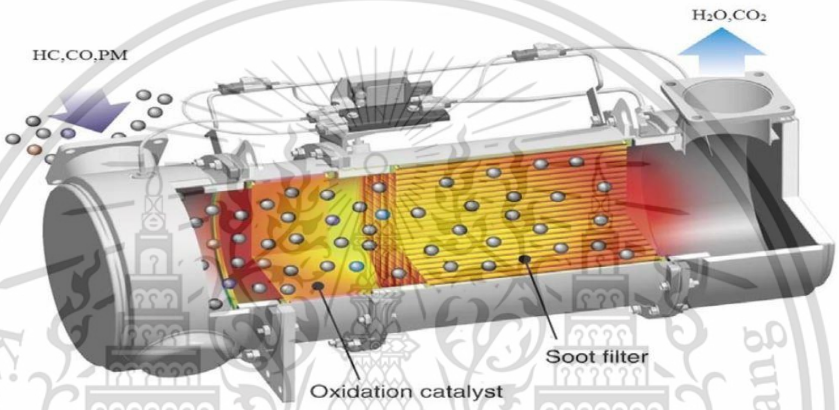

Figure 2.9 Passive regeneration process in DPF [10].

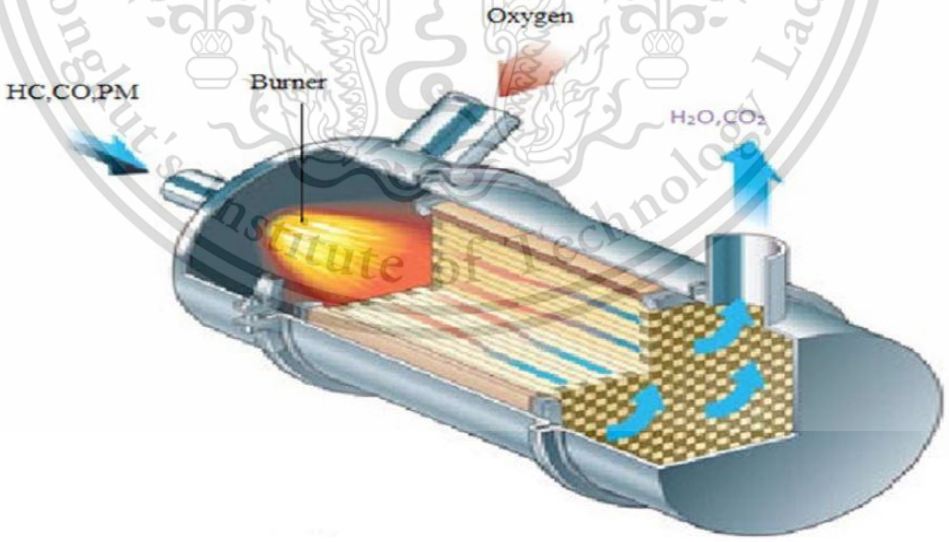

Figure 2.10 Active regeneration process with burner in DPF [10].

2.6 Lubricant Chemistry

Lubricating oil that are used in automotive vehicles are responsible for reducing the friction, heat and metal wear for the moving parts inside the engine. There are two types of lubricants as well as mineral and synthetic oils. Mineral oil is extracted from the crude oil while the synthetic oil is formulated by humans.

The components of conventional lubricants can be mainly divided into base oil and lubricant additives which can promote the performance of base oil. A typical lubricant contains about 80% of base oil and 20% of additives such as dispersant, detergent, anti-wear agent, fiction modifier and others. Composition of both detergents and dispersants are around 70% of the performance package and these are the main components of lubricant additives. Although these metal additives can improve the performance of base oil, drawbacks of formation of ash derived from these metal additives are still challenging matter [11, 12].

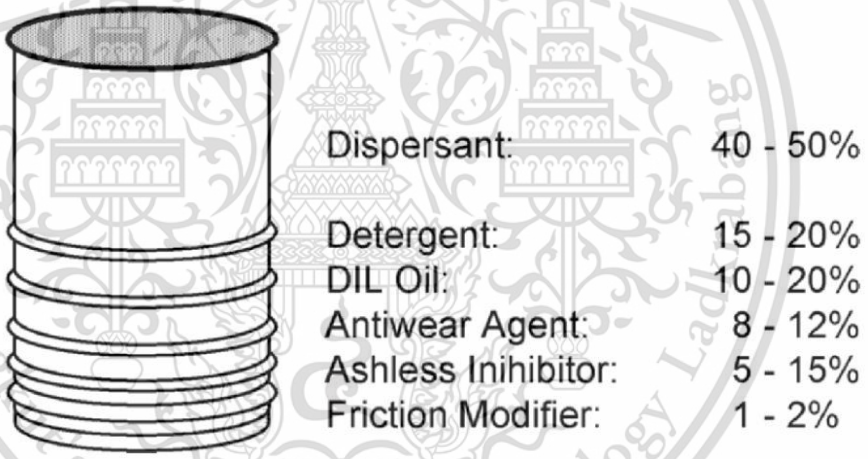

Figure 2.11 Composition of lubricant additives in a typical engine oil [12].

2.6.1 Detergents

The function of detergents from lubricant additive package is to solubilize polar components and overcome corrosion through neutralization of acids. The major components of additives are Calcium (Ca), Magnesium (Mg) or Sodium (Na). Another important function of detergent is the prevention of temperature deposit. Figure 2.12 shows the effect of high temperature deposits on the surface of piston [12].

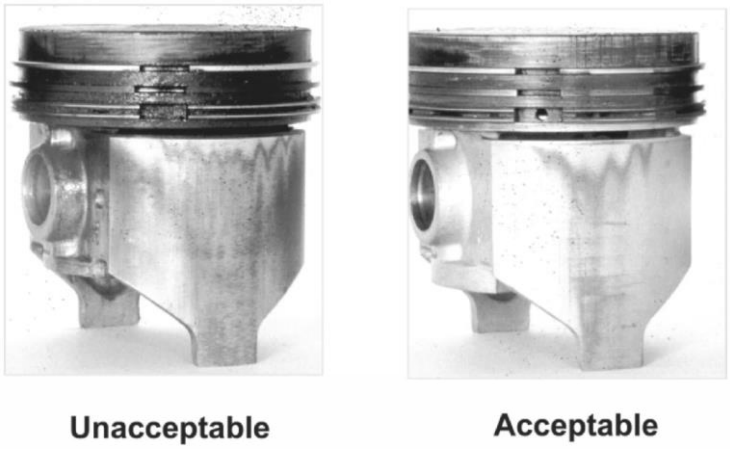

Figure 2.12 Detergents prevent high temperature deposits [12].

2.6.2 Dispersants

Major responsibility of dispersants is to suspend soot to be less (or) small particles inside the crankcase. There are two types of dispersants: (i) succinimide dispersant and (ii) Mannich dispersant. The function of dispersants are similar to detergents to provide for (i) the suspension of soot particles (ii) reduction of metal wear (iii) increasing viscosity of base oil and (iv) prevention of low temperature deposits. The chemistry of dispersant can be defined that the combination of longer hydrocarbon chain and the polar amine head group provide to suspend the soot particles to be smaller as discussed in figure 2.13 [12].

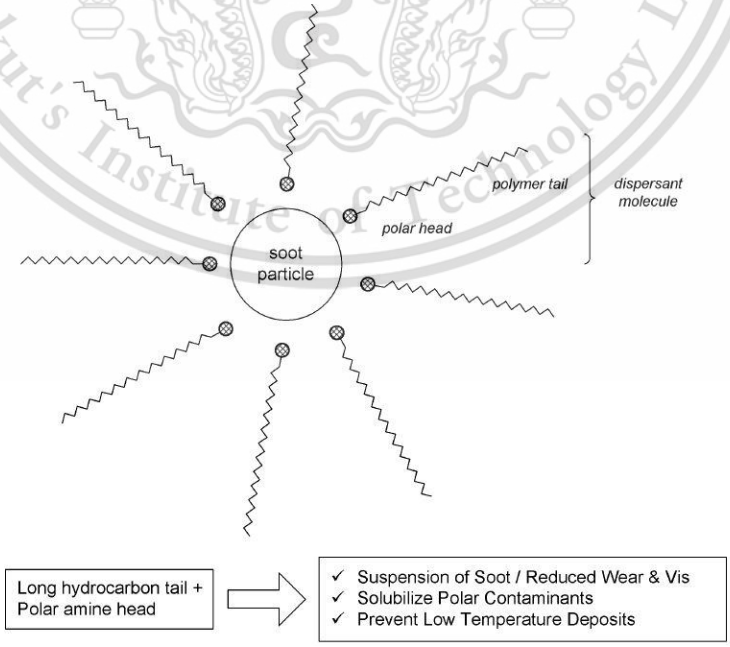

Figure 2.13 Dispersant chemistry [12].

2.7 Impact of Lube Oil Contribution on Diesel Particulate Matter

During combustion in internal combustion engines, lubricants can also participate, and this effect can vary either physical or chemical properties of particulate matters. Y. Wang et al. [13] found that the effect of contribution of lube oil changes the particulate matters' morphology to become more disorder layers, shorter fringe lengths and looser stacked graphite structure compared to PM emitted from pure diesel condition as shown in figures 2.14. L. Dong et al. [14] also found that the concentration of small PM nanoparticles were apparently present when combustion of diesel was blended (0.5% by weight) with lubricating oil as summarized in table 2.4.

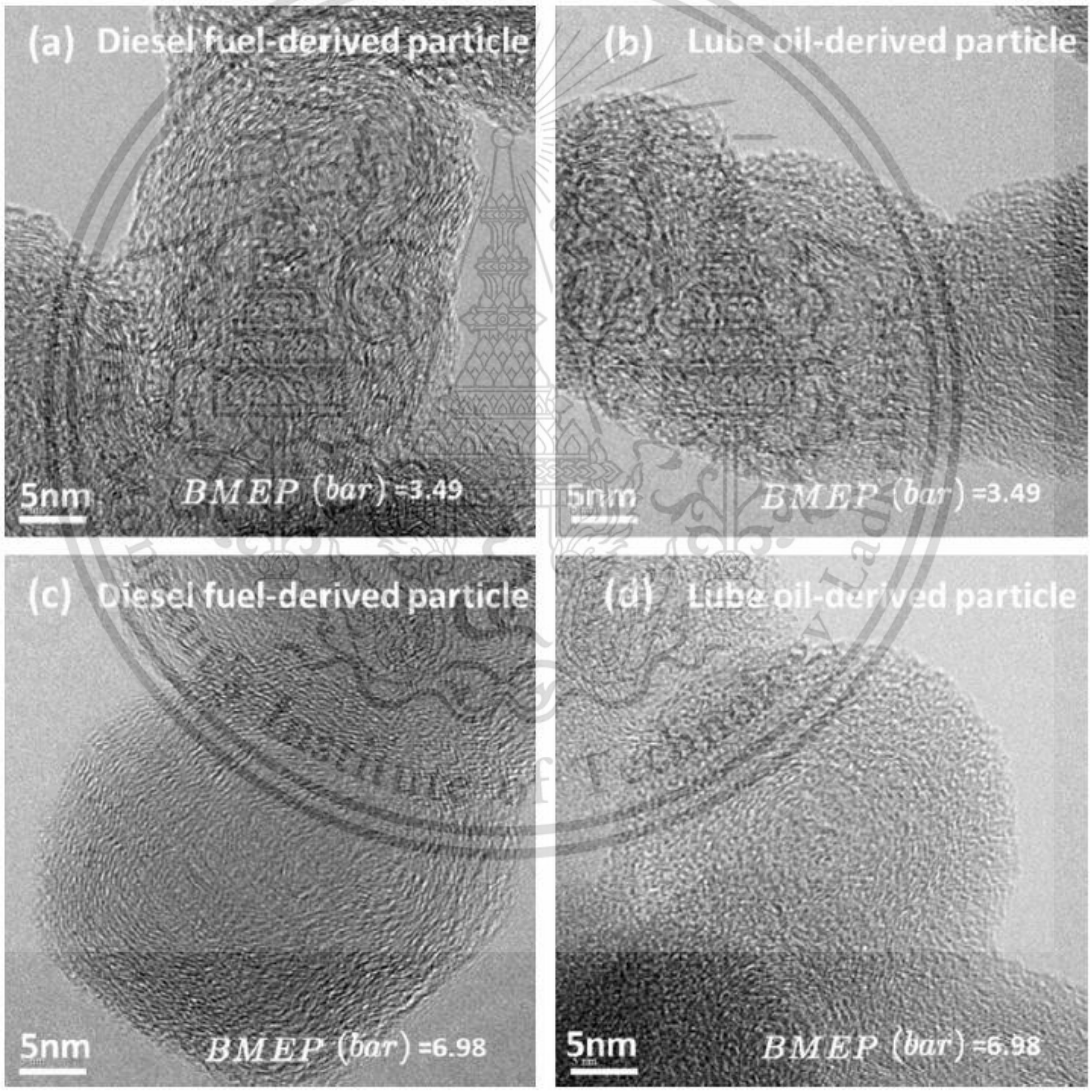

Figures 2.14 Typical HRTEM images of primary particles [13].

Table. 2.3 Diesel blended lube oil particles formation comparison [14].

Load		25%	75%
Pure diesel	Primary particle diameter	23.63 nm	27.21 nm
	Total number concentrations	$4.32e^7$	$1.21e^8$
Diesel blended with oil	Primary particle diameter	27.32 nm	28.46 nm
	Total number concentrations	$1.91e^8$	$1.81e^8$

P. Karin et al. [15] investigated the physical and chemical composition difference between lamp PM and engine PM to point out the effect of soluble organic fraction from the engine. This paper mainly compares the lamp's PM (pure carbon) and engine's PM (soot and ash) as shown in figures 2.15. TEM images of soot from lamp

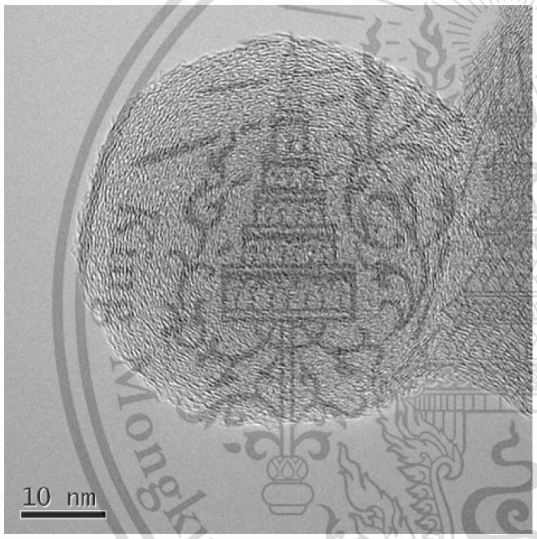

(a) PM from Lamp

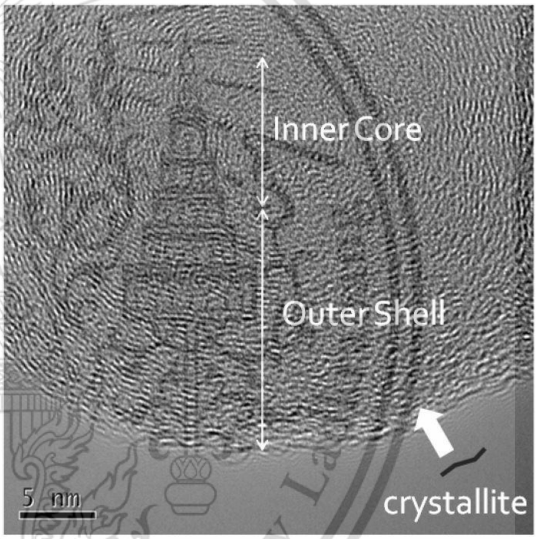

(b) PM from diesel engine combustion

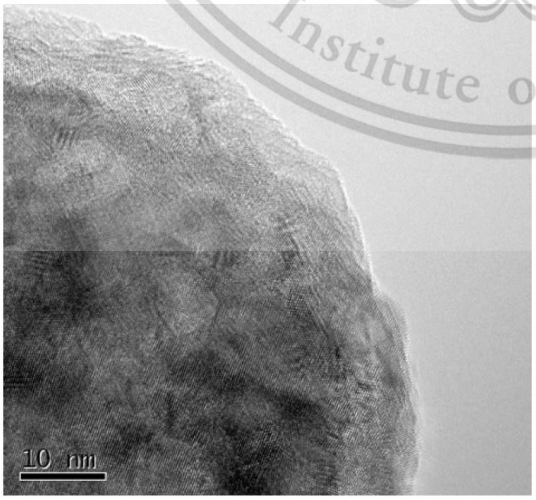

(c) Ash from engine combustion

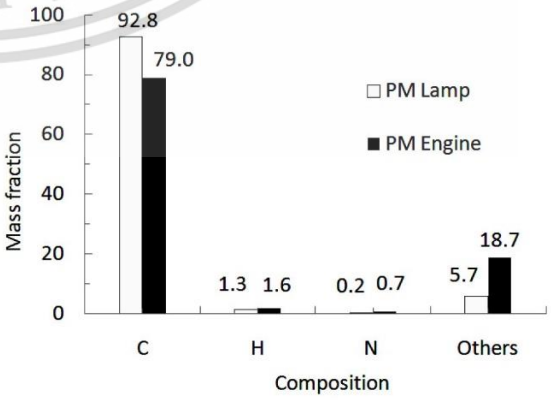

(d) CHN analysis

Figures 2.15 Nanostructure and composition of PMs from lamp and engine [14].

and engine are similar nanostructures. The agglomerated ash was found out from engine PM, and the author concluded that this metallic ash might be derived from lube oil composition of the engine lubrication system. CHNO analysis had conducted to analyze the chemical composition difference between lamp's PM and engine's PM. Carbon composition of lamp's PM was distinctly high while the engine's PMs contain not only soot (carbon) but also higher percentages of soluble organic fraction (Hydrogen, Nitrogen and others such as ash) [15].

2.7.1 Effect of metal additives on particulate matter

According to the discussion that have described in article 2.6, lubricant additives compart as an essential role to promote the performance of base oil. On the other hand, the effect of contamination of lube oil additives can change the particle size distribution, morphology and nanostructures. PM emitted from combustion of fuel dosing with ani-wear additive (0.5 wt%) changed the primary particles' nanostructured to be more disordered nanostructure [16]. H. Jung et al. investigated the influence of cerium additive contamination on number-weighted distribution, light-off temperature and PM oxidation kinetics. The author concluded the oxidation kinetics of PM derived from cerium additive dosing condition has not shown any significance on overall activation energy [17].

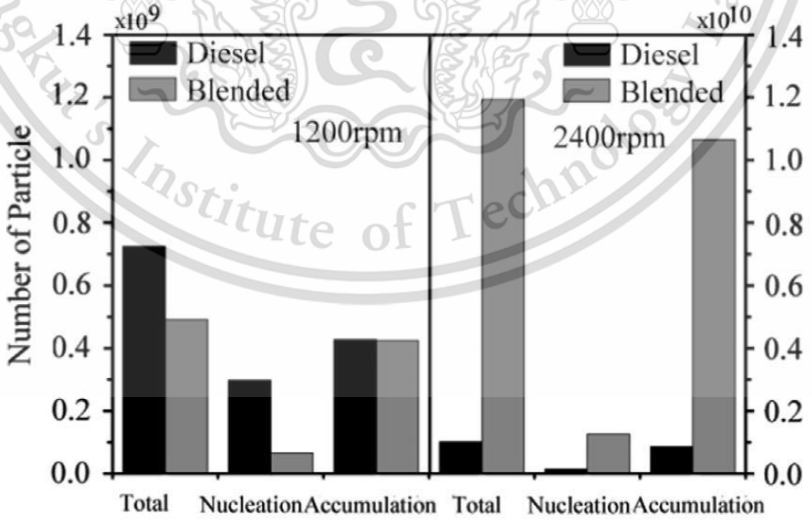

Figure 2.16 Particle number concentration under different conditions [16].

2.8 Ash in Diesel Particulate Filter

Particulate matter emitted from diesel engines mainly composed of solid fraction (soot and ash) and soluble organic fraction (sulfate and nitrate organic compounds). Diesel particulate filter plays an important role to trap the soot and oxidize into carbon dioxide by utilizing DPF regeneration process (as explained in article 2.5.2) effectively. Although DPF regeneration process can oxidize the soot, ash still remains along the inlet channel since ash is incombustible material. Metal oxide ashes are derived from engine oil additives, engine wear, fuel trace metals and some aerosol particles. However, these ashes are mainly derived from engine oil additives and the sources of metal oxide ash shown in percentages are described in figure 2.1.6 [16].

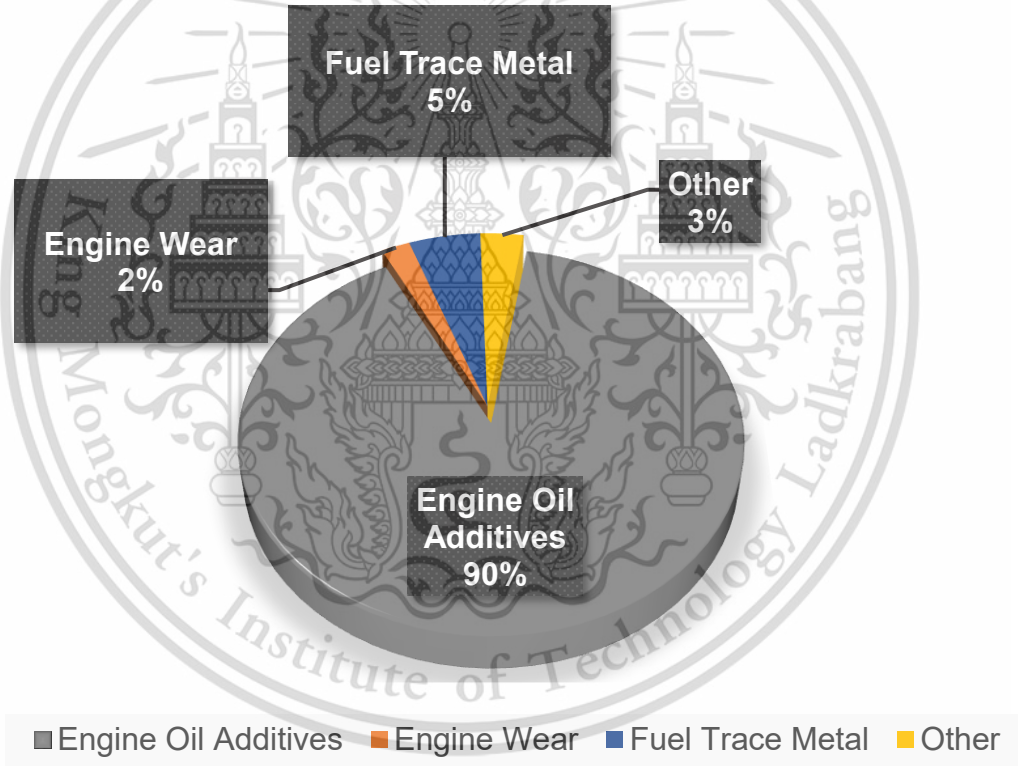

Figure 2.17 Composition of ash from used DPF [16].

2.8.1 Ash accumulation along inlet channels of DPF

Owing to accumulation of incombustible ashes along the inlet channels of DPF, exhaust back pressure is increased due to the blockage of metal oxide ashes upon the pores of DPF channel wall's surface. This effect is leading to reducing the effective soot filtration length. The amount of ash blockage is dependent upon user's regeneration frequency and types of regeneration (i.e. passive regeneration and active regeneration). S. D. Bagi et al. [18] proposed ash build up steps depending on types of regeneration. In this paper, the author discussed the steps of ash bridges formation starting from the ash precursors and concluded that the ash build up by active regeneration get worse impact than passive regeneration as compared in figures 2.18 (a and b).

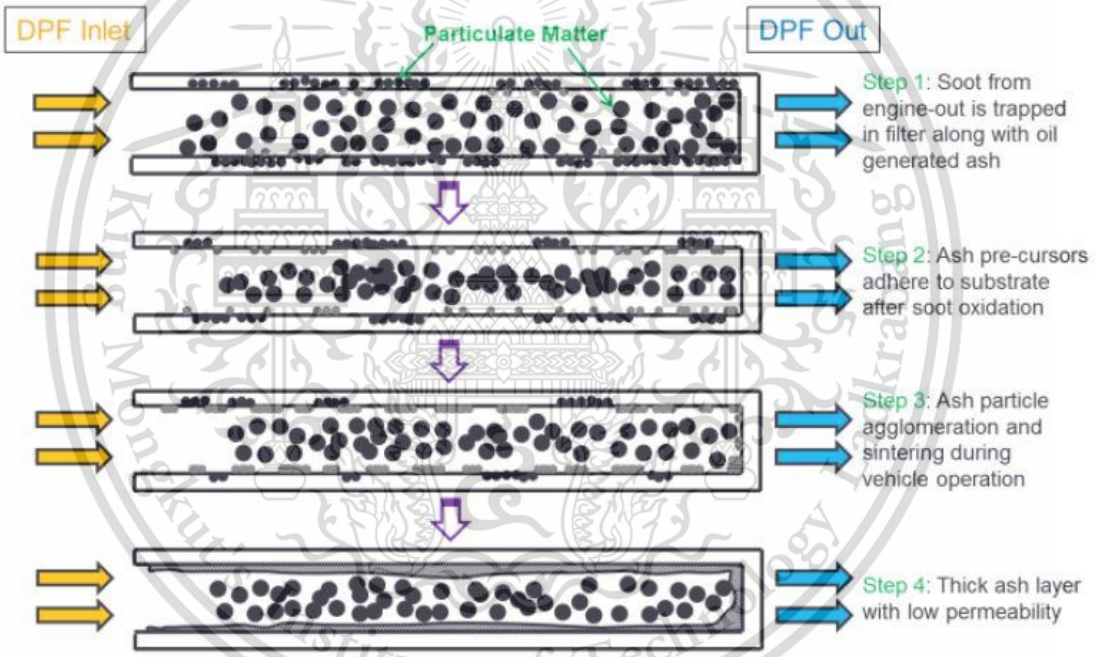

Figure 2.18 (a) Ash distribution in DPF (predominant passive regeneration strategy) [18].

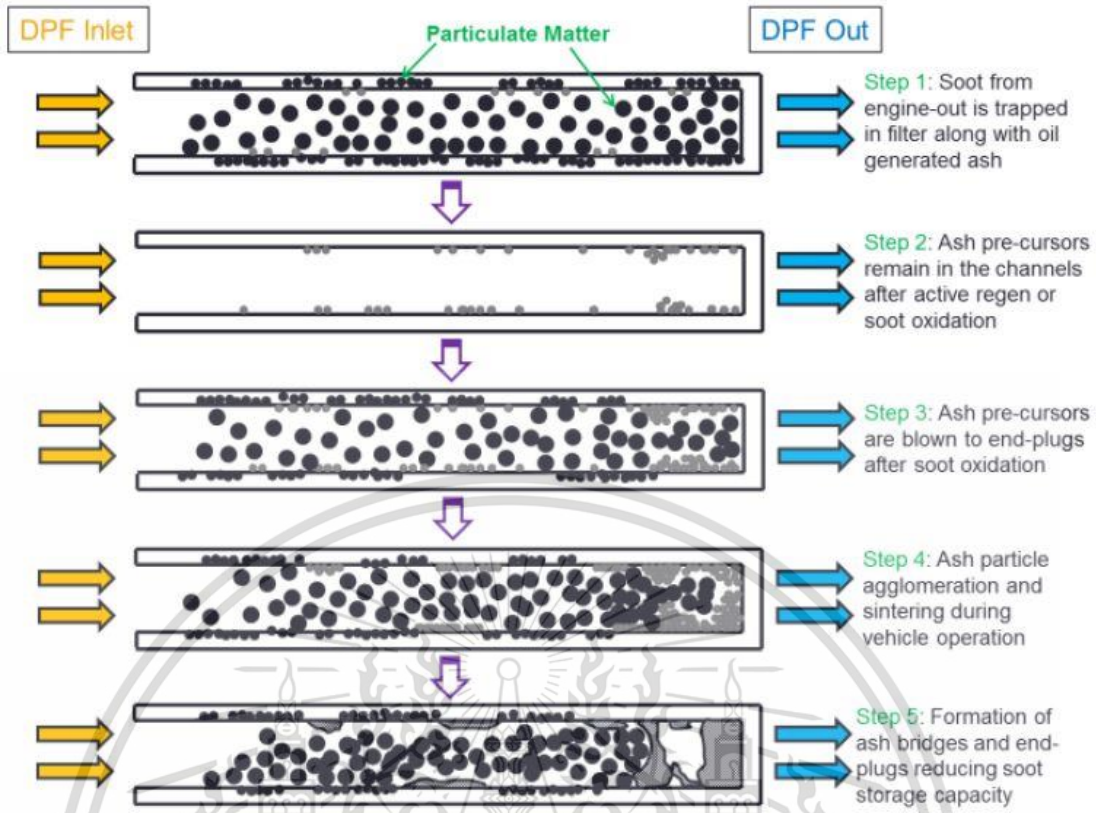

Figure 2.18 (b) Ash distribution in DPF (predominant active regeneration strategy) [18].

2.9 Investigation of Diesel Ash inside Diesel Particulate Filter

A. Liati et al., [19] investigated the electron microscopy analysis of diesel ash on morphology, SEM images of ash accumulated in DPF and chemistry of ash components. Accumulated ash were found out either in loose and powdery or brittle agglomerates sizing in the range of hundreds of nm to a few μm as shown in figure 2.19 (a). Besides, a very fine powdery ash particles were also penetrating through the pores of DPF as described in figure 2.19 (b). SEM images of ash particles showed the minor components such as drop-like particles, glassy particles of Al-silicate composition and a few spherical Fe-oxide particles. The composition of bulk ash was also investigated by using EDX and concluded that various metal oxide compositions were found inside bulk ash as described in table 2.5. Moreover, TEM images of nanostructure of bulk ashes were found out in straight line structures as shown in figures 2.20.

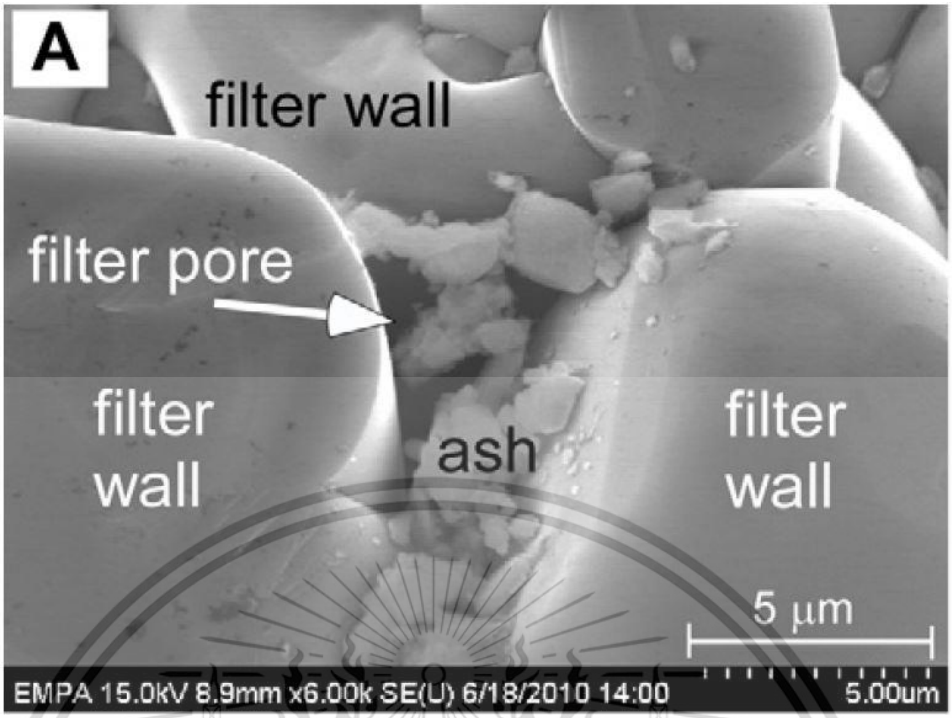

Figure 2.19 (a) SEM image of ash agglomerates in the pores of the channel wall of used DPF [19].

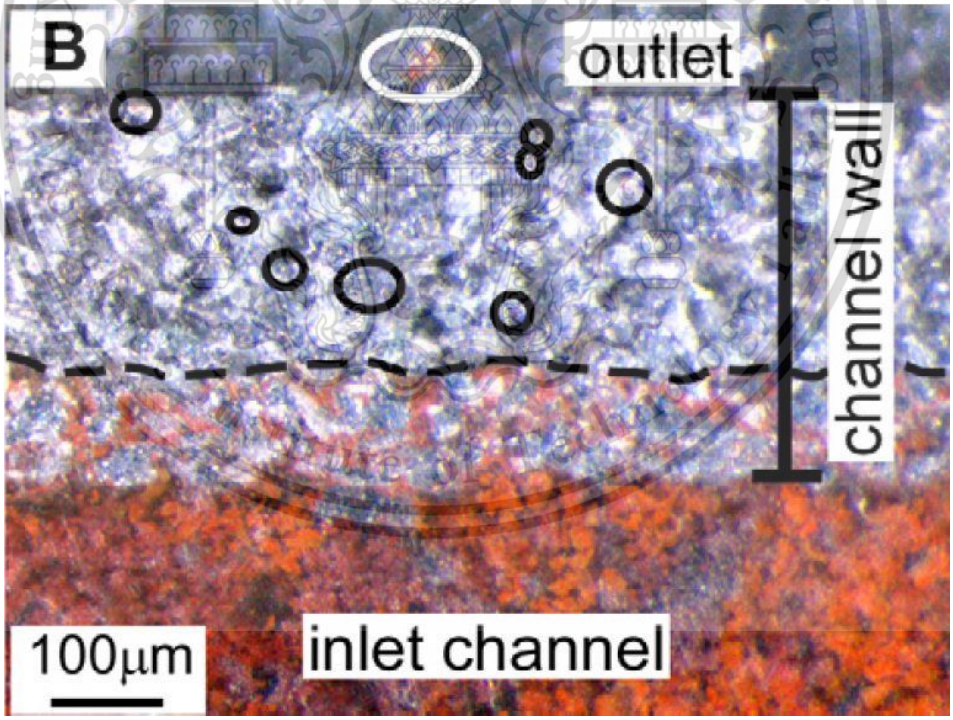

Figure 2.19 (b) SEM image of massive ash penetration in the pores of the channel wall of used DPF [19].

Table 2.4 Chemical composition of bulk ash [19].

Element	Concentration: mol% - (wt%)		
	Light truck		Passenger car
	center	periphery	
CaO	15.7 (9.16)	17.3 (10.2)	20.9 (9.74)
ZnO	9.33 (7.94)	10.5 (9.00)	7.67 (5.20)
P_2O_5	9.50 (14.1)	8.23 (12.3)	8.17 (9.66)
MgO	22.4 (9.45)	22.6 (9.57)	2.47 (0.83)
SO_3	23.0 (19.2)	32.6 (27.5)	5.18 (3.45)
Fe_2O_3	10.3 (17.2)	4.69 (7.88)	>50 (70)
Al_2O_3	4.92 (5.24)	1.35 (1.45)	1.13 (0.96)
Cr_2O_3	1.04 (1.65)	0.49 (0.79)	0.055 (<0.1)
NiO	1.33 (1.04)	0.60 (0.47)	0.55 (0.34)
CuO	1.11 (0.86)	1.22 (0.96)	0.34 (0.21)
SiO_2	1.10 (0.69)	0.21 (0.13)	0.94 (0.47)
MnO	0.34 (0.25)	0.19 (0.14)	0.05 (<0.1)

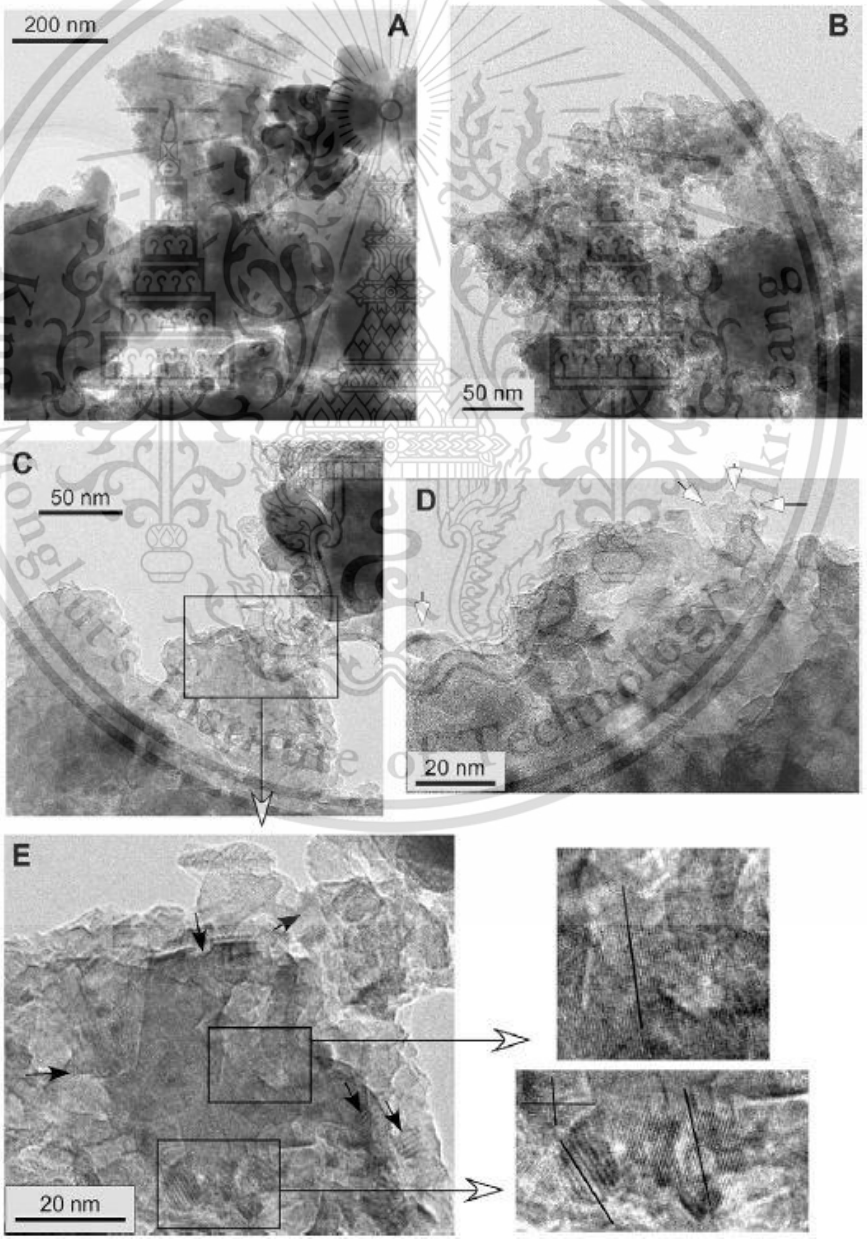

Figure 2.20 TEM images of bulk ash showing straight line structures [19].

2.10 Surface Chemistry and Application of Metal Oxide Catalysts

Metal oxides are used as catalysts due to its great catalytic effects. Naturally, surfaces of metal oxides are very rare to exist as an ideal homogeneous surface. In fact, structure defects (i.e. steps, kink edges and corners) and point defects (i.e. oxygen vacancies) are present [20 – 23]. Bolis. V [20] proposed a schematic diagram of metal oxide's (MgO) surface imperfection presenting surface defects and point defects are shown in figure 2.21.

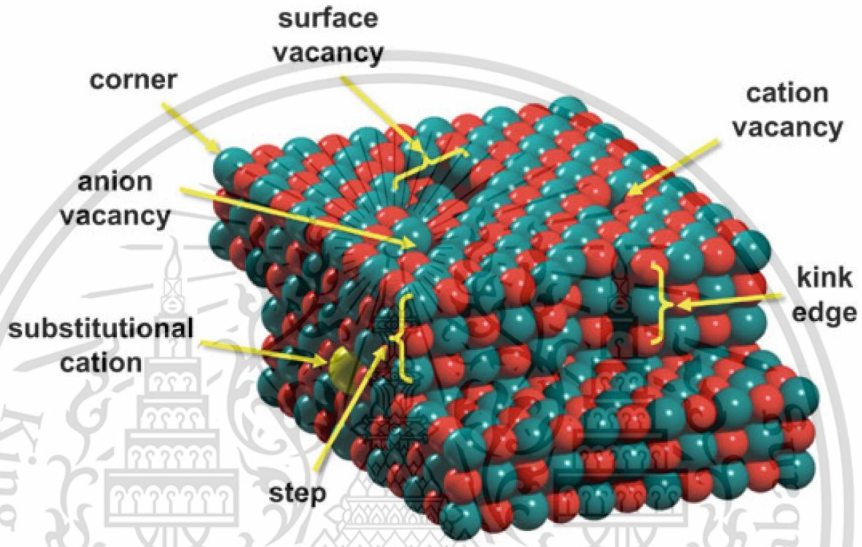

Figure 2.21 Cartoon of a piece of realistic MgO nanocrystal, which exhibits both structural (steps, kinks edges and corners) and point (oxygen vacancy) defects [20].

Among surface defects, oxygen vacancies can adsorb more oxygen. The more oxygen adsorption leads to more desorption and reaction rat is increased. Therefore, metal oxides are widely used as catalysts by increasing the number of oxygen vacancies using doping or nano-structuring. To measure the amount of adsorbed oxygen on metal oxide surfaces, temperature programmed desorption (TPD) method was commonly applied [24]. Scanning tunneling microscope is an essential tool to analyze the oxide surfaces by magnifying until atomic resolution [25]. Diebold. U [26] investigated metal oxide surface's imperfection of Titanium dioxide (TiO_2) surface using scanning tunneling microscopy (STM) images. The author concluded that the oxygen does not stick to fully oxidized surface and the oxygen vacancies on Titanium dioxide's surface were increased by metal oxide reduction. The location of metal ions, oxides and oxygen vacancies obtained from STM images were described as shown in figure 2.22 (a). By presenting point defects (i.e. oxygen vacancy), metal oxide catalyst can offer great

catalytic effects. Solid-gas reaction mechanism, Mars-Van Krevelen mechanism, the oxide surface is directly involved in a solid-gas reaction by using its most reactive oxygen atoms. A weakly bound surface oxygen atom is added to the reactant forming oxygenated compound leaving as anion oxygen vacancy [27].

As shown in figure 2.22 (b), three possible catalytic soot oxidation mechanisms of metal oxide were proposed by Uchisawa, J. et al. [28]. In mechanism (1), active oxygen is released from the lattice by redox reaction of CeO_2 and carbon from soot. Regarding to activity series, carbon (C) is more active than cerium (Ce). Therefore, oxides from CeO_2 can be diffused into carbon as active oxygen. In mechanism (2), oxygen molecules from supply gas are dissociative adsorbed on metal oxide surface, move onto the soot surface and reacts with soot. In mechanism (3), active oxygen species (O_2^-) are formed on surface oxygen vacancy sites generated by the reduction of CeO_2 and the vacancies can accept the oxygen molecules from supplied gas and oxidize the soot. Moreover, phenomena of oxygen vacancy from mechanism (3) is mainly based on solid-gas reaction of Mars-Van Krevelen mechanism.

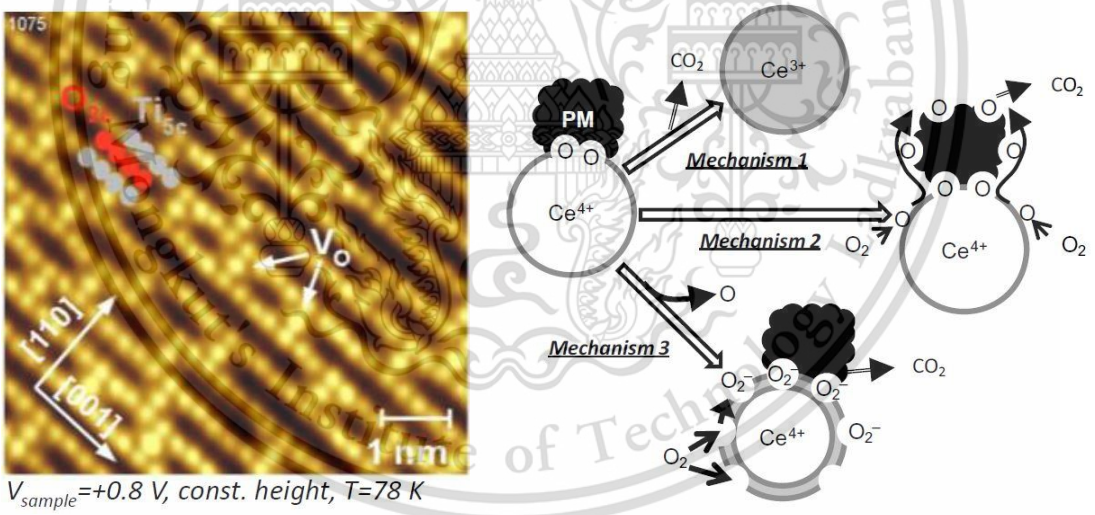

(a) STM image of TiO_2 [26] **(b)** Catalytic soot oxidation mechanisms[28]

Figure 2.22 (a) STM image of TiO_2 surface showing (Ti) metal ions, oxygen atoms and anion oxygen vacancies (V_o) and **(b)** Catalytic soot oxidation mechanisms.

CHAPTER 3

RESEARCH METHODOLOGY

3.1 Experimental Equipment

3.1.1 Engine specification

A natural aspirated, single cylinder, direct injection, compression ignition engine (Kubota RT 140 DI) was used to generate the particulate matters. Engine displacement volume is 709 cm^3 and compression ratio is 18:1. Details of engine specifications are briefly described in Table 3.1 and engine performance curves are shown in figure 3.1.

Table 3.1 Engine specification

Items	Details
Engine type	1-cylinder, natural aspirated, direct injection, compression ignition engine
Bore x Stroke	(97 x 96) mm
Displacement	709 cm^3
Compression ratio	18:1
Power	9.2 kW @2400 RPM
Injection timing	19°CA bTDC
Injection pressure	22 MPa

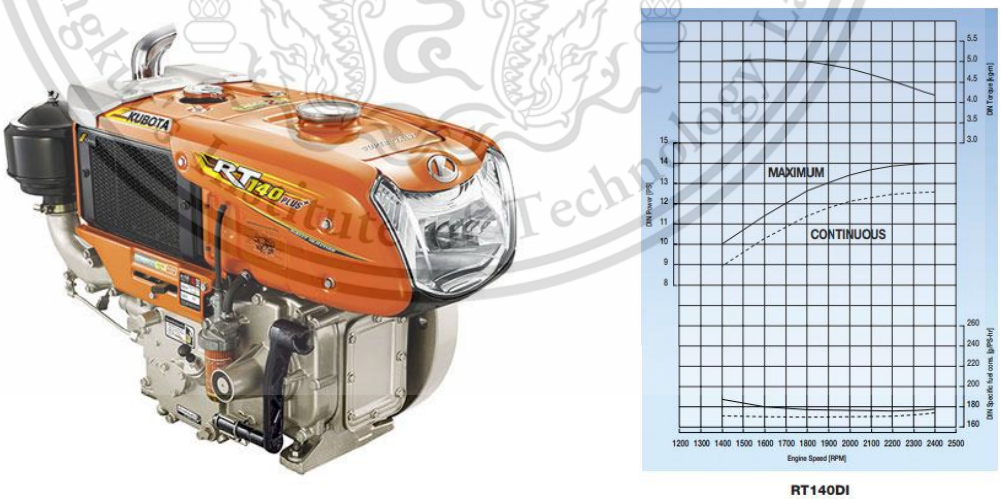

Figure 3.1 Engine performance curve of Kubota RT-140 DI CI engine.

3.1.2 Engine dynamometer

As shown in figure 3.2, an eddy current engine dynamometer (Tokyo plant model ED-60-Horizontal) was used to control the desired engine speed and load conditions. Engine propeller shaft (drive shaft) is mounted on the dynamometer and the torque arm is connected to the load cell to measure the outcoming torque from the engine. The measurable torque can be converted into power for calculating the brake power of the engine. Dynamometer is controlled by control unit which is worked by the aid of Lab-view program. Various speed and load conditions was applied to obtain the information under different engine operating conditions. Details of various engine operating conditions for each experiment are described in Table. 3.2 and schematic diagram of engine dynamometer is shown in figure 3.3.

Figure 3.2 Eddy current engine dynamometer.

Table 3.2 Various engine speed and load conditions.

Experiments	Speed (rpm)	Load (%)
Engine performance	1600, 2000,2400	20, 50, 80, Full load
Smoke intensity		
Soot powder	2400	Full load

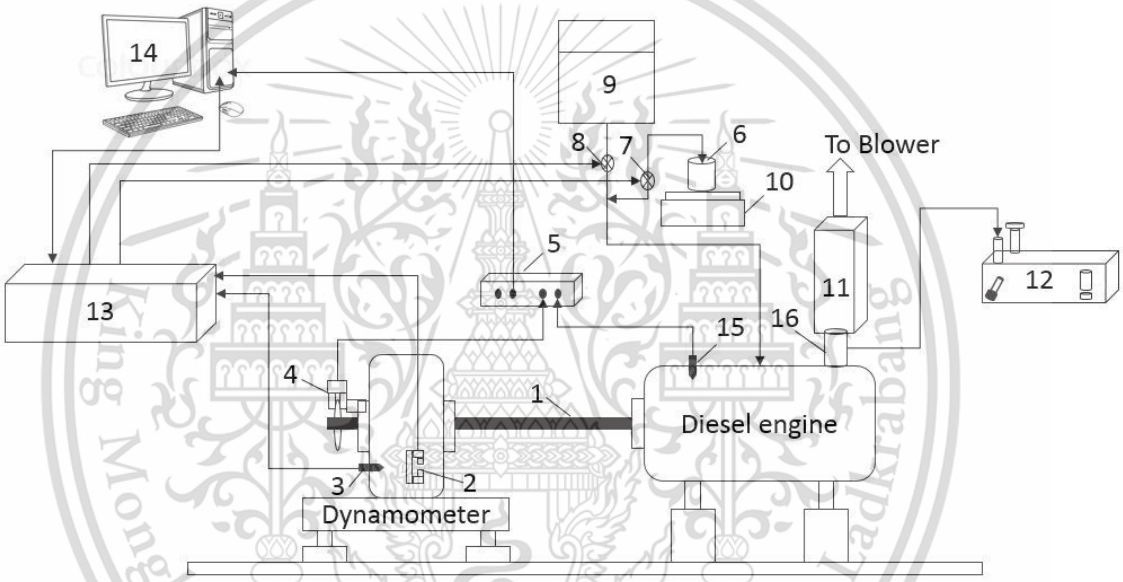

Figure 3.3 Schematic diagram of engine experiment.

Labels:

1) Propeller shaft
2) Load cell
3) Dyno cooling water temperature sensor
4) Crank angle encoder sensors
5) Data acquisition unit
6) Fuel beaker
7) Solenoid valve (1)
8) Solenoid valve (2)
9) Fuel supply
10) Weight scale
11) Soot powder collector
12) Smoke meter
13) Data logger
14) Computer (Lab-view)
15) Pressure sensor
16) Exhaust muffler

3.1.3 Test fuels

Conventional diesel (B7) and hydrotreated vegetable oil (HVO) were used as ideal fuels. Secondly, designed lubricating oil with excess oil additives were blended directly into diesel and HVO fuels by the exact amount of (10%) by mass. The properties of test fuels and blending lubricant oil properties are shown in Table 3.3 and Table 3.4.

Table 3.3 Properties of test fuels.

Properties	Standard	Diesel	HVO
Density @30°C (g/cm^3)	ASTM D4052	0.824	0.778
Kinematic viscosity @40°C (mm^2/s)	ASTM D445	3.24	2.64
Carbon content (%)	ASTM D5291	85.73	84.24
Hydrogen content (%)	ASTM D5291	13.22	15.05
Oxygen content (%)	ASTM D5599	0.00	0.00
Cetane Index	ASTM D4737	60.43	76.89
Distillation T10 (°C)	ASTM D8611b	207.7	227.4
Distillation T50 (°C)	ASTM D8611b	287.9	278.2
Distillation T90 (°C)	ASTM D8611b	352.3	293.2
Auto ignition temperature (°C)	ASTM 659	288	288

Table 3.4 Properties of blending lubricant tested by Bangchak Corporation.

Test	Method	Result
Density @15°C (g/mL)	ASTM D4052-15	0.8960
Density @30°C (g/mL)	ASTM D4052-15	0.8866
Viscosity @40°C (mm^2/s)	ASTM D445-15a	154.8
Viscosity @100°C (mm^2/s)	ASTM D445-15a	15.05
Magnesium (%wt)	ASTM D6481	0.1816
Zinc (%wt)	ASTM D6481	0.0798
Phosphorous (%wt)	ASTM D6481	0.0856

3.1.4 Smoke meter

Okuda DSM – 240 was introduced to measure the smoke intensity of the exhaust emission. At first, engine was controlled under desired operating condition for (3) minutes running time. After that, gas detector was inserted into the exhaust muffler for (7) seconds in order to reach the exhaust gas along the pipe. Finally, the pump must be released by pressing the lever and waiting for (3) seconds. At last, after the exhaust gas passed through filter paper, it was detected by light detector to measure the soot contamination by expressing percentage. Smoke meter and filter paper that are used in this experiment are shown in figure 3.4.

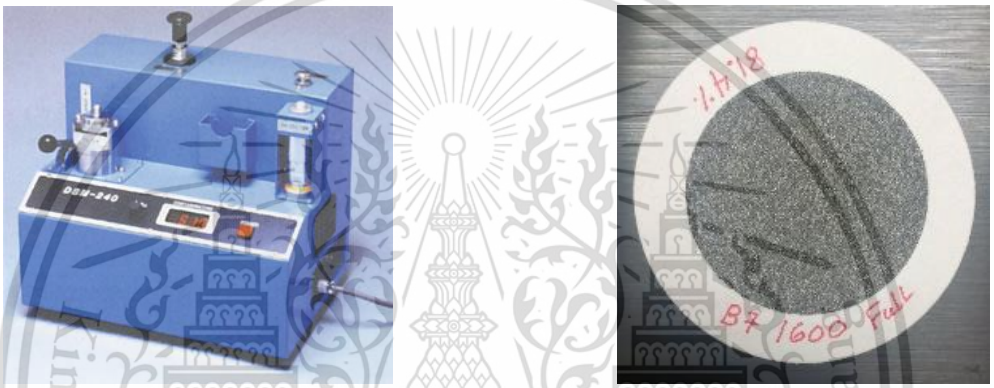

Figure 3.4 Opacity smoke meter (Okuda DSM – 240) and filter paper.

3.1.5 Pressure sensor

Kistler high temperature pressure sensor (Type 6052C) was used at a pre-installed pressure mounting sleeve as shown in figure 3.5. Sensor was mounted directly in the cylinder head with a tightening torque of 1.5 Nm. Sensor's front is (M5x0.5) bore and it was installed prescribed guidelines to obtain the optimal pressure measurements inside cylinder through the experiments.

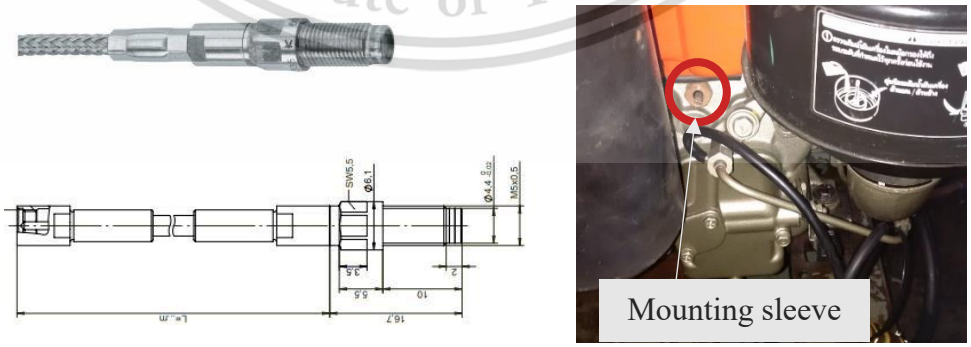

Figure 3.5 Engine combustion pressure analyzer and location of mounting sleeve.

3.1.6 Encoder sensors

To observe the combustion pressure according to the crank angle position, crank angle encoder (CA-RIE-360) was used. The marker disk with 360° slits (outer diameter 120 mm) was installed at the end of the flywheel path. An infrared beam is emitted and the marker disk including slits will pass inbetween the sensor unit. Encoder sensor and marker disk are shown in figure 3.6.


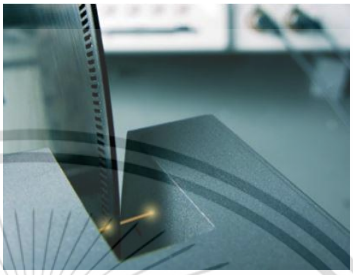


Encoder sensors

	Models	Pulses per revolution	Resolution	Diameter of disc	Max. rpm	Max. Output freq. [kHz]	General description	Applications
CA-RIE-xxx	CA-RIE-360	360	1°	121.6 mm (4.79 in.)	12000	125	Rugged industrial encoder sensor with 1 zero puls per revolution	Combustion Analysis
	CA-RIE-720	720	0.5°	236.2 mm (9.30 in.)	10000	125	Optimized for use with DEWE-CRANKANGLE-CPU [1] to reach resolutions up to 0.1° Sensor size: 25.5 x 39.5 x 47.5 mm (1.0 x 1.55 x 1.87 in.) Temp. Range -10 °C to 60 °C (extented temp. range on request)	Torsional Vibration Rotational Vibration
CA-ENCODER-xxx	CA-ENCODER-900	900	0.4°	-	9000	300	Incremental hollow shaft encoder IP65 protected 12 mm shaft diameter (end to end hollow shaft) incl. fixturing and 10 m cable Size: 72 x 45 x 51 mm (2.81 x 1.76 x 2 in.) Temp. Range -20 °C to 85 °C	Combustion Analysis
	CA-ENCODER-3600	3600	0.1°	-	5000	300		

[1] *The DEWE-CRANKANGLE-CPU is already integrated in DEWE-xxxx-CA2-PROF systems!*

Figure 3.6 Encoder sensors (CA-RIE-360).

3.1.7 Data acquisition (DAQ) system

DAQ system connects the data information between engine and computer. As shown in figure 3.7, “DEWESoft SIRIUSi-HS-CA” was used in this experiment.

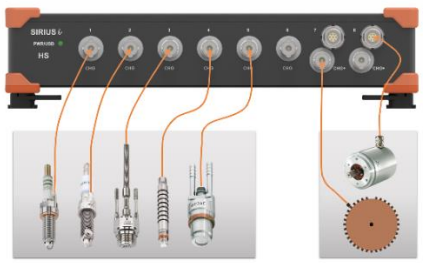

Figure 3.7 Data acquisition (DAQ) system.

3.2 Experimental Procedure

3.2.1 Combustion characteristics

For the combustion characteristics analysis, 12 various engine speed and load conditions (as previously described in Table 3.2) were conducted to investigate the performance of the engine for each fuel conditions. Measureable torque, brake specific fuel consumption, engine speed values resulting from lab-view program were used to calculate the brake specific energy consumption and brake thermal efficiency to compare each fuel. By using pressure – crank angle data from pressure sensor, Pressure-Volume relationship (PV diagram) can be transformed as shown in figures 3.8.

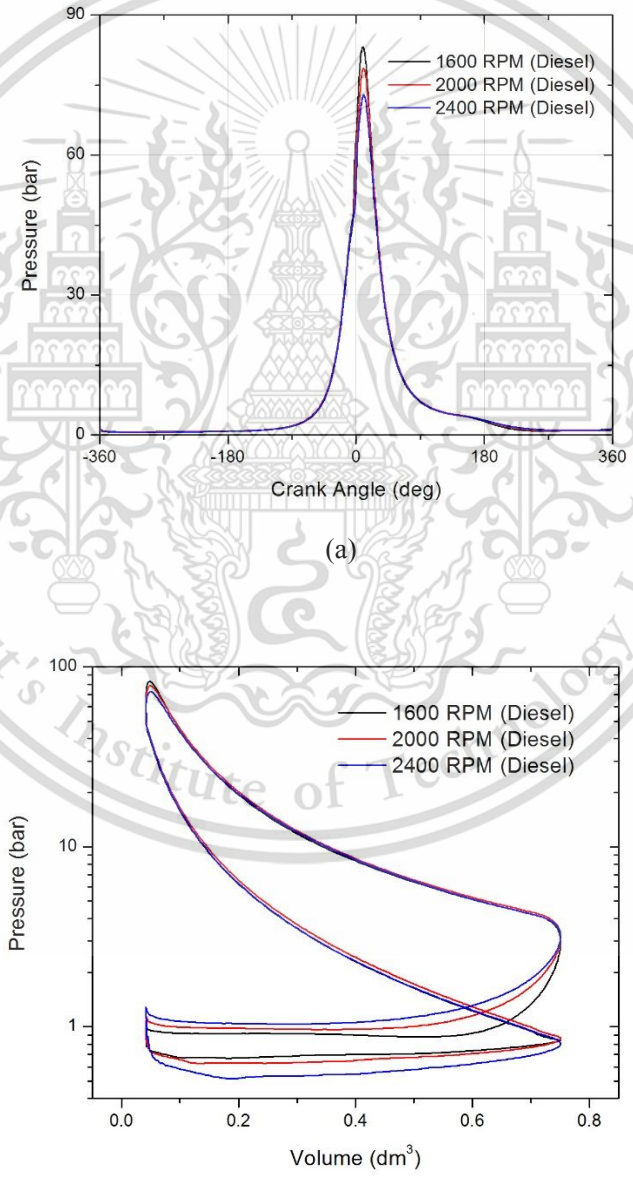

Figure 3.8 Combustion pressure analysis of (a) Pressure-Crank angle and (b) PV diagram.

3.2.2 Physical characterization of particulate matters

Scanning electron microscope (FE – SEM SU8030: magnification 20X to 800, 000X) as shown in figure 3.9 was used to investigate the agglomerate structure of particulate matters (in the range of PM2.5, PM10) in micro- scales. Particulate matters trapped by the filter paper was used to investigate the morphology of PM in micro-scales. (1000x, 10,000x) magnification was introduced to observe the agglomerate structure of PM.

Transmission electron microscope (JEM – 2100 Plus) as shown in figure 3.10 was used to investige the nanostructure of ultrafine agglomerate particles and single primary particles in nano-scales. PM powders which was collected by the soot collecter were used. (30,000x) magnification was introduced to observe the ultrafine agglomerate particles and (600,000x and 800,000x) magnifications were introduced to observe clearly the single primary nanostructure of particulate matters.

Figure 3.9 Investigation of agglomerate structure of PM using Scanning Electron Microscopy (SEM).

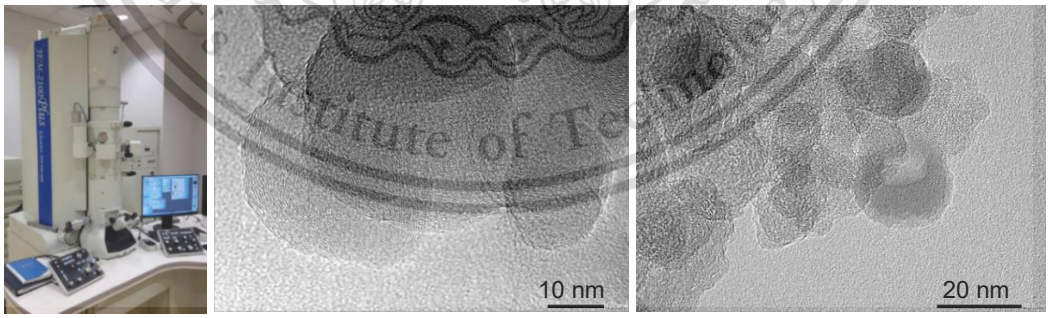

Figure 3.10 Investigation of single primary nanostructure of PM using Transmission Electron Microscopy (TEM).

To investigate the skeletonized nanostructure of single primary particles as shown in figure 3.11, ImageJ software was used. At first, TEM image (25nm x 25nm) was cropped into (5nm x 5nm) image. This (5nm x 5nm) image was transformed into black and white binary image without outliers. Finally, black and white binary image was transformed into skeletonized image to see the different crystallites structure of particulate matters in nano- scales.

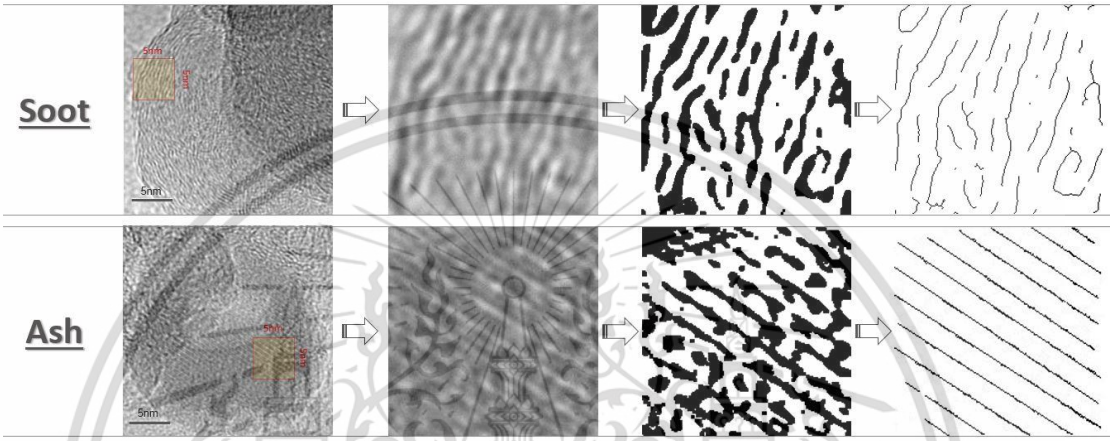

Figure 3.11 Investigation of skeletonized nanostructrure of diesel soot and metal oxide ash using ImageJ.

3.2.3 Chemical composition analysis of particulate matters

To investigate the chemical composition of particulate matters as shown in figure 3.12, electron dispersive x-ray spectroscopy was introduced by the aid of scanning electron microscopy. PMs from filter paper were detected by electron beam and it was determined by their x-ray energies. (3) spectrums were observed to each samples for fairly comparison.

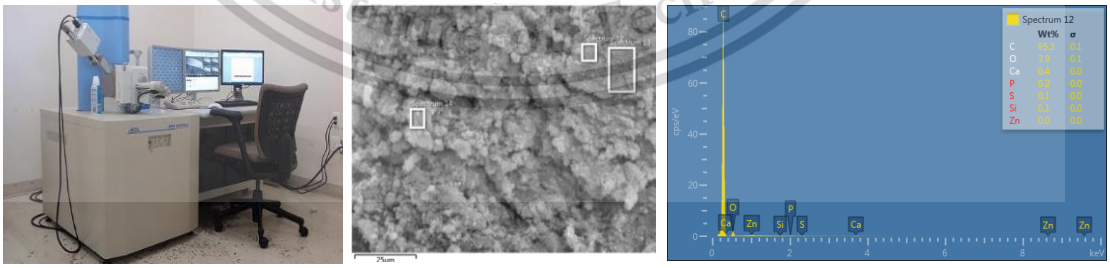

Figure 3.12 Chemical composition analysis of diesel blending lube oil PMs showing unburned metallic additives by using Electron Dispersive X-ray Spectroscopy (SEM-EDS) analysis.

3.2.4 Elemental analysis of particulate matters

To investigate the elemental analysis of particulate matters in nano- scales, electron dispersive x-ray spectroscopy was introduced by the aid of transmission electron microscopy as shown in figure 3.13. Electron beam with the intensity of (0 – 40 keV) was chosen according to different x – ray energies of each elements. Same magnification as TEM image (600,000x and 800,000x) was introduced to observe the elemental composition in nano- scales.

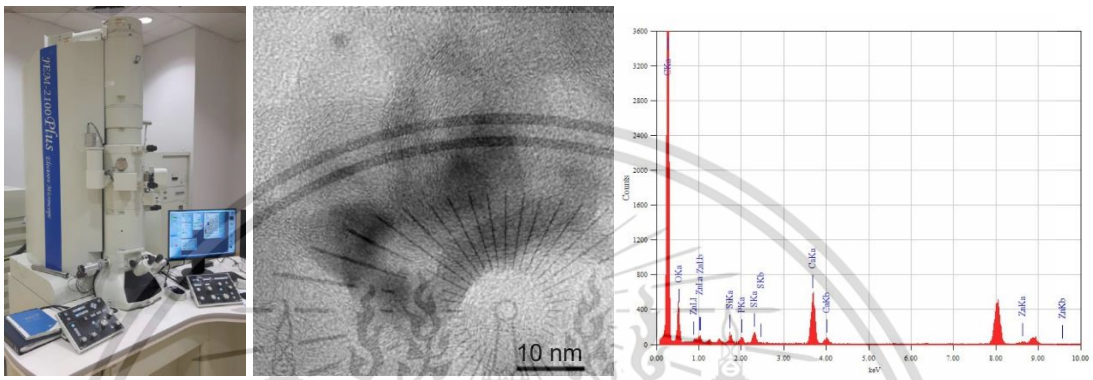

Figure 3.13 Elemental analysis of EDS spectra focusing on metal oxide ash showing metallic elements.

3.2.5 Oxidation kinetics of particulate matters

Thermogravimetric analyzer (NETZSCH) was used to investigate the oxidation kinetics of particulate matters. Operating temperature was increased by isothermal and the operating atmosphere was maintained with pure air. Only nitrogen gas was introduced until the operating temperature was reached. After reaching operating temperature, the properable amount of O_2 was introduced to be pure air atmosphere. (550, 575, 600, 625, 650) degree celcius were chosen to oxidize the PM.

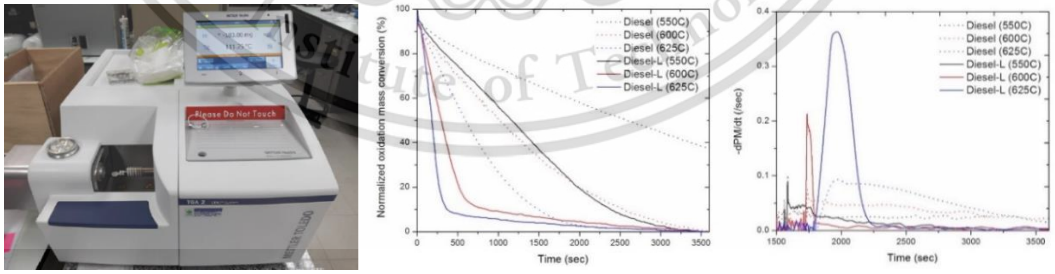

Figure 3.14 Thermogravimetric analysis of diesel blending lube oil PMs showing faster mass conversion rate due to influence of metal oxide ash acting as catalyst on oxidation kinetics.

CHAPTER 4

RESULTS AND DISCUSSION

4.1 Combustion Characteristics of Diesel and HVO Fuels

Engine combustion characteristics of diesel and Hydrotreated Vegetable Oil (HVO) fuels were successfully conducted using 1-cylinder small CI engine. Combustion pressure, brake specific fuel consumption, engine performance, heat release rates and also indicated and brake thermal efficiency of HVO fuel combustion were analyzed by comparing diesel fuel combustion characteristics. Soot contamination percentage under different engine operating conditions were also measured using a smoke meter. Regarding to second generation biodiesel properties of HVO, oxygen molecules has been removed to be mostly identity with diesel fuel properties. Not only combustion characteristics but also less smoke intensity advantages of HVO fuel combustion were found out in this experiment.

4.1.1 Chemical properties of test fuels

Conventional diesel (B7) and synthetic biodiesel: Hydrotreated Vegetable Oil (HVO) were used as reference fuels in the experiment. Chemical properties of each fuel are described in Table 4.1. HVO fuel has lower fuel density and lower energy density compared to conventional diesel since auto ignition temperature are identity. One of the prominent advantages of HVO is higher cetane index which could shorten the ignition delay during combustion. As shown in figure 4.1, fuel distillation test was conducted to analyze the fuel molecules. During fuel distillation experiment, test fuel was placed inside the distillation column and temperature was increased steadily. Results are recorded as volume fraction in percentage. Fuel with lower fuel molecules are easier to distillate than the fuel composed of greater fuel molecules and the results are described as T10, T50 and T90 which is meant for distilled volume fraction of (10%, 50% and 90%). According to fuel distillation result, HVO needs lower temperature to reach the distilled volume fraction of 50% and 90%. This information confirmed that HVO is composed of smaller fuel molecules compared to conventional diesel.

Table 4.1 Chemical properties of test fuels.

Properties	Diesel	HVO
Chemical formula	$C_{14.11}H_{26.23}$	$C_{14.03}H_{29.86}$
Density@30°C (g/cm^3)	0.824	0.778
Lower Heating Value (kJ/g)	45.86	46.86
Energy Density (kJ/cm^3)	37.79	36.45
Carbon content (%)	85.73	84.24
Hydrogen content (%)	13.22	15.05
Oxygen content (%)	0.00	0.00
Cetane Index	60.43	76.89
Distillation T10 (°C)	207.7	227.4
Distillation T50 (°C)	287.9	278.2
Distillation T90 (°C)	352.3	293.2
Auto ignition temperature (°C)	288	288

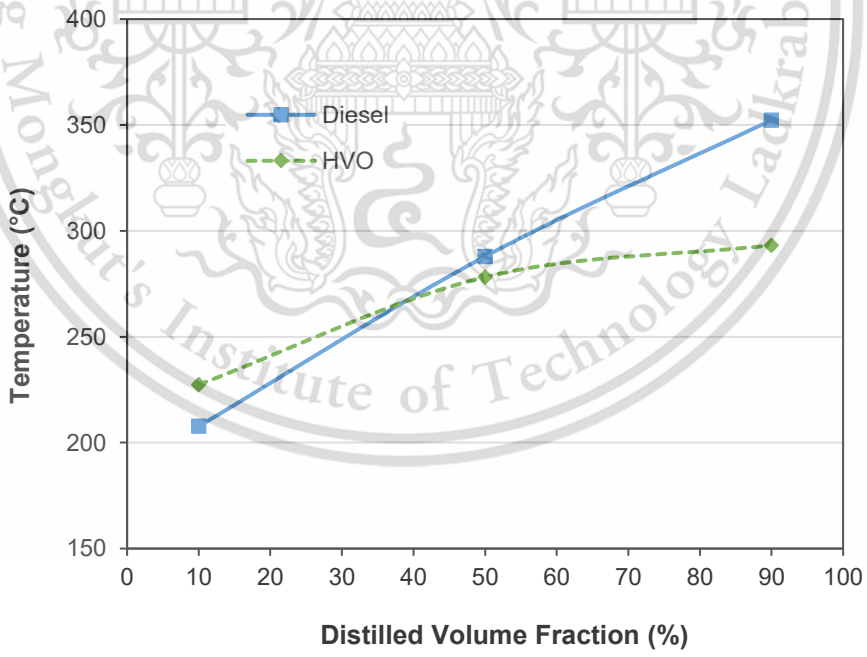

Figure 4.1 Fuel distillation test result.

4.1.2 Combustion pressure

Combustion characteristics analysis of diesel and HVO fuel combustion have been initiated with pressure – crank angle measurement which gives rise to the pressure – volume (PV) diagram. Pressure – crank angle and PV diagrams from various speed condition (1600, 2000, 2400) rpm under full engine load condition are described in figures 4.2. According to each operating engine speed under full load condition, HVO fuel combustion offers slightly greater combustion pressure.

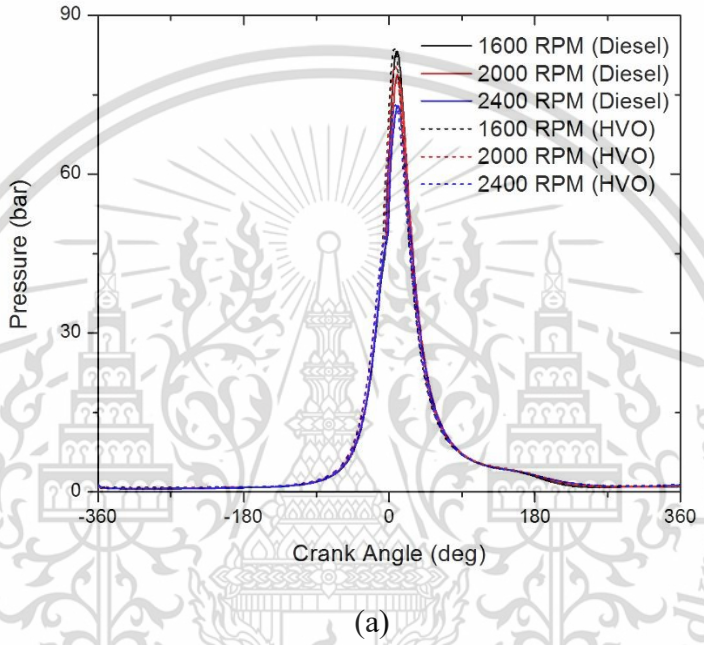

(a)

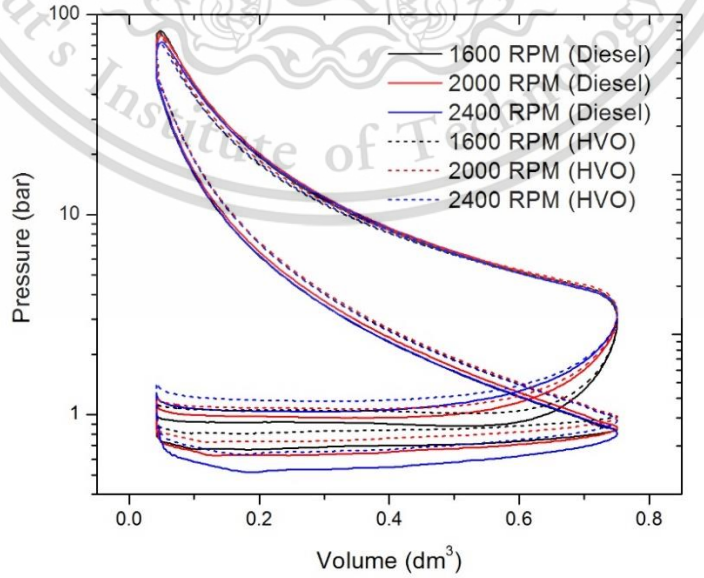

(b)

Figures 4.2 Combustion characteristics of (a) Pressure – crank angle (b) PV diagram.

4.1.3 Engine performance

Engine performance curves of both diesel and HVO combustion are described in figure 4.3 in terms of speed (rpm) and torque (Nm). When the engine speed is increased, the torque delivered by the engine is decreased. HVO fuel combustion produce lower torque compared to diesel especially in high engine load condition (i.e. 2400 rpm). This result might be related to different fuel properties of density (g/cm^3) and lower heating Q_{LHV} (kJ/g) values of diesel and HVO. Energy density (kJ/cm^3) can be calculated as shown in Table 4.1 by using density and lower heating values. Diesel nozzle inject same volume of fuel in the cylinder. Energy density means how much energy can be obtained according to each fuel injected volume. Lower fuel density of HVO can offer lower energy per volume (i.e. energy density) and this effect might be leading to lower torque. Therefore, indicated work of HVO is lower than diesel fuel combustion. Calculated indicated work W_i for diesel and HVO combustion were 641 Nm and 515 Nm respectively.

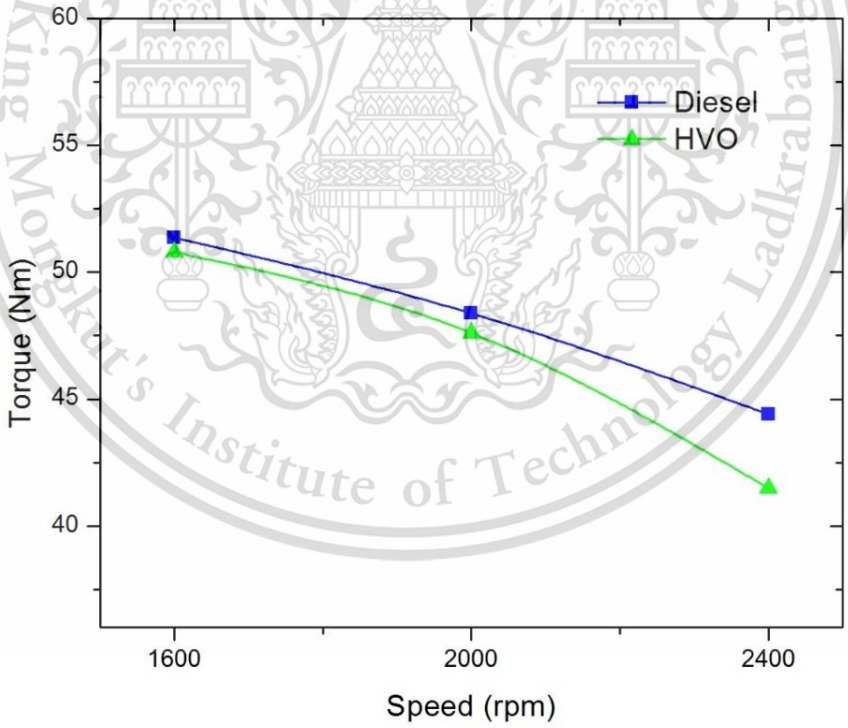

Figure 4.3 Engine performance curve.

4.1.4 Heat release rate

Heat release rates of diesel and HVO fuel combustion under full engine load condition with various speed conditions were briefly described in figure 4.4. Heat release rate curves can be divided into 3 different stages such as (i) vaporization (ii) premix combustion (iii) mixing control combustion. The injected fuel is start vaporized at vaporization stage and premix combustion occurs where the peak of heat release rate can be produced. Finally, mixing control combustion is followed by the continuous fuel injection. Fuel vaporization of HVO was better than diesel and it leads to greater fuel atomization which could significantly reduce the heat release rate at the vaporization stage as shown in figure 4.4. Moreover, HVO fuel offers shorter ignition delay due to attaining the higher cetane number compared to convention diesel.

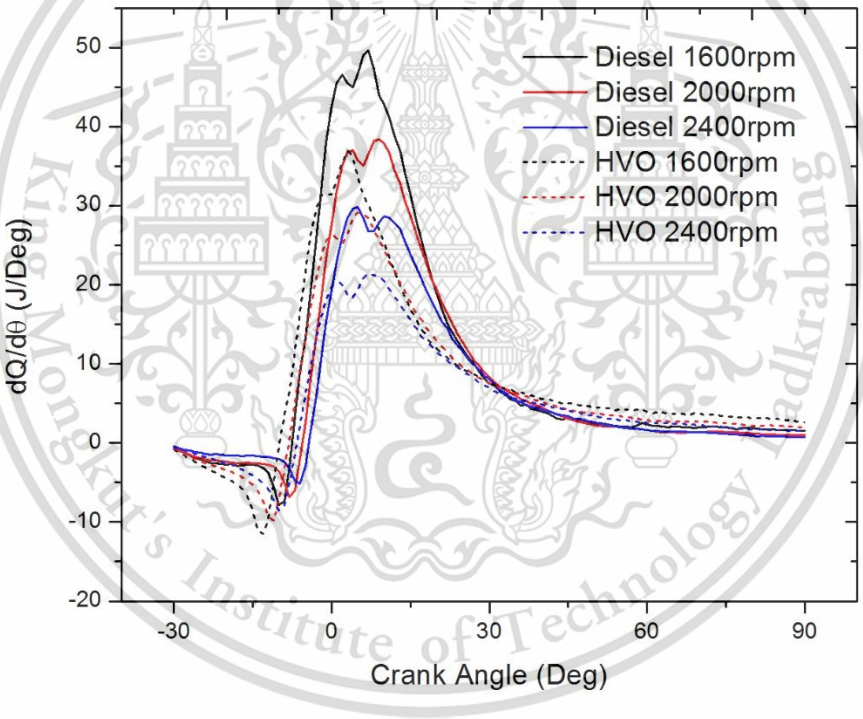

Figure 4.4 Heat release rates under engine full load condition.

4.1.5 Brake specific fuel consumption and thermal efficiency

Brake specific fuel consumption, indicated and brake thermal efficiency of diesel and HVO fuel combustion results were compared as shown in figures 4.5 to 4.7. Less fuel consumption, higher cetane index and greater Q_{LHV} of HVO might be the reasons to achieve better thermal efficiency compared to conventional diesel. Engine experiment has also been conducted under part load operation which is operating under 20%, 50% and 80% of engine full load condition at 2400 rpm. Brake specific fuel consumption, combustion pressure data and indicated thermal efficiency were measured to confirm the previous variable speed and engine full load condition as shown in figures 4.8 and 4.9.

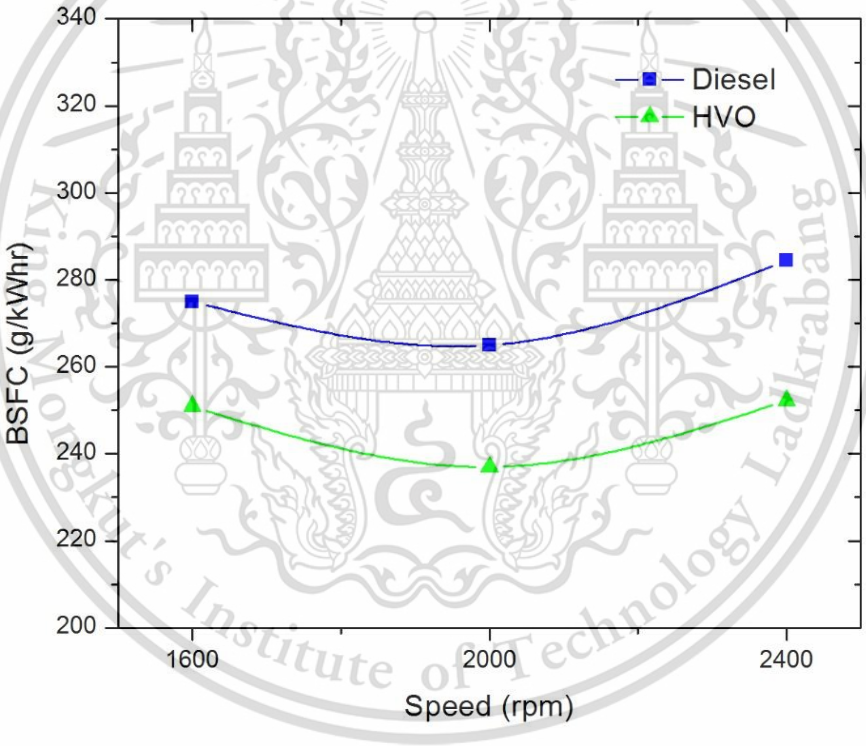

Figure 4.5 Brake specific fuel consumption.

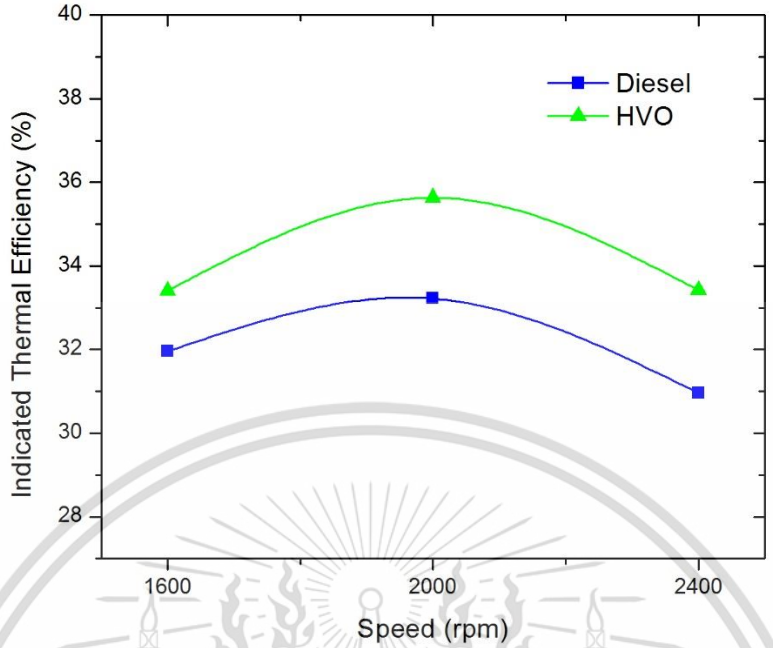

Figure 4.6 Indicated thermal efficiency.

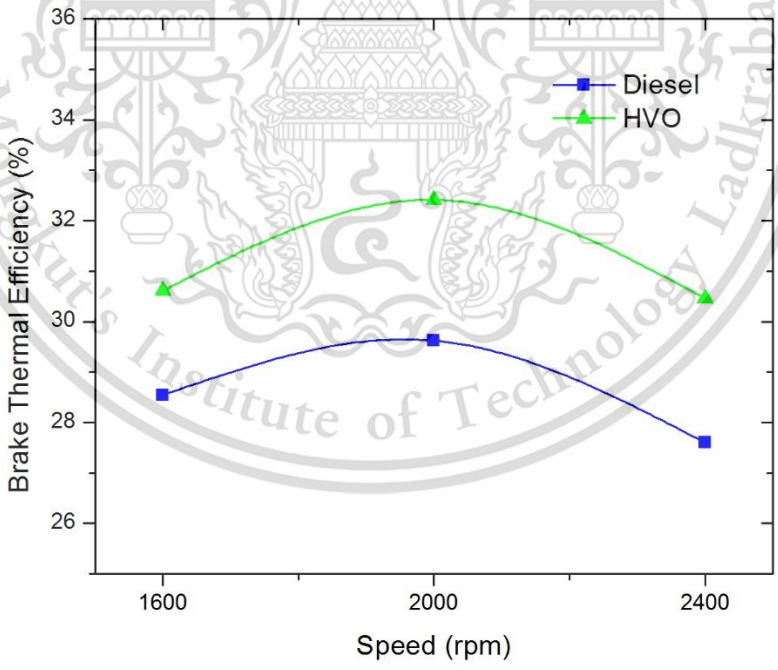

Figure 4.7 Brake thermal efficiency.

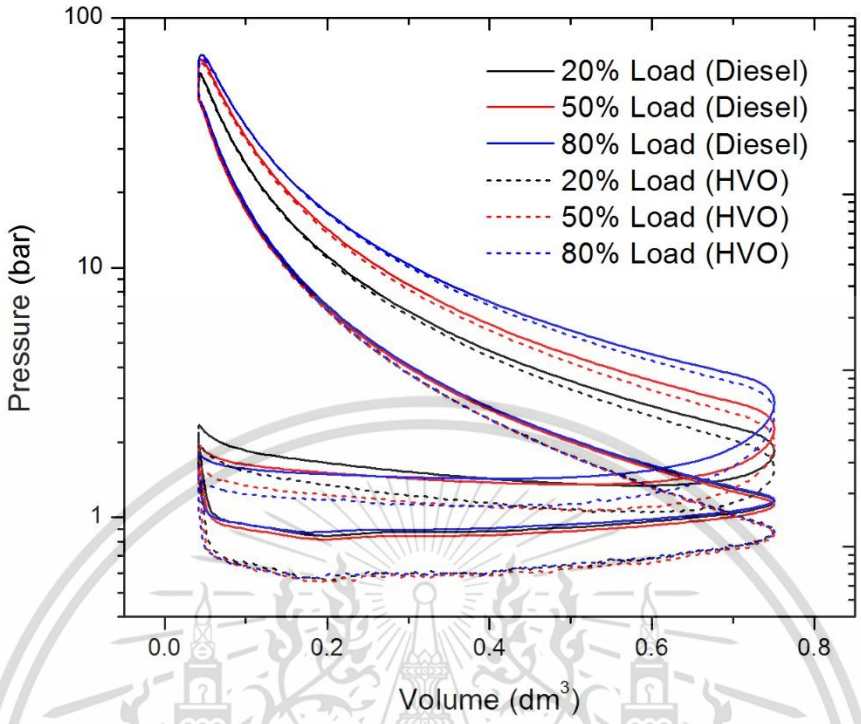

Figure 4.8 PV diagram of diesel and HVO operating under part load conditions.

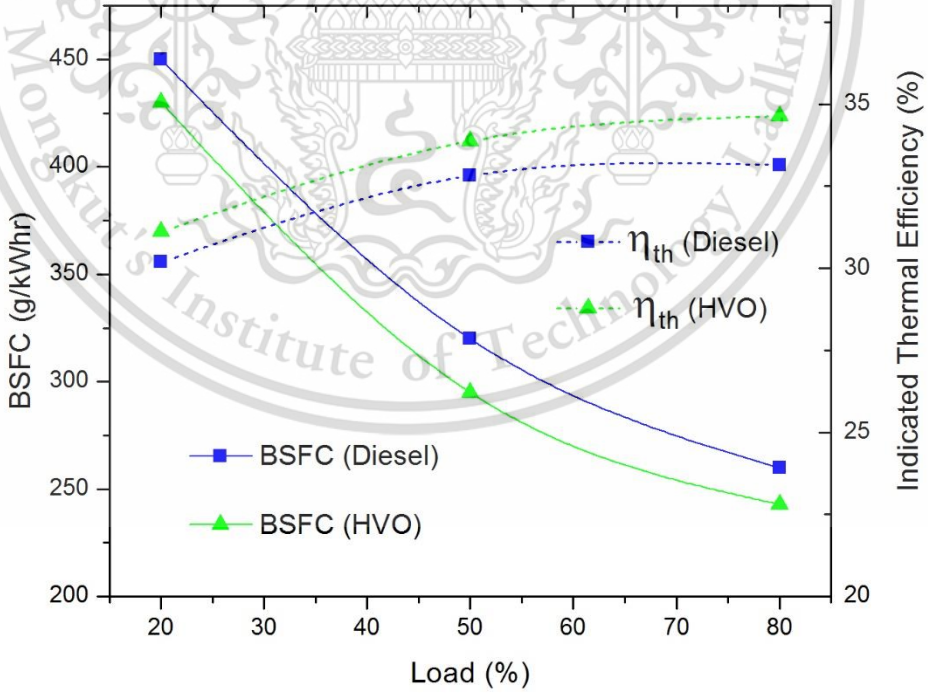

Figure 4.9 BSFC (indicating as solid lines) and Indicated Thermal Efficiency (indicating as dashed lines) under part load condition.

4.1.6 Smoke Intensity

The amount of unburned hydrocarbon (soot) contamination percentage were compared between diesel and HVO fuel combustion under different engine's speed and load conditions as shown in figures (4.10) and (4.11) . Contamination of soot (smoke intensity) was increased according to higher engine's speed and load conditions. Engine combustion from HVO fuel emits less smoke intensity than diesel. HVO fuel is composed of smaller hydrocarbon molecules and injected fuel were more efficiently vaporized due to better fuel atomization. Unlike conventional diesel, HVO fuel is a synthetic paraffinic fuel, lower density and higher cetane index which might lead to more complete combustion and less soot contamination.

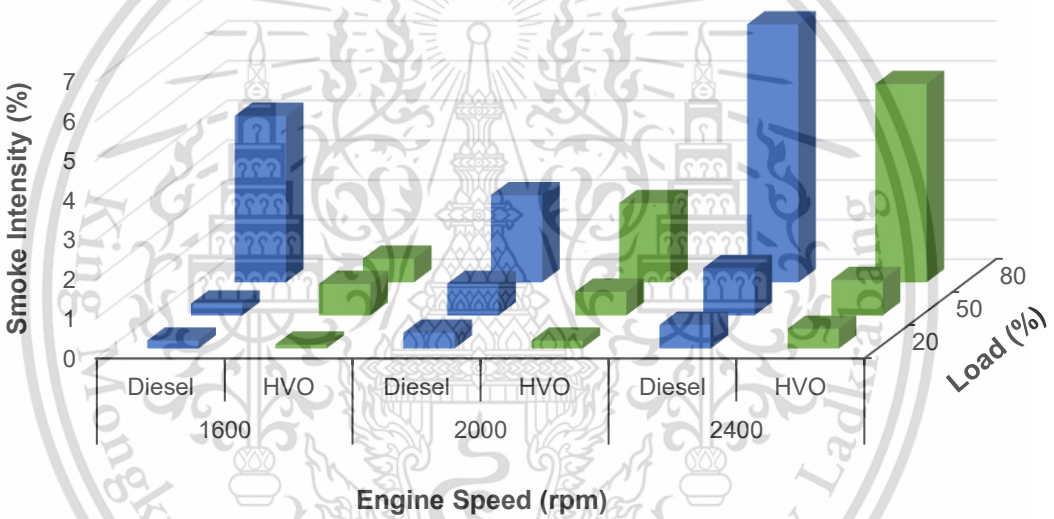

Figure 4.10 Smoke intensities under part load condition.

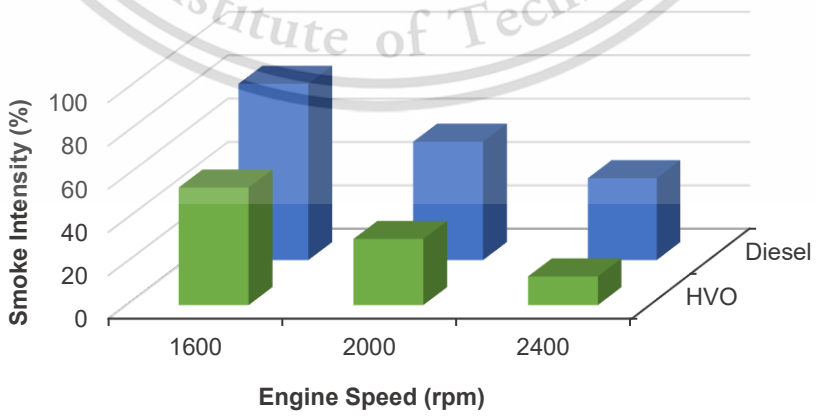

Figure 4.11 Smoke intensities under engine full load condition.

4.2 Characterization of Particulate Emission from Diesel & HVO

Physicochemical characterization of particulate matters emitted from diesel and HVO fuel combustion were briefly compared. Physical characterization such as agglomerate structures in micro- scales, ultrafine agglomerate structures in nano- scales and morphology of single primary particles nanostructures using electron microscopy (SEM and TEM). Measurement of fringe lengths by applying Image-J software were investigated. As a chemical characterization, isothermal thermogravimetric analysis was conducted to analyze the oxidation kinetics of particulate matters and also activation energy were calculated by using Arrhenius equation.

4.2.1 Agglomerate structure of particulate matters

Figures 4.12 compare the SEM image of agglomerate structure of diesel and HVO PM emitted from 2000 rpm engine full load condition which were collected by paper filter using opacity smoke meter. As in the micro- scales, PM sizing in the range of PM 2.5 (less than 2.5 μm) and PM 10 (less than 10 μm) were grouped to become an agglomerated structure. Regarding to SEM image, there is no significant difference between the agglomerate structure of diesel and HVO PMs.

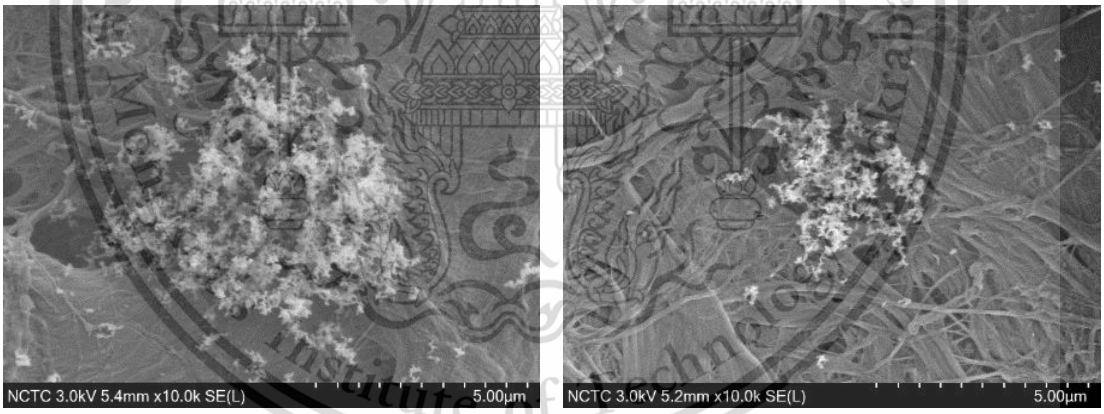

(a) Agglomerate structure of diesel PM (b) Agglomerate structure of HVO PM

Figures 4.12 SEM image of agglomerate structure of (a) diesel PM and (b) HVO PM emitted from 2000 rpm engine full load condition.

4.2.2 Ultrafine agglomerate particles

Morphology of ultrafine agglomerate particles were also analyzed by the aid of TEM image of PM nanoparticles which is derived from 2400 rpm engine full load condition. Single primary particles were combined each other to become an ultrafine agglomerate particle. According to TEM image of ultrafine agglomerate structure of diesel and HVO PMs, single primary particles from both PMs were agglomerated in similar structures.

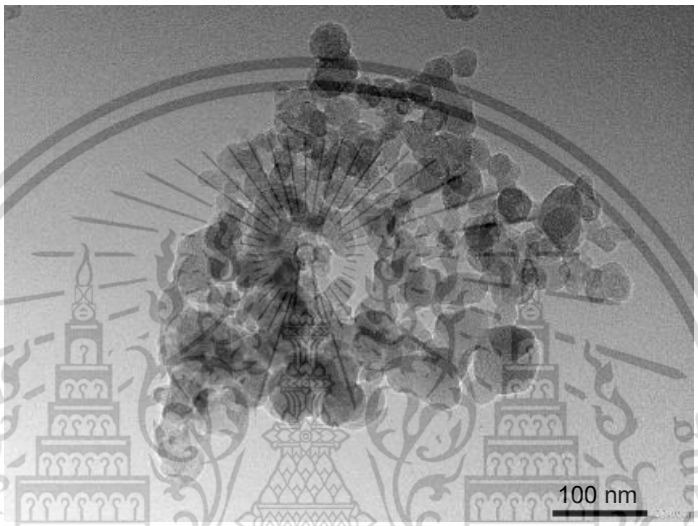

(a) Ultrafine agglomerate structure of diesel PM

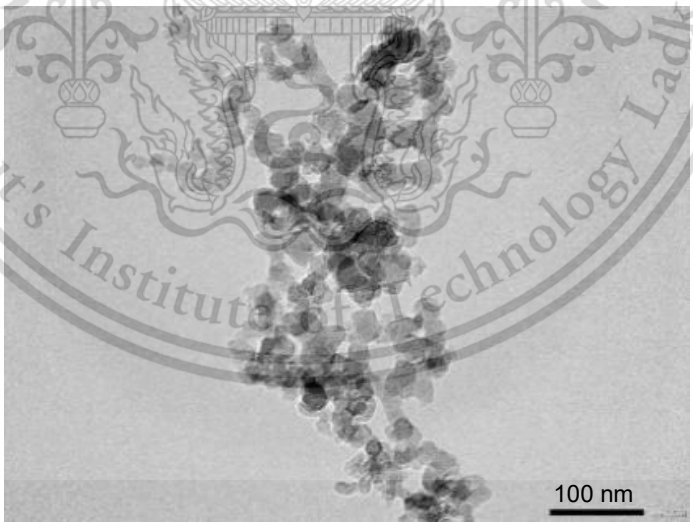

(b) Ultrafine agglomerate structure of HVO PM

Figures 4.13 TEM image of ultrafine agglomerate structure of (a) diesel PM and (b) HVO PM emitted from 2400 rpm engine full load condition.

4.2.3 Nanostructures of single primary particles

Transmission electron microscopy was used to investigate the single primary particle nanostructure of diesel and HVO PMs. PM powders were collected under 2400 rpm engine full load condition. 600k and 800k magnifications were introduced to take the TEM images. A single primary particle nanostructure from both diesel and HVO soot are spherical shapes composed of curve-line crystallites and single primary particles from both PMs are sizing in the range of 10 – 60 nm. Therefore, single primary particle nanostructure of diesel and HVO soot are also physically similar morphologies as shown in figures 4.14.

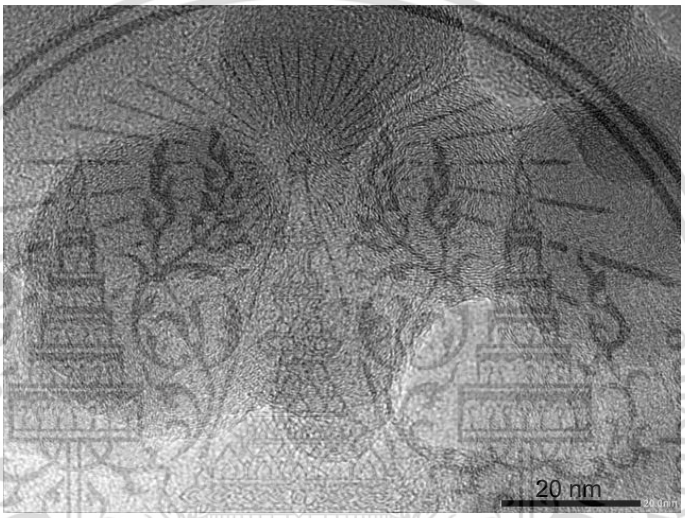

(a) Single primary nanostructure of diesel PM

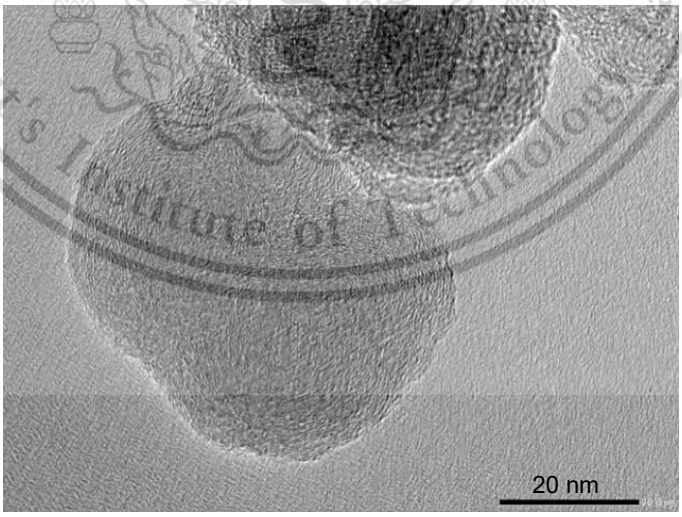

(b) Single primary nanostructure of HVO PM

Figures 4.14 TEM images of single primary nanostructure of (a) diesel PM and (b) HVO PM emitted from 2400 rpm engine full load condition.

4.2.4 Skeletonized nanostructure of particulate matters

As in figures 4.15, transformation of TEM image of soot into skeletonized nanostructure is described to investigate mainly for the carbon fringe lengths and crystallite structures. Image J software was used to achieve the skeletonized patterns. First, TEM image was cropped into 10nm x 10nm image to cover either inner core or outer shell and this cropped image was changed into black and white textures and finally skeletonized structure was transformed. The skeletonized nanostructure of both diesel and HVO soot has similar curve line carbon crystallites.

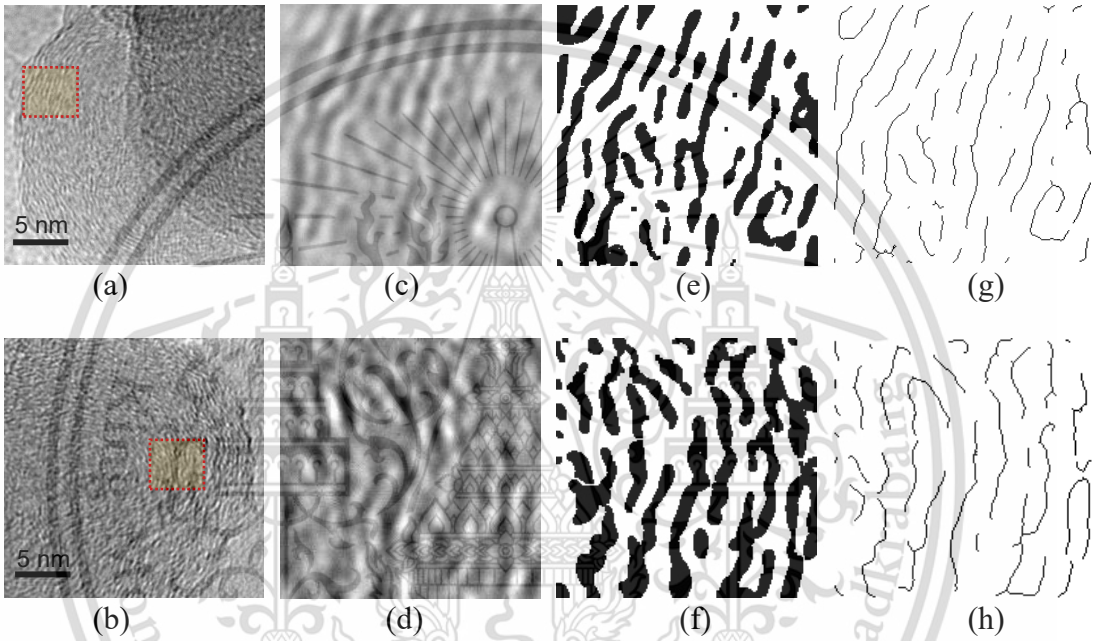

Figures 4.15 TEM images of soot from (a) diesel (b) HVO, (5nm x 5nm) cropped images of soot from (c) diesel (d) HVO, black and white binary images of soot from (e) diesel (f) HVO, skeletonized images of soot from (g) diesel (h) HVO.

4.2.5 Fringe length distribution

Carbon fringe lengths from soot were measured using TEM image by the aid of Image J software. Single primary particle nanostructure of engine's soot can be divided as inner core and outer shell. Inner core has much number of shorter fringe lengths while the outer shell is composed of less number of longer fringe lengths. Carbon fringe lengths were measured upon (3) different zones such as (i) 10nm x 10nm cropped area which covers for both inner core and outer shell (ii) inner core and (iii) outer shell. Measurements has been conducted on (3) different samples for all focused zones. According to 10nm x 10nm cropped area, the average fringe lengths from both diesel and HVO were mostly in the range of 0.3 – 1.8 nm. Besides, the fringe lengths from the inner core were mostly in the range of 0.3 to 1.0 nm while the outer core fringe

lengths were 0.9 to 1.8 nm. Moreover, the average fringe lengths derived from both diesel and HVO soot in all (3) different zones are not significantly different as shown in figures 4.16.

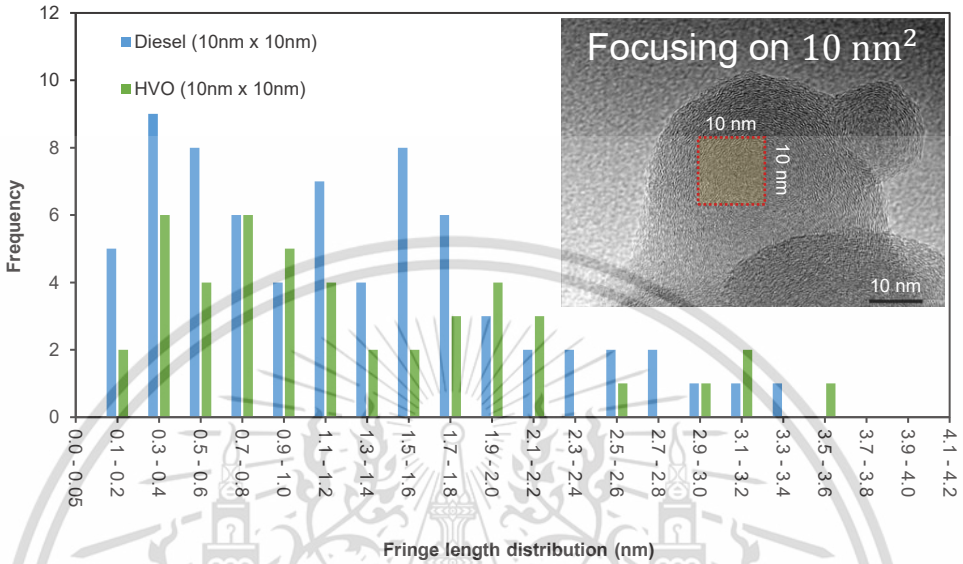

(a) Fringe length distribution in 12nm x 12nm area

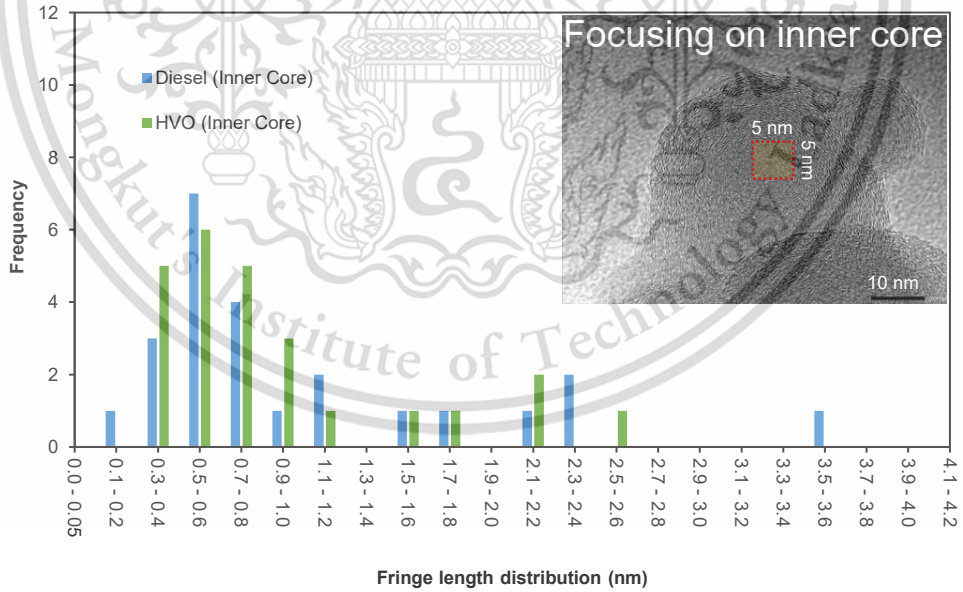

(b) Fringe length distribution at inner core area

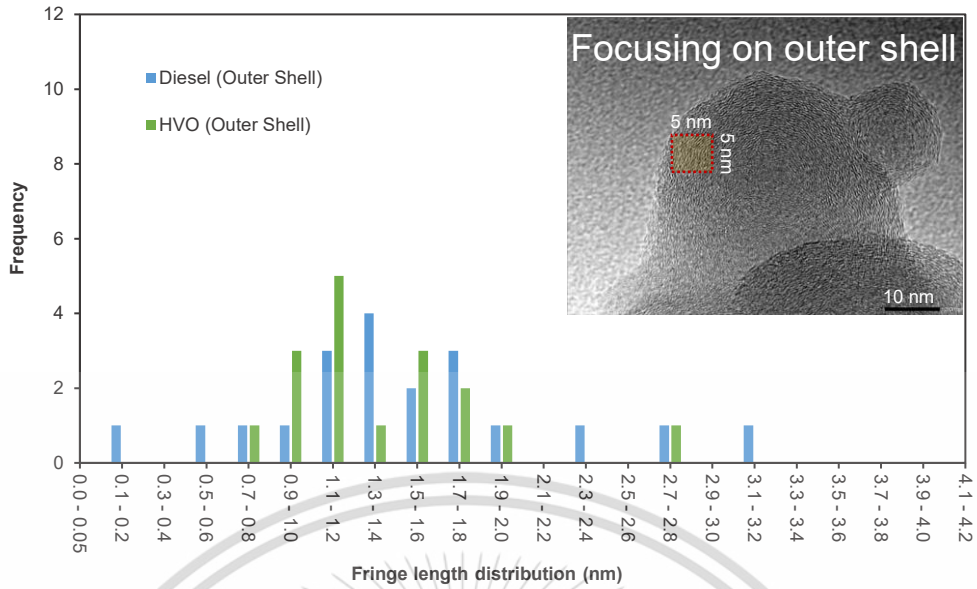

(b) Fringe length distribution at outer shell area

Figures 4.16 Fringe length distribution of (a) 10nm x 10nm(b) inner core (c) outer shell.

4.2.6 Oxidation mass conversion of particulate matters

Isothermal thermogravimetric analysis was conducted to investigate the oxidation kinetics of particulate matters. PM samples were heated with increasing temperature starting from 550°C which is the enough amount of temperature to initiate the soot burning by pure air atmosphere according to previous literatures. Nitrogen gas was used until reaching the operating temperature and operation has been done under pure air atmospheric condition with different temperatures such as 550°C, 575°C, 600°C, 625°C and 650°C. Mass conversion of test sample was recorded for each 0.3 seconds discrepancy. Mass conversion of TGA can be distinguished into (3) sections such as vaporization, carbon oxidation and unburned fraction oxidation. Less than 10% of soluble organic fraction and water vapor are vaporized during increasing temperature with nitrogen atmosphere. When the operating temperature has reached, oxygen was injected, and carbon oxidation is initiated. After all of the combustible carbon is oxidized, a very few fractions of incombustible materials will be oxidized, and the process is terminated. Regarding to TGA mass conversion result, particulate matters derived from HVO fuel combustion were easier to oxidize than diesel PM as described in figure 4.17. Chemical properties of particulate matters are mainly dependent upon the engine operating conditions, fuel properties and types of lubricant. Unlike conventional diesel, HVO fuel has no aromatic since it is a paraffinic fuel with lower

fuel density. Besides, smaller fuel molecules composition of HVO might become the advantages to oxidize faster.

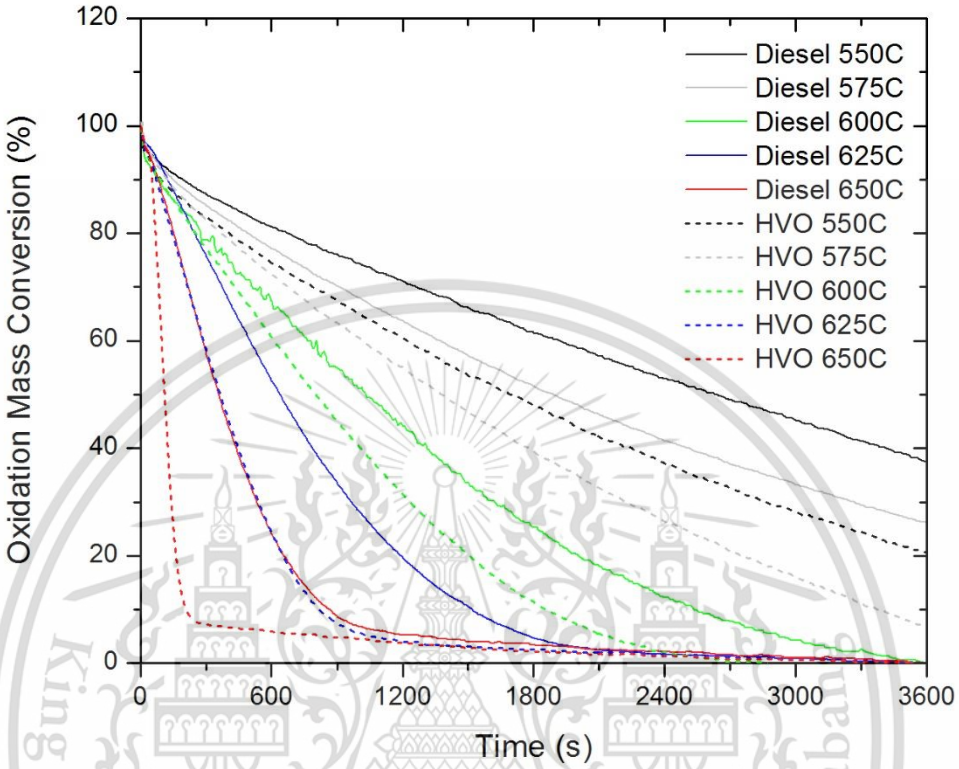

Figure 4.17 Oxidation mass conversion of particulate matters.

4.2.7 Oxidation kinetics and apparent activation energy (E_a)

Higher PM oxidation rates of HVO can be found out due to faster mass conversion as shown in figure 4.18. HVO PM oxidation rate at 650°C is the highest oxidation rate since oxidation rate is directly proportional to temperature according to Arrhenius equation as shown in following equations.

$$PM + O_2 = CO_2 \tag{4.1}$$

$$\frac{-dPM}{dt} = A\, e^{\frac{-E_a}{RT}} [PM]^n [O_2]^m \tag{4.2}$$

$$ln\left[\frac{1}{[PM]^n}\frac{-dPM}{dt}\right] = \frac{-E_a}{R}\left[\frac{1}{T}\right] + ln\, A + mln[O_2] \tag{4.3}$$

Apparent activation energy between the reaction of carbon and oxygen molecules can be estimated by using different temperature oxidation rates which is linearly straight line corelated as in figure 4.19. Regarding to the calculation from Arrhenius equation, faster oxidation kinetics of HVO PMs utilize lower activation energy compared to diesel PM. Calculated activation energies of diesel and HVO PMs were 154.9 kJ/mol and 140.6 kJ/mol respectively.

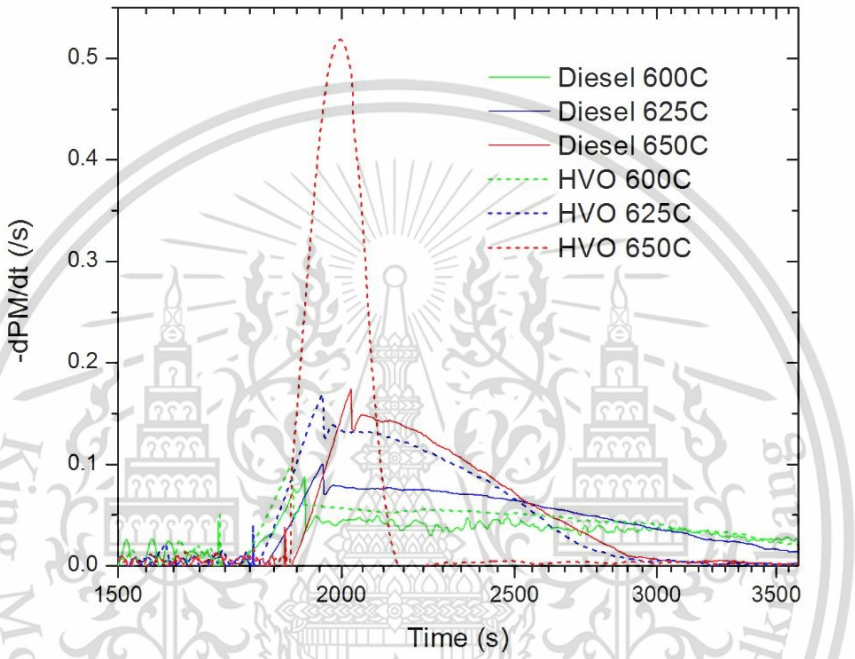

Figure 4.18 Oxidation rate of diesel and HVO PMs.

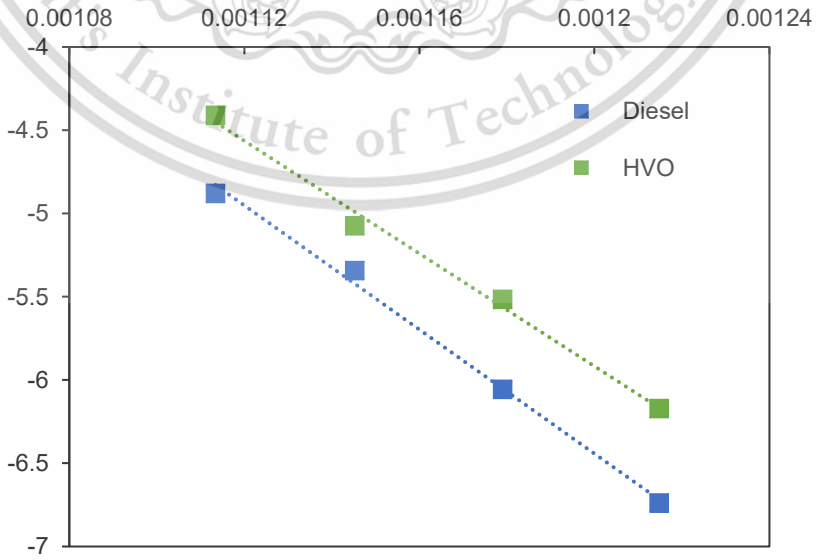

Figure 4.19 Arrhenius plot of PM oxidation rates.

4.3 Impact of Engine Oil's Additives on Particulate Emission

During combustion inside the engine cylinder, lubricants can also participate. Contamination of lubricants can vary the physical and chemical properties of particulate matter. In this study, physicochemical characterization of impact of engine oil's additives on particulate matter formation were investigated by using electron microscopy, electron dispersive x-ray spectroscopy and thermogravimetric analysis

Contamination of engine oil during engine combustion can cause the formation of metal oxide ash among particulate matter composition. These metal oxide ashes cannot be burnt by DPF regeneration process and it reduces effective filtration length of DPF leading to blockage overtime. In this study, a designed lubricating oil containing excess amount of additives were blended 10% by mass directly into the reference fuels (i.e. diesel and HVO). The chemical composition and properties of designed lube oil is shown in Table 4.2. According to lube oil additive composition test (ASTM D5185), composition of sulfur could not be detected for designed lube oil. The purpose of blending excess additive lube oil directly into the fuel is in order to increase the ash formation percentage amongst particulate matter composition since these metal oxide ashes are mainly originated from the unburned engine oil additives.

Table 4.2 Chemical properties of designed lubricating oil.

Test	Test Method	Units	Result
Density @15°C	D4052-15	g/mL	0.896
Density @30°C	D4052-15	g/mL	0.8866
Viscosity @40°C	D445-15a	mm^2/s	154.8
Viscosity @100°C	D445-15a	mm^2/s	15.05
Viscosity index	D2270	-	97
Calcium	D5185	PPM	1942
Phosphorous	D5185	PPM	757
Zinc	D5185	PPM	846
Silicon	D5185	PPM	5.6

4.3.1 Agglomerate structure of particulate matter

Scanning electron microscopy (SEM) was used to investigate the agglomerate structure of particulate matters in micro- scales as shown in figures 4.19. Figure (a) describes the agglomerate microstructure of particulate matter from diesel condition and figure (b) shows the agglomerate microstructure of particulate matter derived from diesel blending lube oil condition respectively. According to the SEM images, the agglomerate structure of lubricant oil related particles has not shown significant different in micro- scales. In other words, the agglomerate structure of lubricant oil related particles was similar to agglomerate structure of diesel PM.

(a) Agglomerate structure of diesel PM

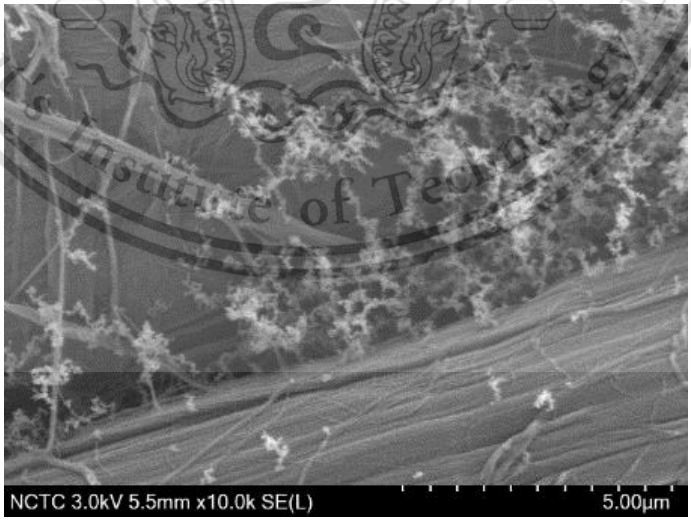

(b) Agglomerate structure of diesel blending lube oil PM

Figures 4.19 SEM image of agglomerate structure of (a) diesel PM and (b) diesel blending lube oil PM emitted from 2000 rpm engine full load condition.

4.3.2 Ultrafine agglomerate structure of particulate matter

Transmission Electron Microscopy (TEM) images were used to determine the ultrafine agglomerate primary particle nanostructures as shown in figures 4.20. Soot powders were collected under 2400 rpm engine full load condition since this engine condition is suitable to generate the soot efficiently according to previous smoke intensity results. TEM images showed that the agglomerate structure of ultrafine particles from diesel blending lube oil condition were not significant different compared to neat diesel engine's ultrafine particles.

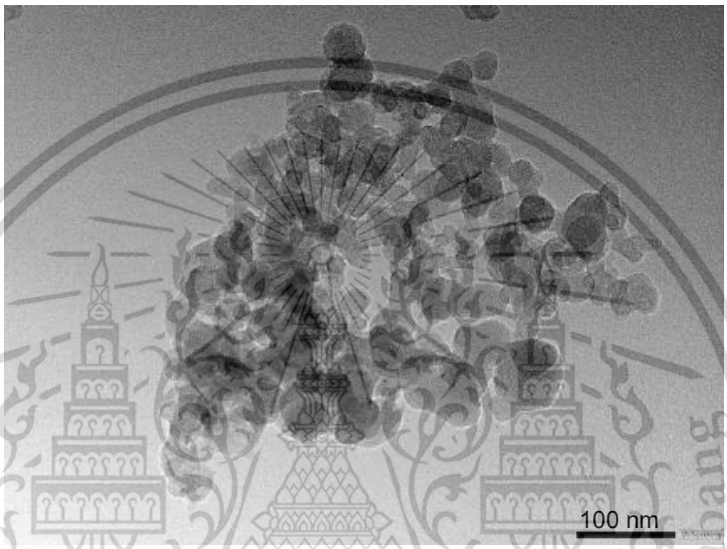

(a) Ultrafine agglomerate structure of diesel PM

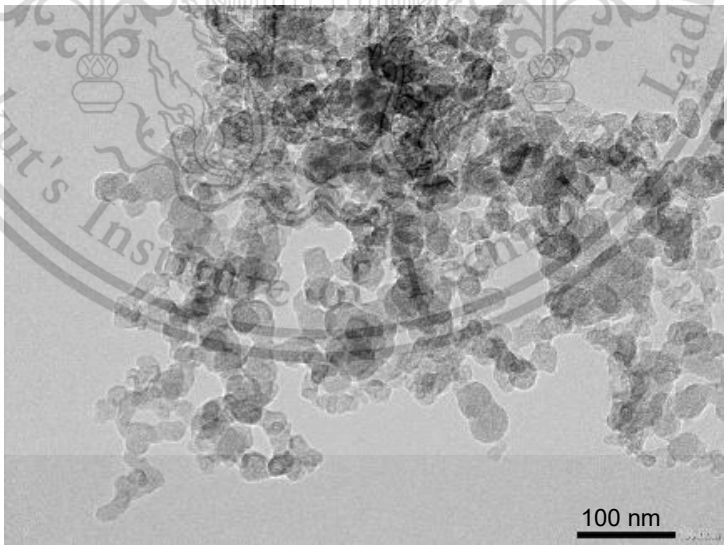

(b) Ultrafine agglomerate structure of diesel blending lube oil PM

Figures 4.20 TEM images of ultrafine agglomerate structure of (a) diesel PM and (b) diesel blending lube oil PM emitted from 2400 rpm engine full load condition.

4.3.3 Single primary particle nanostructures of fuel blending lube oil PMs

As described in figures 4.21, nanostructure of diesel blending lube oil PM in figure (a) and HVO blending lube oil PM in figure (b) were analyzed using TEM images. Particles from both fuel blending lube oil conditions were combined together with soot and metal oxide ash. These metal oxide ashes are mainly derived from engine oil additives. Nanostructure of metal oxide ashes were composed of lattice fringes showing parallel straight-line hatch patterns.

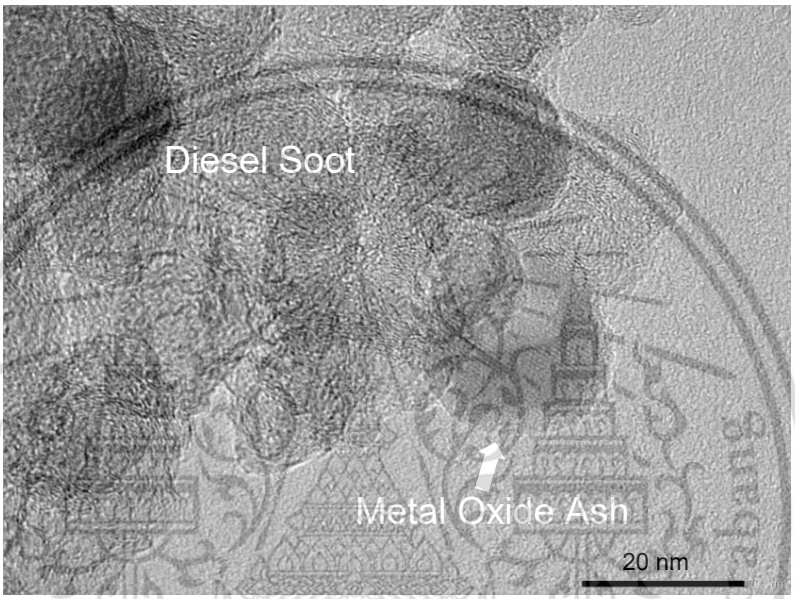

(a) Single primary nanostructure of diesel blending lube oil PM

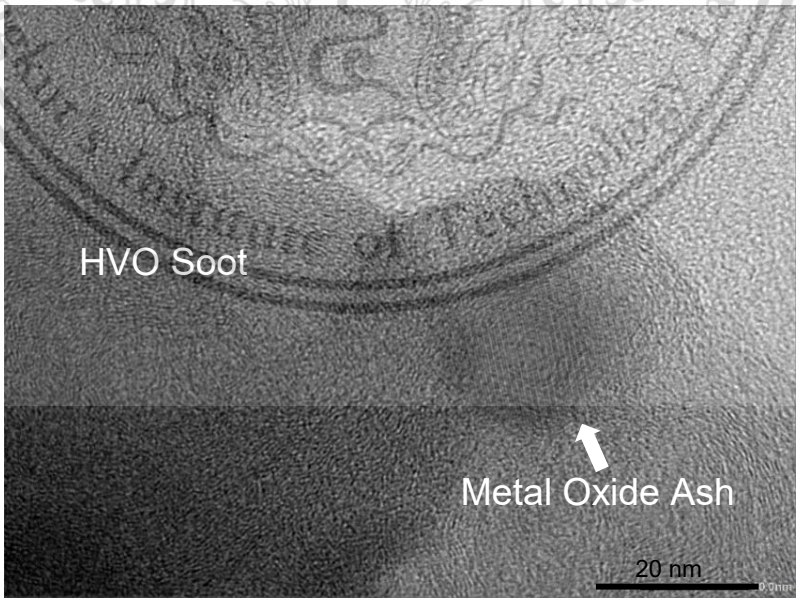

(b) Single primary nanostructure of HVO blending lube oil PM

Figures 4.21 TEM images of single primary nanostructure of metal oxide ash from (a) diesel blending lube oil PM and (b) HVO blending lube oil PM.

4.3.4 Skeletonized nanostructures of metal oxide ashes

To investigate the skeletonized nanostructures of metal oxide ash derived from diesel blending lube oil conditions and HVO blending lube oil conditions, ImageJ software was applied to transform the TEM images into skeletonized images. Firstly, (25nm x 25nm) TEM image was cropped into (5nm x 5nm) image. Secondly, (5nm x 5nm) image was transformed into black and white binary images by removing some outliers. Finally, black and white binary image was transformed into skeletonized image. The consequent transformation steps from TEM image to skeletonized images were briefly described in figures 4.22. According to the skeletonized images, primary particle's skeletonized nanostructure of ashes from both fuel blending lube oil PMs were composed of parallel straight-line lattice fringes.

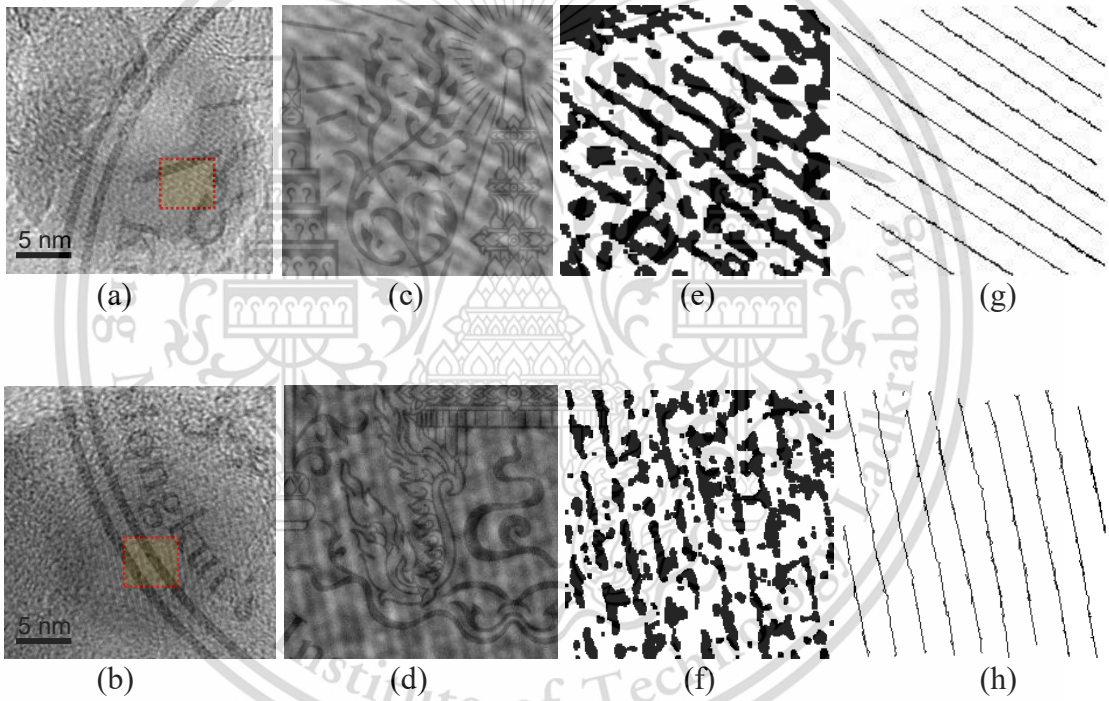

Figures 4.22 TEM images of metal oxide ash from (a) diesel-L (b) HVO-L, (5nm x 5nm) cropped images of metal oxide ash from (c) diesel-L (d) HVO-L, black and white binary images of metal oxide ash from (e) diesel-L (f) HVO-L, skeletonized images of metal oxide ash from (g) diesel-L and (h) HVO-L.

4.3.5 Chemical composition of diesel blending lube oil PMs

SEM-EDS analysis determined the chemical composition of PM from both blending and without blending lubricant oil condition as shown in figures 4.23 a and b. Results showed that diesel PM mainly contains elemental composition of Carbon (C) from soot which is unburned hydrocarbon (HC) derived from engine combustion. However, SEM-EDS result of diesel blending lubricant oil condition showed not only Carbon (C) but also additional metallic elements such as Calcium (Ca), Phosphorous (P), Magnesium (Mg), Silicon (Si) and Zinc (Zn) which all are originated from engine lubricant additives. Therefore, SEM-EDS result pointed out that metallic additives from engine lubricating oil cannot be burned during engine combustion.

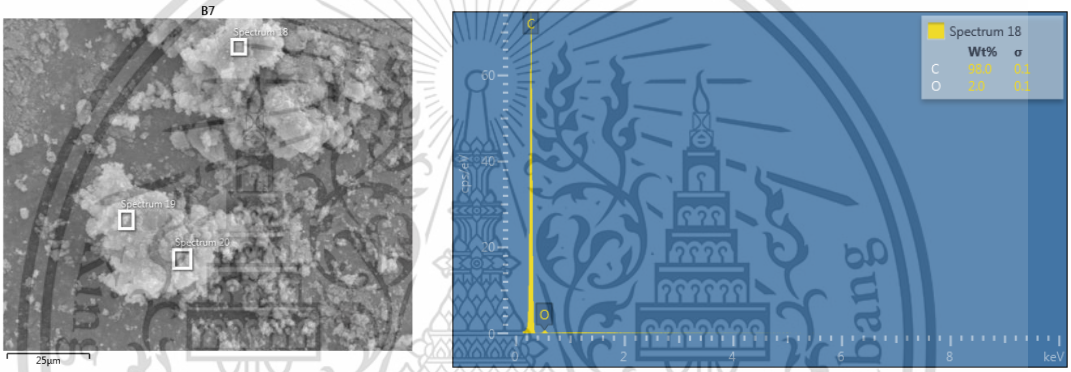

(a) Chemical composition of diesel PM

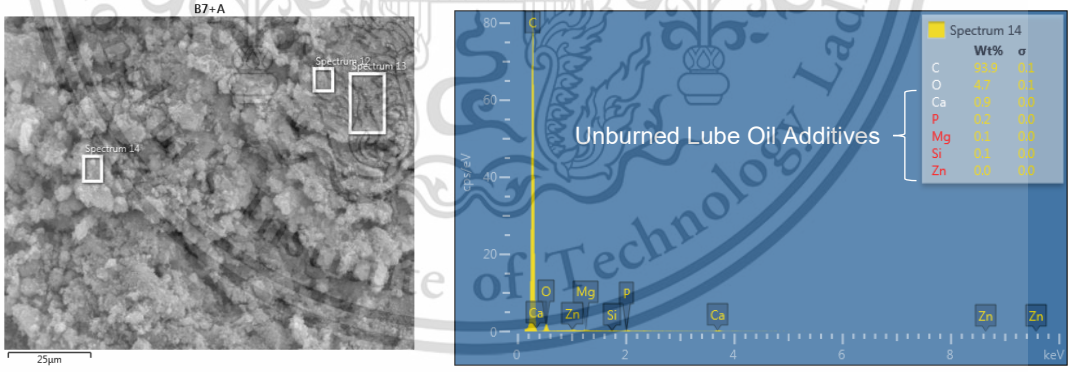

(b) Chemical composition of diesel blending lube oil PM

Figures 4.23 SEM-EDS analysis of chemical composition analysis of (a) diesel PM and (b) diesel blending lube oil PM emitted from 2000 rpm engine full load condition.

4.3.6 Elemental composition of diesel blending lube oil PMs

The elemental composition of particulate matters from diesel condition and diesel blending lube oil condition were analyzed using electron dispersive x-ray spectroscopy (TEM – EDS). Regarding to the qualitive analysis of EDS, the electron beam is exerted onto the particles and determined the elements according to x-ray energies. PM nanoparticles from diesel blending lube oil condition as in figure 4.24 (b) contain not only carbon but also unburned metallic additive elements which all are derived from engine oil additives and confirmed as an identity with previous SEM-EDS analysis. Quantitative TEM-EDS analysis results are summarized in table 4.3.

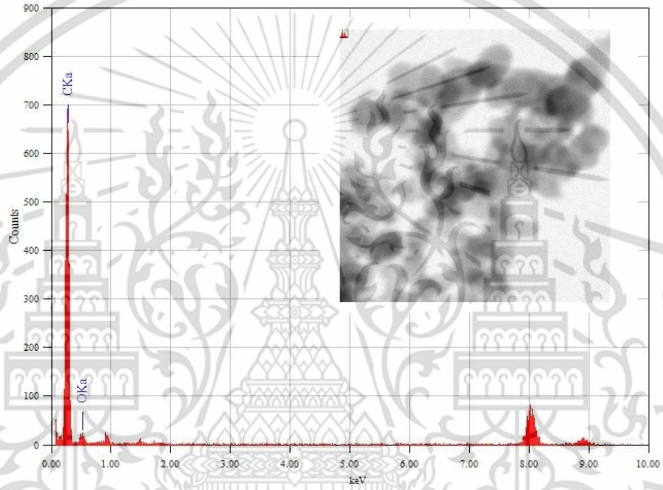

(a) Elemental analysis of diesel PM

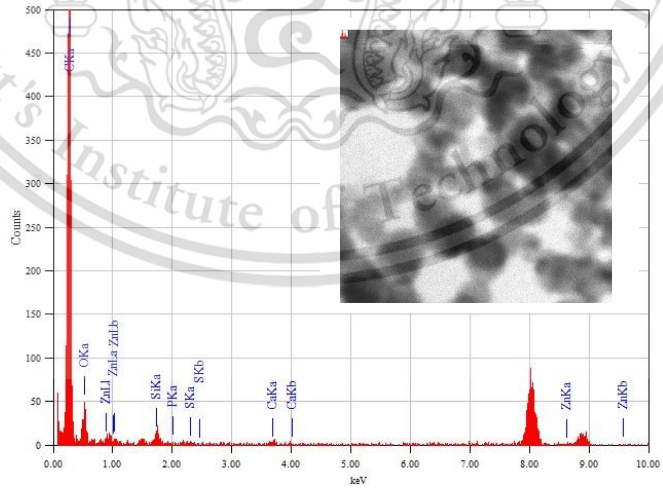

(b) Elemental analysis of diesel blending lube oil PM

Figures 4.24 Qualitative TEM-EDS spectrums of elemental analysis of (a) diesel PM and (b) diesel blending lube oil PM.

Table 4.3 Quantitative analysis of PM nanoparticles.

Element	(keV)	Composition (%)	
		Diesel PM	Diesel-L PM
C	0.277	99.208	97.243
O	0.525	0.792	1.386
Si	1.739	-	1.32
P	2.013	-	0.001
S	2.307	-	0.021
Ca	3.690	-	0.036
Zn	8.630	-	0.003

4.3.7 Elemental analysis of metal oxide ash

Either qualitative or quantitative elemental analysis of metal oxide ash has been conducted to determine the composition by using TEM-EDS as shown in figure 4.25. A single primary ash particle was exerted by electron beam as a focused point and investigated the elemental components. The intensity of electron beam was within (0 – 40) keV which is sufficient to analyze all of the elements containing in the sample. 600k magnification was used to focus only on the single primary particle of ash. TEM-EDS qualitative result showed that ash is composed of metallic components coordination with higher composition of oxygen to become metal oxide ash.

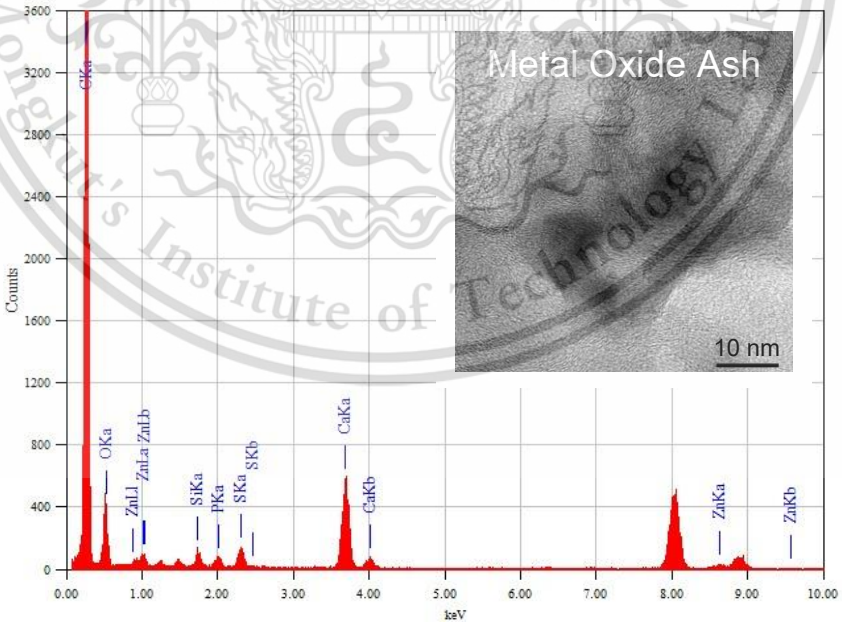

Figure 4.25 Qualitative analysis of metal oxide ash.

Among metallic composition, highest number of Calcium (Ca) was found out since the designed blending lubricant consists of excess amount of Ca additives. Therefore, these metal oxide ashes found out in this research can be regarded as plenty of Calcium Oxide (CaO) ashes.

4.3.8 Oxidation mass conversion of fuel blending lube oil PMs

In order to investigate the contamination of metal oxide ash on soot oxidation kinetics, thermogravimetric analysis was introduced using pure air atmospheric condition. Isothermal method was used under (3) different temperatures such as 550°C, 575°C and 625°C as shown in figure 4.26. Nitrogen gas was used to reach the operating temperature and oxidation process was started by injecting oxygen gas. Starting from oxidation, mass conversion data were recorded for each 0.3 seconds.

Particulate matters from diesel blending lube oil condition have faster oxidation kinetics compared to pure diesel PMs as shown in figure 4.26. Furthermore, particulate matters from HVO blending lube oil condition (HVO-L) were easier to oxidize than diesel blending lube oil PMs as described in figure 4.27 since pure HVO PMs were also faster carbon mass conversion than pure diesel PMs that have discussed in article 4.2.6.

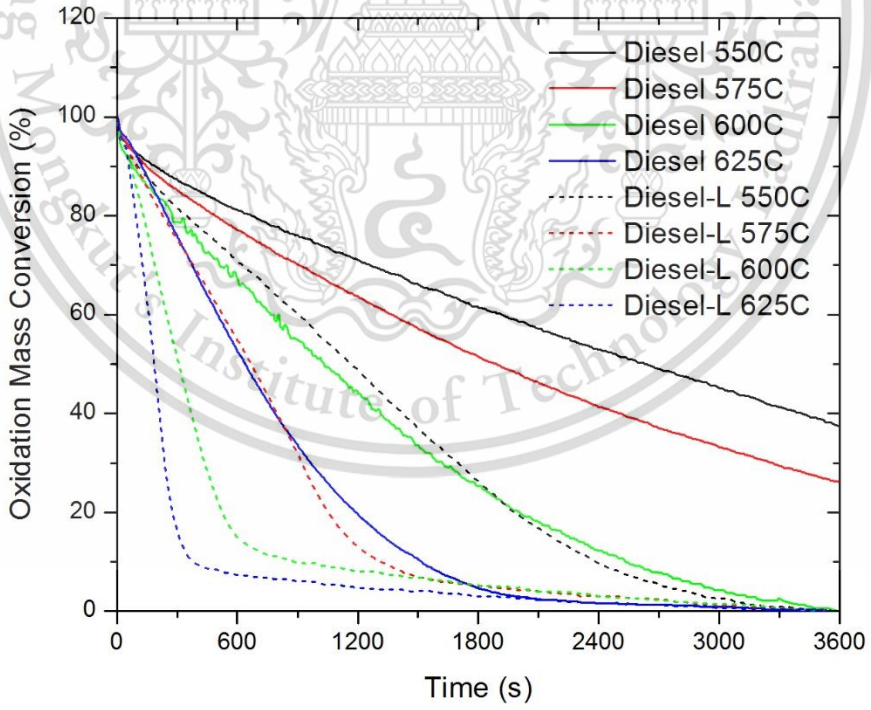

Figure 4.26 Oxidation mass conversion of particulate matter.

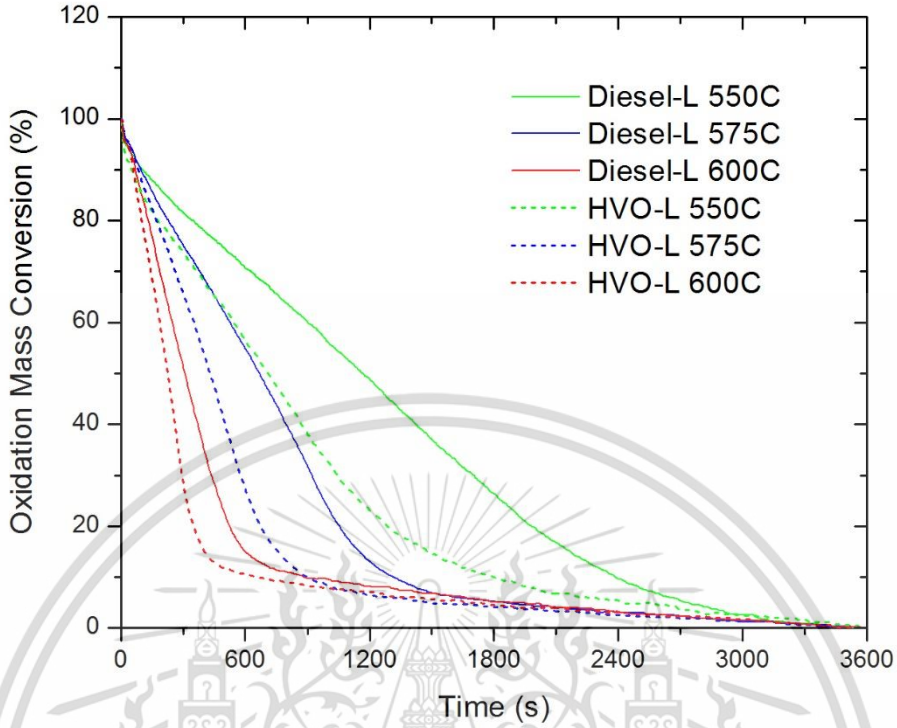

Figure 4.27 Oxidation mass conversion of particulate matter.

4.3.9 Oxidation kinetics and apparent activation energy

As shown in figure 4.28, HVO blending lube oil PMs have higher oxidation rate compared to diesel blending lube oil PMs. Arrhenius plot for both fuel blending lube oil PMs were plotted in figure 4.29. Activation energy of diesel blending lube oil PMs and HVO blending lube oil PMs were 134.1 kJ/mol and 121.8 kJ/mol respectively.

As a summary, influence of metal oxide ash contamination on soot showed prominent faster oxidation kinetics in both diesel and HVO blending lube oil conditions due to presence of ashes acting as catalyst on soot oxidation kinetics. Among four different conditions of (diesel, HVO, diesel-L and HVO-L) PM, fastest mass conversion rate can be found out in HVO blending lube oil condition with lowest activation energy.

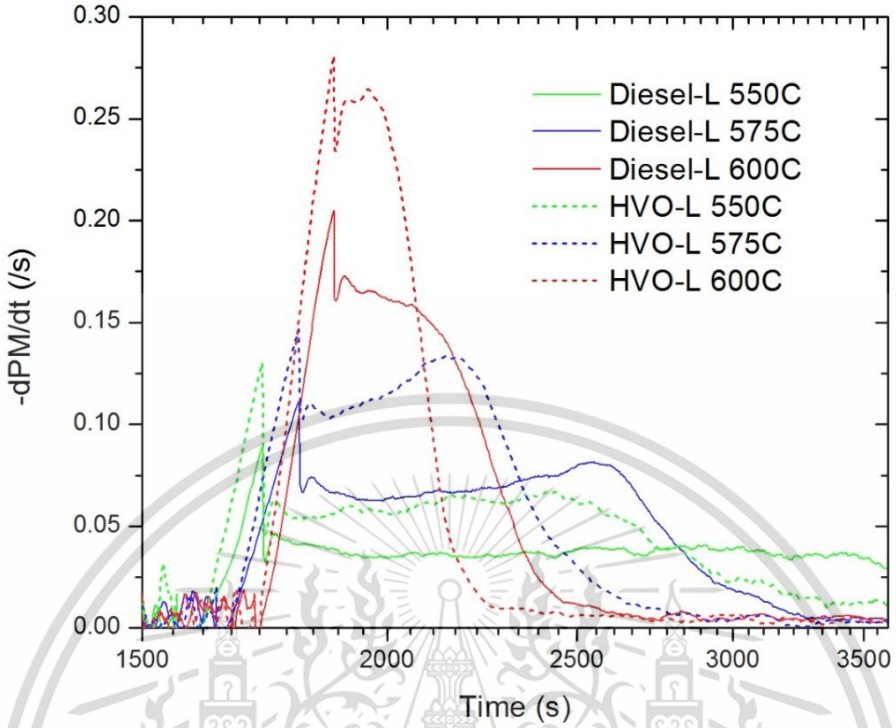

Figure 4.28 Oxidation rate of diesel-L and HVO-L PMs.

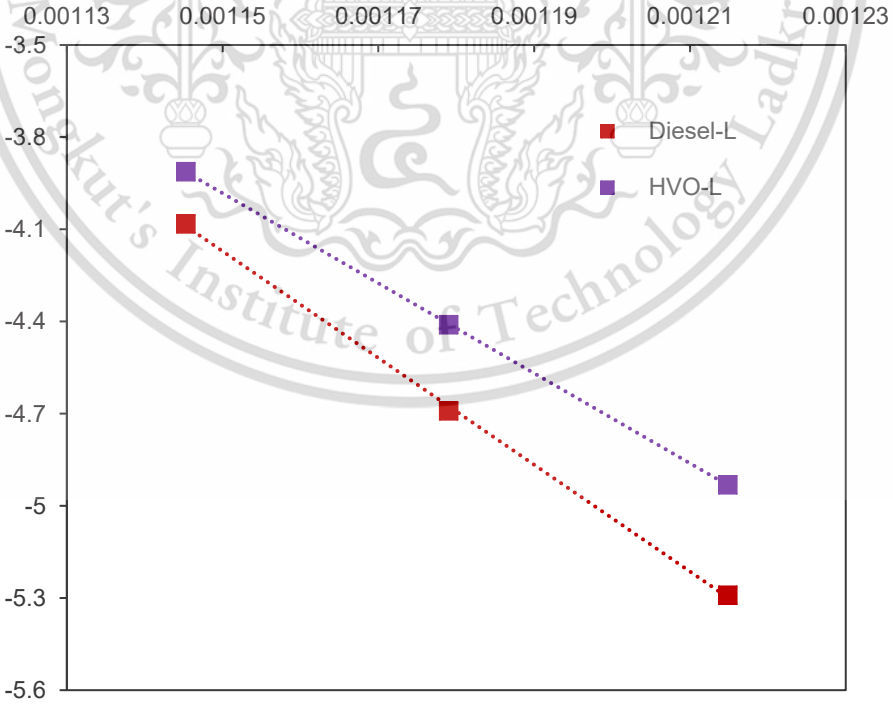

Figure 4.29 Arrhenius plot of Diesel-L and HVO-L PMs.

CHAPTER 5

CONCLUSIONS AND DISCUSSION

5.1 Combustion Characteristics of Hydrotreated Vegetable Oil

In this research, combustion characteristics of Hydrotreated Vegetable Oil (HVO) fuel such as combustion pressure, brake specific fuel consumption, engine performance, heat release rates and thermal efficiency have been investigated by comparing with conventional diesel.

HVO fuel has higher cetane index and lower fuel density than diesel. Combustion pressure of HVO fuel is slightly higher and it delivers lower torque. However, less fuel consumption and better fuel atomization of HVO can be regarded as great advantages that might lead to higher thermal efficiency. Besides, a synthetic paraffinic fuel containing no aromatics with higher cetane index of HVO delivered more complete combustion with less soot contamination.

5.2 Particulate Emission of HVO Fuel Combustion

Electron microscopy image analysis was used to investigate the physical morphology of particulate matters by capturing agglomerate structure of PM in micro-scales and ultrafine agglomerate structure in nano- scales. Single primary particles from both PMs were spherical shape sizing in the range of 10 – 60 nm and these are composed of curve line crystallites. Fringe length distribution within three different zones were measured and the results showed similar fringe lengths between diesel and HVO PMs. The inner core is made up of large number of shorter fringe lengths (ranging between 0.3 to 1.0 nm) while the outer shell has less number of longer fringe lengths (ranging between 0.9 to 1.8 nm).

According to isothermal thermogravimetric analysis under pure air atmospheric condition, particulate matters emitted from HVO fuel combustion were easier to oxidize than diesel PMs and the apparent activation energies for diesel and HVO PMs were 154.9 kJ/mol and 140.6 kJ/mol respectively.

5.3 Impact of Engine Oil Additives on Particulate Emission

To investigate the impact of contamination of engine oil's additives on particulate matter, physicochemical characterization has been conducted by using electron microscopy, electron dispersive x-ray spectroscopy and thermogravimetric analysis.

According to electron microscopy, morphology of agglomerate structure in micro- scales and ultrafine agglomerate structure in nano- scales were not significantly different between diesel PMs and diesel blending lube oil PMs. However, the single primary particle nanostructure from both diesel and HVO PMs were spherical shapes composed of curve line crystallites (carbon fringes). Regarding to the TEM images of diesel blending lube oil PMs and HVO blending lube oil PMs, metal oxide ashes were combined together with soot. Unlike soot, single primary particle nanostructure of metal oxide ashes were composed of lattice fringes showing parallel straight-lined hatch patterns as described in figures 5.1 (c and d).

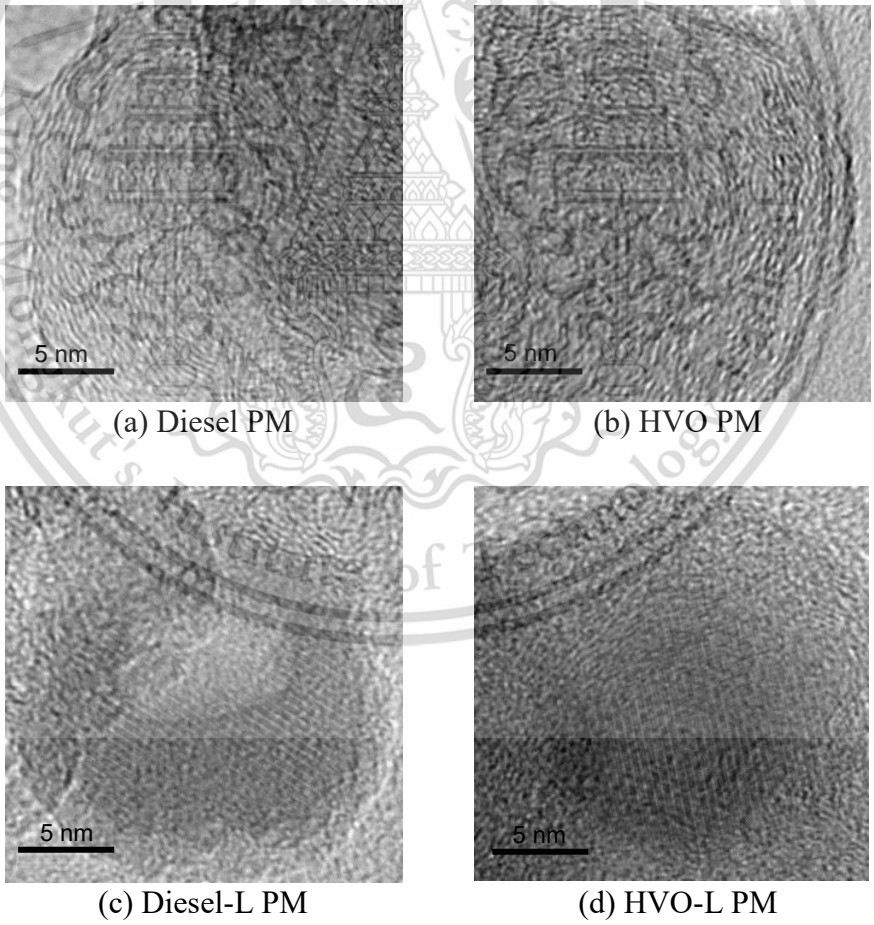

(a) Diesel PM (b) HVO PM

(c) Diesel-L PM (d) HVO-L PM

Figures 5.1 TEM images of nanostructures of soot from (a) diesel PM (b) HVO PM, nanostructure of metal oxide ashes from (c) diesel blending lube oil condition and (d) HVO blending lube oil condition.

Chemical composition analysis of SEM-EDS and TEM-EDS pointed out that metallic additives from lubricating oil cannot be burnt by engine combustion. Qualitative and quantitative elemental analysis also confirmed that these metal oxide ashes were contained unburned metallic composition and higher composition of oxygen to become metal oxide ash.

Regarding to investigate the influence of metal oxide ash contamination on soot oxidation, isothermal thermogravimetric analysis was conducted using pure air atmospheric condition for all of four different PMs (diesel PM, HVO PM, diesel blending lube oil PM and HVO blending lube oil PM). Results showed that particulate matters derived from blending lube oil condition has higher oxidation kinetics than pure diesel and HVO PMs. In fact, the contamination of metal oxide ashes might promote soot oxidation rate acting as catalysts on soot oxidation kinetics. By following Arrhenius equation, a reaction which has faster oxidation rate needs lower activation energy. The faster oxidation kinetics and lower activation energy of diesel and HVO blending lube oil PMs were found out due to the impact of metal oxide ash acting as catalyst on soot oxidation kinetics.

REFERENCES

[1] Eastwood, P. (2008). Particle Emission from Vehicles. John Wiley & Sons, Ltd, England.

[2] Dec, J. (1997). A Conceptual Model of DI Diesel Combustion Based on Laser-Sheet Imaging. SAE Technical Paper 970873.

[3] Tree, D. (2007). Soot Process in Compression Ignition Engines. Progress in Energy and Combustion Science 33 pp. 272-309.

[4] Srivastava, D. (2011). Effect of Engine Load on Size and Number Distribution of Particulate Matter Emitted from a Direct Injection Compression Ignition Engine. Aerosol and Air Quality Research 11 pp. 915-920.

[5] Virtanen, A. (2004). Effect of Engine Load on Diesel Soot Particles. Environmental Science & Technology 38 pp. 2551-2556.

[6] Man, X. (2015). Effect of Diesel Engine Operating Conditions on the Particulate Size, Nanostructure and Oxidation Properties When using Wasting Cooking Oil Biodiesel. Energy Procedia 66 pp. 37-40.

[7] Boonsakda, J. (2016). Effect of Palm Methyl Ester Blends Diesel on Small CI Engine Particulate Matter Quantity and Nanostructure. The 7th TSME International Conference on Mechanical Engineering. AEC0018.

[8] Karin, P. (2017). Morphology and Oxidation Kinetics of CI Engine's Biodiesel Particulate Matters on Cordierite Diesel Particulate Filters using TGA. International Journal of Automotive Technology 18 pp. 31-40.

[9] Karin, P. (2015). Oxidation Kinetics of Small CI Engine's Biodiesel Particulate Matter. International Journal of Automotive Technology 16(2) pp, 211-219

[10] Mohankumar, S. (2017). Particulate Matter Formation and Its Control Methodologies for Diesel Engine: A Comprehensive Review. Renewable and Sustainable Energy Reviews 80 pp. 1227-1238.

[11] Mortier, R. (1992). Chemistry and Technology of Lubricants. Springer Science & Business Media, New York.

[12] Burrington, J. (2007). Challenges in Detergents and Dispersants for Engine Oils. https://www.researchgate.net/publication/225244054.

[13] Wang, Y. (2016). Impact of Lubricating Oil Combustion on Nanostructure, Composition and Graphitization of Diesel Particles. Fuel 190 pp. 237-244.

[14] Dong, L. (2015). Comparative Study on Particles Formation in a Diesel Engine When Lubricating Oil Involved in Fuel Combustion. Journal of Chemistry 839879.

[15] Karin, P. (2012). Nanostructures and Oxidation Kinetics of Diesel Particulate Matters. Journal of Research and Applications in Mechanical Engineering 1 pp. 3-7.

[16] Wang, Y. (2015). Effects of an Anti-wear Oil Additive on the Size Distribution, Morphology, and Nanostructure of Diesel Exhaust Particles. Tribology International 92 pp. 379-386.

[17] Jung, H. (2005). The Influence of a Cerium Additive on Ultrafine Diesel Particle Emissions and Kinetics of Oxidation. Combustion and Flame 142 pp. 276-288.

[18] Bagi, S. (2016). Investigation into Ash from Field Returned DPF Units: Composition, Distribution, Cleaning Ability and DPF Performance Recovery. SAE Technical Paper 2016-01-0928.

[19] Liati, A. (2012). Investigation of Diesel Ash Particulate Matter: A Scanning Electron Microscope and Transmission Electron Microscope Study. Atmospheric Environment 49 pp. 391-402.

[20] Bolis, V. (2013). Fundamentals in Adsorption at the Solid-Gas Interface. Concepts and Thermodynamics. Springer Series in Materials Science 154.

[21] Henrich, V. (1999). Metal Oxide Surfaces and Their Interaction with Aqueous Solutions and Microbial Organisms. US Department of Energy Publications 1-1-1999.

[22] Neeft, J. (1996). Metal Oxides as Catalysts for the Oxidation of Soot. The Chemical Engineering Journal 64 pp. 295-302.

[23] Arora, A. (2016). Metal/Mixed Metal Oxides and Their Applications as Adsorbents. International Journal of Science 14 pp. 3215-3227.

[24] Iwamoto, M. (1978). Oxygen on Oxides. Journal of Physics and Chemistry 82 2564.

[25] Davies, P. (2016). Thin Oxide Films. Science and Technology 2001 pp. 6601-6605.

[26] Diebold, U. (2002). The Surface Science of Titanium dioxide. Surface Science Reports 48 pp. 53-229.

[27] Pacchioni, G. (2017). Increasing Oxide Reducibility: The Role of Metal/Oxide Interfaces in the Formation of Oxygen Vacancies. American Chemical Society Catalysis 2017 pp. 6493-6513.

[28] Uchisawa, J. et al. (2015). Soot Oxidation in Particulate Filter Regeneration. Handbook of Advanced Methods and Process in Oxidation Catalysts. pp. 25 – 50.

APPENDIX A :

BLENDING LUBE OIL TEST REPORTS

BANGCHAK CORPORATION PUBLIC COMPANY LIMITED

Head Office : 2098 M Tower Building, 8th Floor, Sukhumvit Road, Bangchak, Phrakanong, Bangkok 10260 Thailand
Lubricant Supply Chain and Technical Marketing Division Tel : 66 (0) 2335 4537, 66 (0) 2335 4527

CERTIFICATE OF ANALYSIS

PRODUCT : Engine Oil API CD/SF SAE 40 (BCP 1060 4.4%)

LOT NO. : -

PRODUCT SOURCE : SB

CONTROL TEST	UNIT	METHOD	SPEC	RESULT
APPEARANCE	-	VISUAL	B&C	B&C
COLOUR (ASTM)	-	ASTM D1500	REPORT	L 2.0
DENSITY @ 15 °C	g/mL	ASTM D4052-15	REPORT	0.8960
DENSITY @ 30 °C	g/mL	ASTM D4052-15	REPORT	0.8866
FLASH POINT (COC)	°C	ASTM D92-12b	230 MIN.	248
FOAM TENDENCY (Sequence I)	ml	ASTM D892	25/0 MAX.	NIL/0
FOAM TENDENCY (Sequence II)	ml	ASTM D892	50/0 MAX.	10/0
FOAM TENDENCY (Sequence III)	ml	ASTM D892	25/0 MAX.	NIL/0
COPPER STRIP CORROSION	-	ASTM D130	1B MAX.	1A
MAGNESIUM (Mg)	% wt	ASTM D6481	0.170-0.208	0.1816
ZINC (Zn)	% wt	ASTM D6481	0.070-0.086	0.0798
PHOSPHORUS (P)	%wt	ASTM D6481	0.077-0.095	0.0856
POUR POINT	°C	ASTM D 6749-02 (Reapp. 2012)	-6 MAX.	-9
TOTAL BASE NUMBER	mgKOH/g	ASTM D2896(B)-11	4.9 MIN.	5.8
VISCOSITY @ 40 °C	cSt	ASTM D445-15a	REPORT	154.8
VISCOSITY @ 100 °C	cSt	ASTM D445-15a	14.50-15.50	15.05
VISCOSITY INDEX	-	ASTM D2270	95 MIN.	97
WATER CONTENT	% Vol	ASTM D95	NIL	NIL

Remark :

Reported Results refer to the submitted sample only.

This report shall not be advertising and reproduced, except in full, without the written permission from the Lubricant Supply Chain and Technical Marketing Division.

Approve By :

Miss Panita Klintong

Chemist

Date of Issue : 16/5/2018

A-1: Designed lube oil test report by Bangchak Corporation BCP

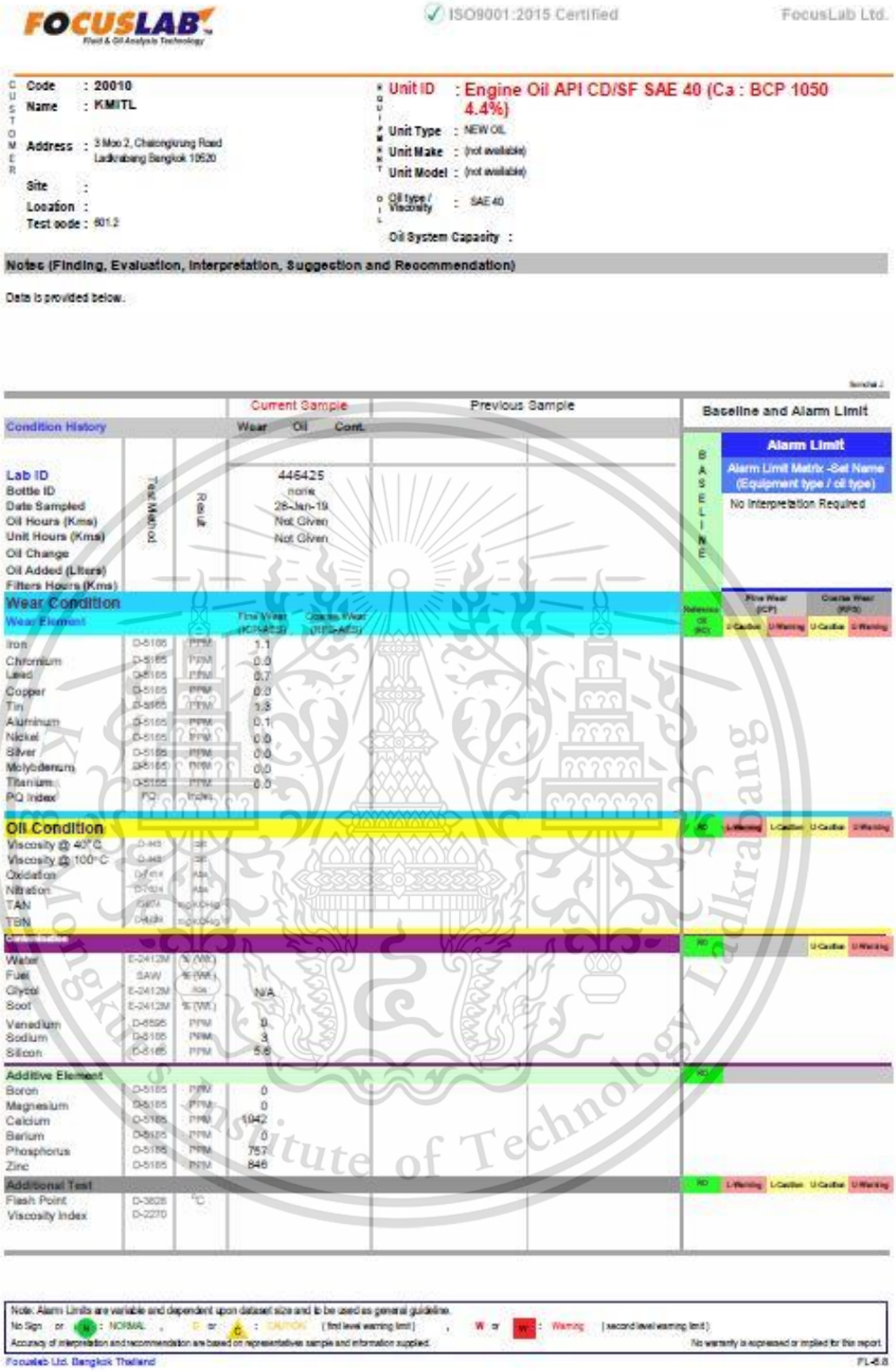

FOCUSLAB Fluid & Oil Analysis Technology

ISO9001:2015 Certified — FocusLab Ltd.

CUSTOMER
Code : 20010
Name : KMITL
Address : 3 Moo 2, Chalongkrung Road Ladkrabang Bangkok 10520
Site :
Location :
Test code : 601.2

EQUIPMENT
Unit ID : Engine Oil API CD/SF SAE 40 (Ca : BCP 1050 4.4%)
Unit Type : NEW OIL
Unit Make : (not available)
Unit Model : (not available)

OIL
Oil type / Viscosity : SAE 40
Oil System Capacity :

Notes (Finding, Evaluation, Interpretation, Suggestion and Recommendation)

Data is provided below.

Condition History	Test Method	Result	Current Sample Wear Oil Cont.	Previous Sample	Baseline and Alarm Limit
Lab ID			446425		Alarm Limit
Bottle ID			none		Alarm Limit Matrix -Set Name (Equipment type / oil type)
Date Sampled			28-Jan-19		No Interpretation Required
Oil Hours (Kms)			Not Given		
Unit Hours (Kms)			Not Given		
Oil Change					
Oil Added (Liters)					
Filters Hours (Kms)					
Wear Condition					
Wear Element			Fine Wear (ICP-AES) / Coarse Wear (RDE-AES)		Reference Oil (RO) / Fine Wear (ICP) L-Caution / L-Warning / Coarse Wear (RPS) U-Caution / U-Warning
Iron	D-5185	PPM	1.1		
Chromium	D-5185	PPM	0.0		
Lead	D-5185	PPM	0.7		
Copper	D-5185	PPM	0.0		
Tin	D-5185	PPM	1.3		
Aluminum	D-5185	PPM	0.1		
Nickel	D-5185	PPM	0.0		
Silver	D-5185	PPM	0.0		
Molybdenum	D-5185	PPM	0.0		
Titanium	D-5185	PPM	0.0		
PQ Index	PQ	Index			
Oil Condition					RO / L-Warning / L-Caution / U-Caution / U-Warning
Viscosity @ 40°C	D-445	cSt			
Viscosity @ 100°C	D-445	cSt			
Oxidation	D-7624	Abs			
Nitration	D-7624	Abs			
TAN	D974	mgKOH/g			
TBN	D4739	mgKOH/g			
Contamination					RO / U-Caution / U-Warning
Water	D-2412M	% (Wt.)			
Fuel	SAW	% (Wt.)			
Glycol	D-2412M	Abs	N/A		
Soot	D-2412M	% (Wt.)			
Vanadium	D-5185	PPM	0		
Sodium	D-5185	PPM	3		
Silicon	D-5185	PPM	5.6		
Additive Element					RO
Boron	D-5185	PPM	0		
Magnesium	D-5185	PPM	0		
Calcium	D-5185	PPM	1042		
Barium	D-5185	PPM	0		
Phosphorus	D-5185	PPM	757		
Zinc	D-5185	PPM	846		
Additional Test					RO / L-Warning / L-Caution / U-Caution / U-Warning
Flash Point	D-3828	°C			
Viscosity Index	D-2270				

Note: Alarm Limits are variable and dependent upon dataset size and to be used as general guideline.
No Sign or N : NORMAL , C or C : CAUTION (first level warning limit) , W or W : Warning (second level warning limit)
Accuracy of interpretation and recommendation are based on representatives sample and information supplied. No warranty is expressed or implied for this report.

Focuslab Ltd. Bangkok Thailand FL-6.8

A-2: Designed lube oil test report by FOCUSLAB

APPENDIX B :

EXPERIMENTAL ANALYSIS REPORTS

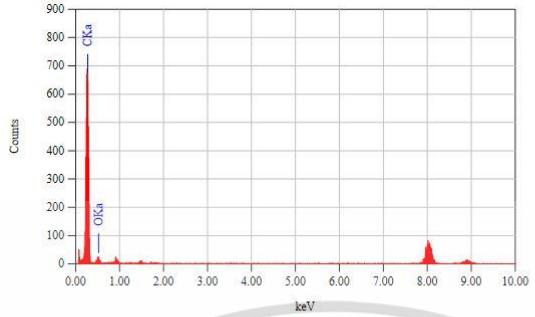

Acquisition Parameter
Instrument : JEM-2100(URP)
Acc. Voltage : 200.0 kV
Probe Current: 1.00000 nA
PHA mode : T3
Real Time : 50.22 sec
Live Time : 50.00 sec
Dead Time : 0 %
Counting Rate: 184 cps
Energy Range : 0 - 40 keV

ZAF Method Standardless Quantitative Analysis
Fitting Coefficient : 0.2871

Element	(keV)	Mass%	Sigma	Atom%	Compound	Mass%	Cation	K
C K	0.277	96.45	0.56	97.31				99.5190
O K	0.525	3.55	0.28	2.69				0.4810
Total		100.00		100.00				

(a)

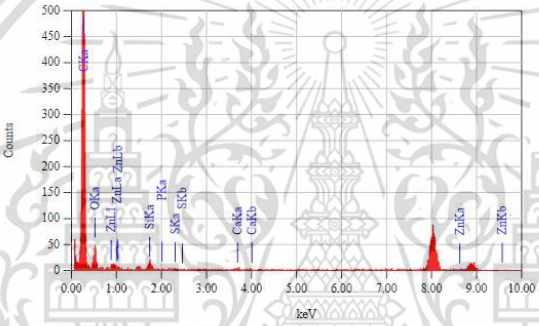

Acquisition Parameter
Instrument : JEM-2100(URP)
Acc. Voltage : 200.0 kV
Probe Current: 1.00000 nA
PHA mode : T3
Real Time : 50.17 sec
Live Time : 50.00 sec
Dead Time : 0 %
Counting Rate: 179 cps
Energy Range : 0 - 40 keV

ZAF Method Standardless Quantitative Analysis
Fitting Coefficient : 0.2898

Element	(keV)	Mass%	Sigma	Atom%	Compound	Mass%	Cation	K
C K	0.277	92.25	0.56	94.56				97.2426
O K	0.525	6.17	0.23	4.75				1.3899
Si K	1.739	1.57	0.18	0.69				1.3115
P K	2.013	0.00	0.00	0.00				0.0006
S K	2.307	0.00	0.00	0.00				0.0207
Ca K	3.690	0.00	0.00	0.00				0.0388
Zn K	8.630	0.00	0.00	0.00				0.0028
Total		100.00		100.00				

(b)

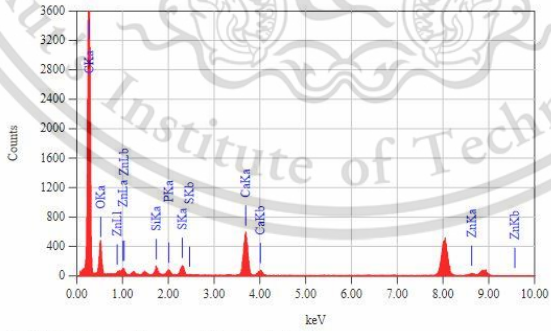

Acquisition Parameter
Instrument : JEM-2100(URP)
Acc. Voltage : 200.0 kV
Probe Current: 1.00000 nA
PHA mode : T3
Real Time : 50.69 sec
Live Time : 50.00 sec
Dead Time : 1 %
Counting Rate: 1317 cps
Energy Range : 0 - 40 keV

ZAF Method Standardless Quantitative Analysis
Fitting Coefficient : 0.2679

Element	(keV)	Mass%	Sigma	Atom%	Compound	Mass%	Cation	K
C K	0.277	89.96	0.21	92.81				94.8900
O K	0.525	8.33	0.12	6.45				2.0766
Si K	1.739	1.81	0.06	0.67				1.2800
P K	2.013	0.04	0.00	0.01				0.2557
S K	2.307	0.08	0.00	0.03				0.5204
Ca K	3.690	0.08	0.00	0.02				0.9575
Zn K	8.630	0.00	0.00	0.00				0.0197
Total		100.00		100.00				

(c)

B-1: TEM-EDS analysis reports of (a) Diesel (b) Diesel-L and (c) Ash focus point

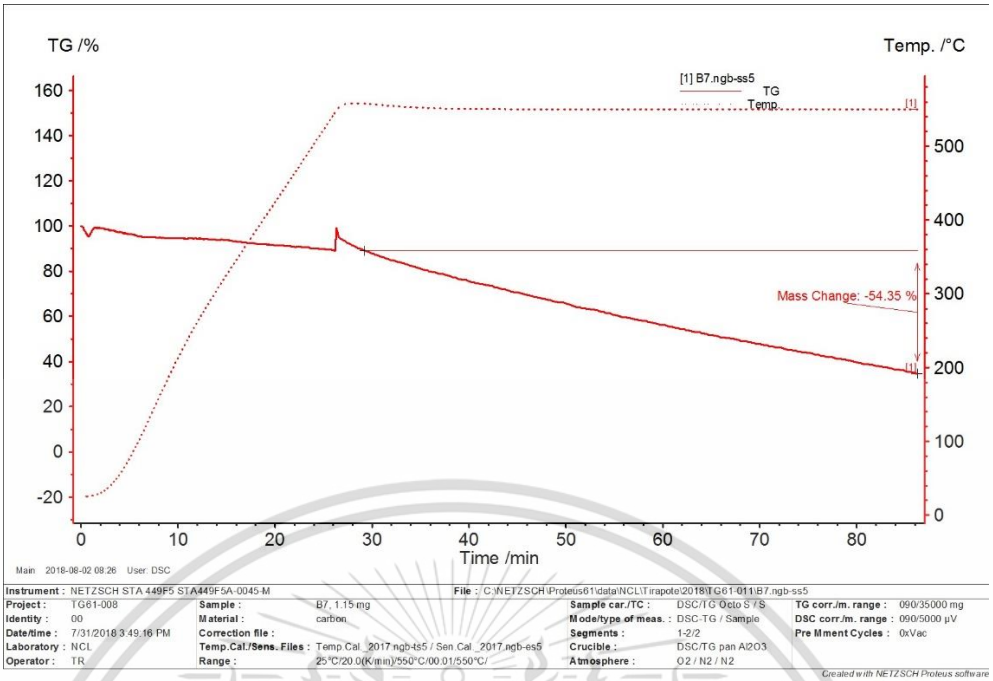

B-2: Thermogravimetric analysis report of Diesel PM at isothermal 550°C with pure air atmospheric condition.

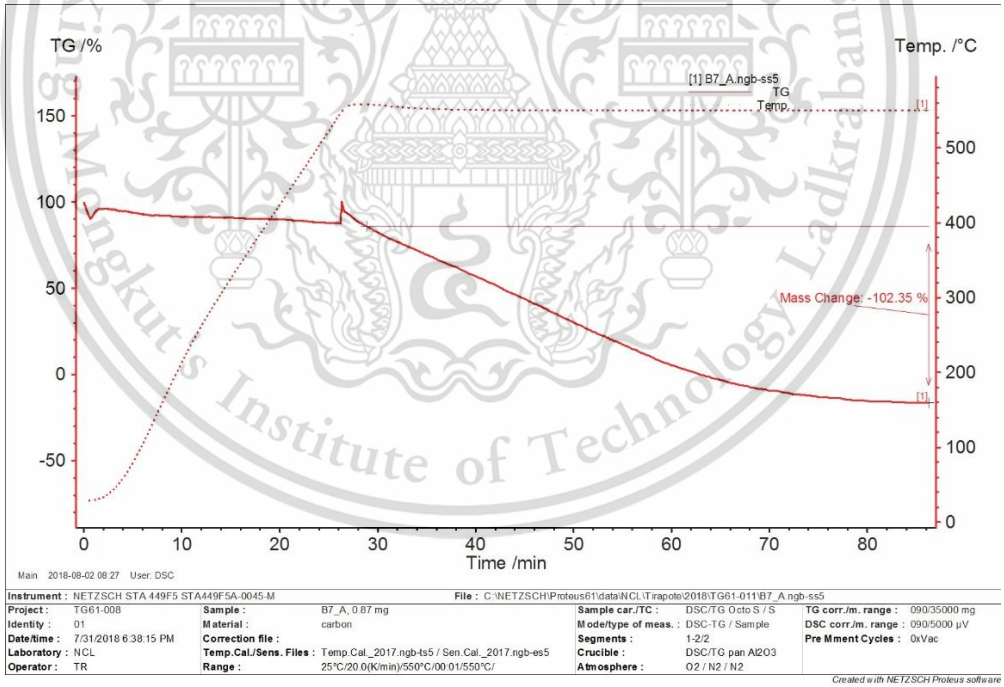

B-3: Thermogravimetric analysis report of Diesel-L PM at isothermal 550°C with pure air atmospheric condition.

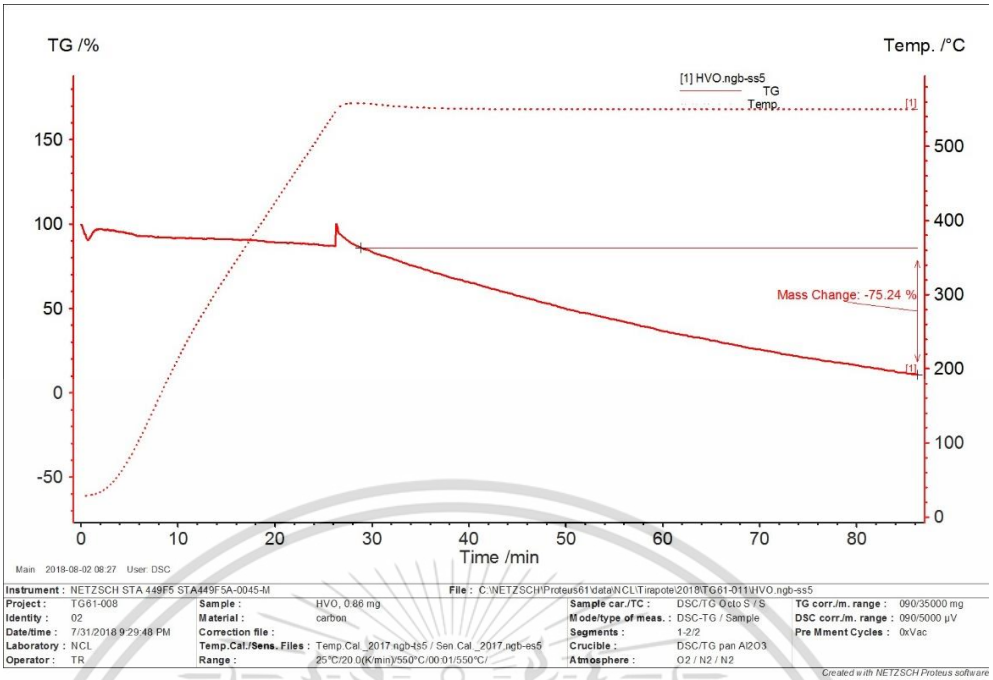

B-4: Thermogravimetric analysis report of HVO PM at isothermal 550°C with pure air atmospheric condition.

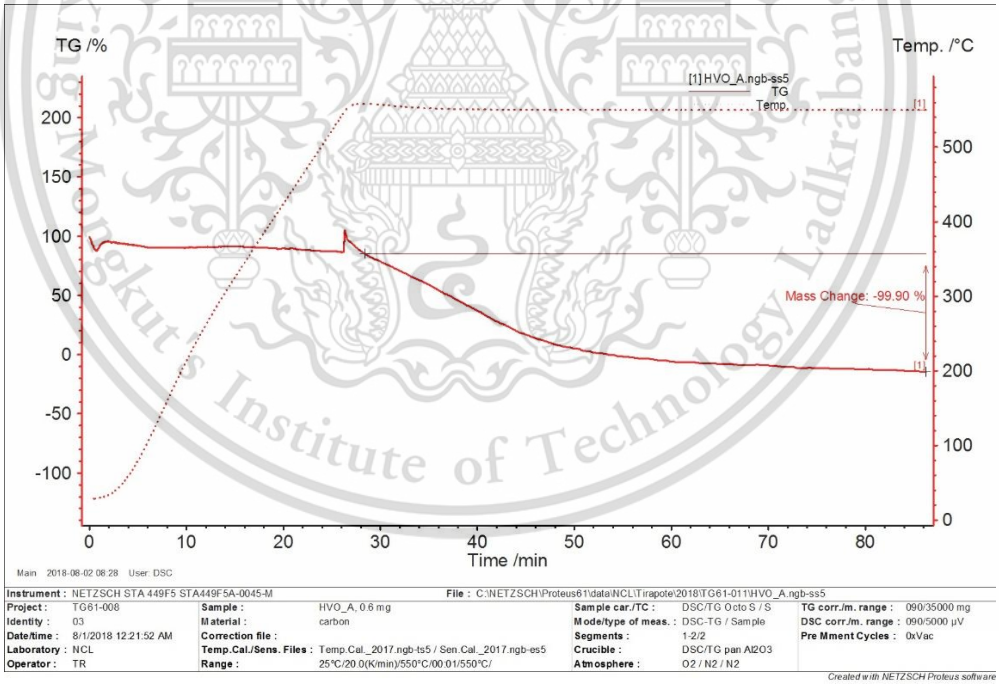

B-5: Thermogravimetric analysis report of HVO-L PM at isothermal 550°C with pure air atmospheric condition.

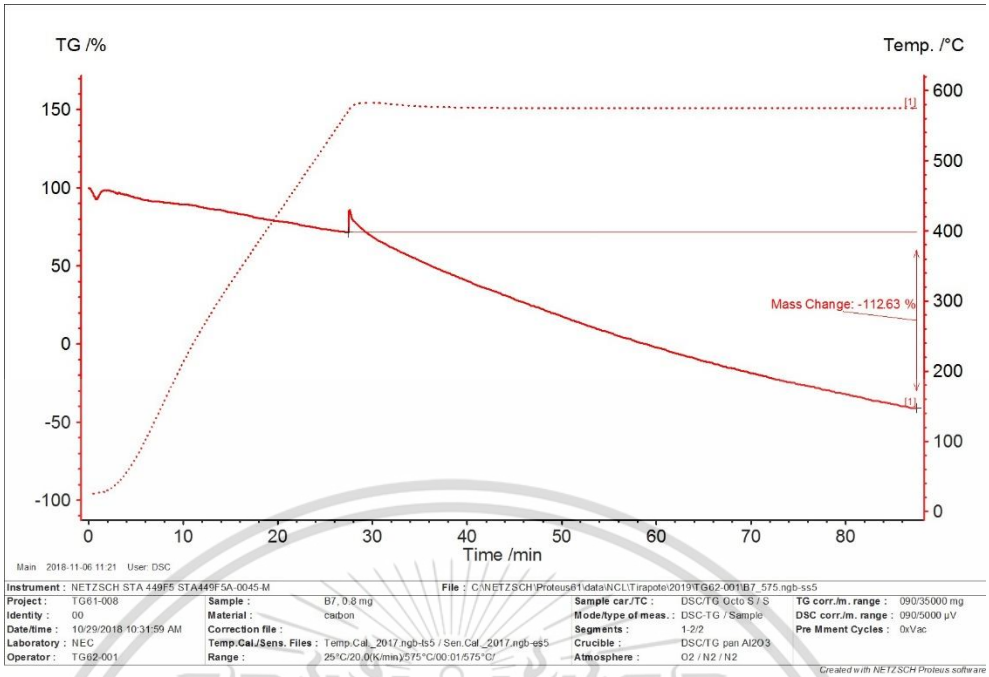

B-6: Thermogravimetric analysis report of Diesel PM at isothermal 575°C with pure air atmospheric condition.

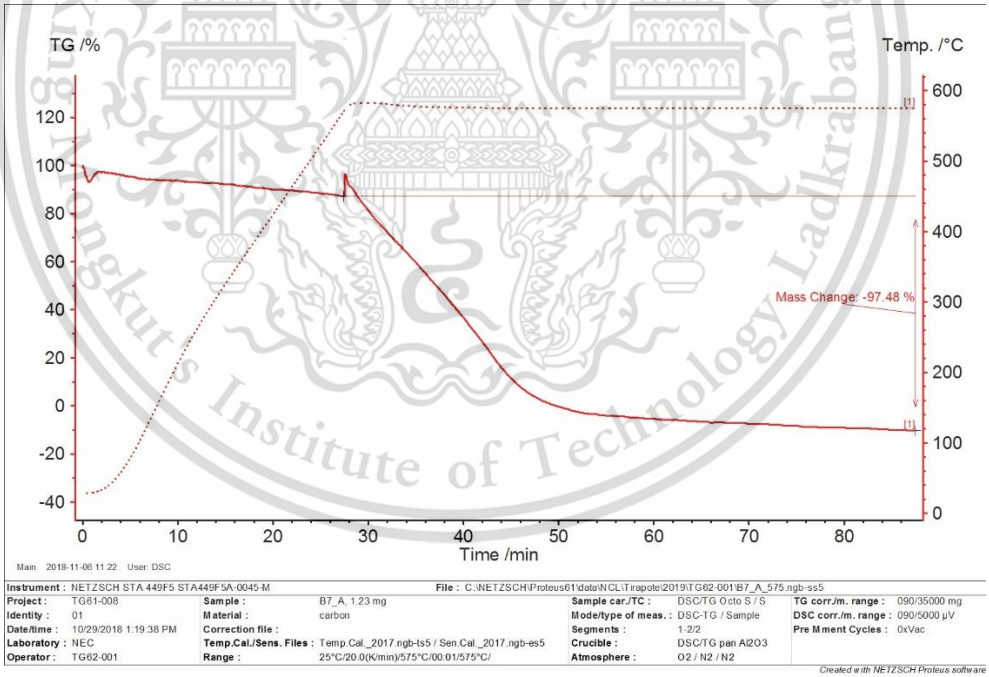

B-7: Thermogravimetric analysis report of Diesel-L PM at isothermal 575°C with pure air atmospheric condition.

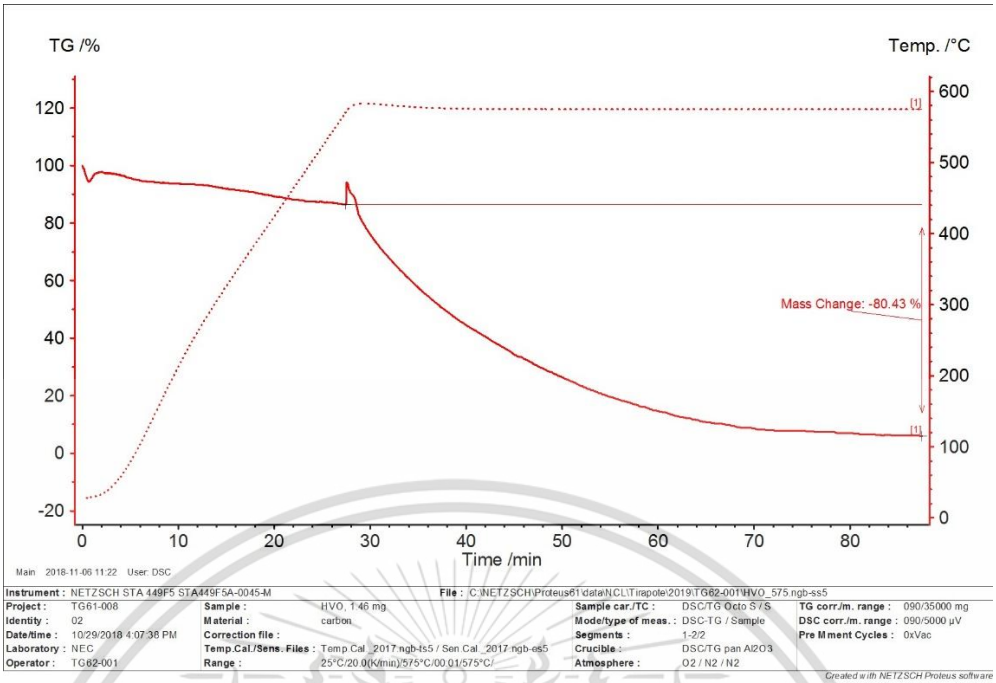

B-8: Thermogravimetric analysis report of HVO PM at isothermal 575°C with pure air atmospheric condition.

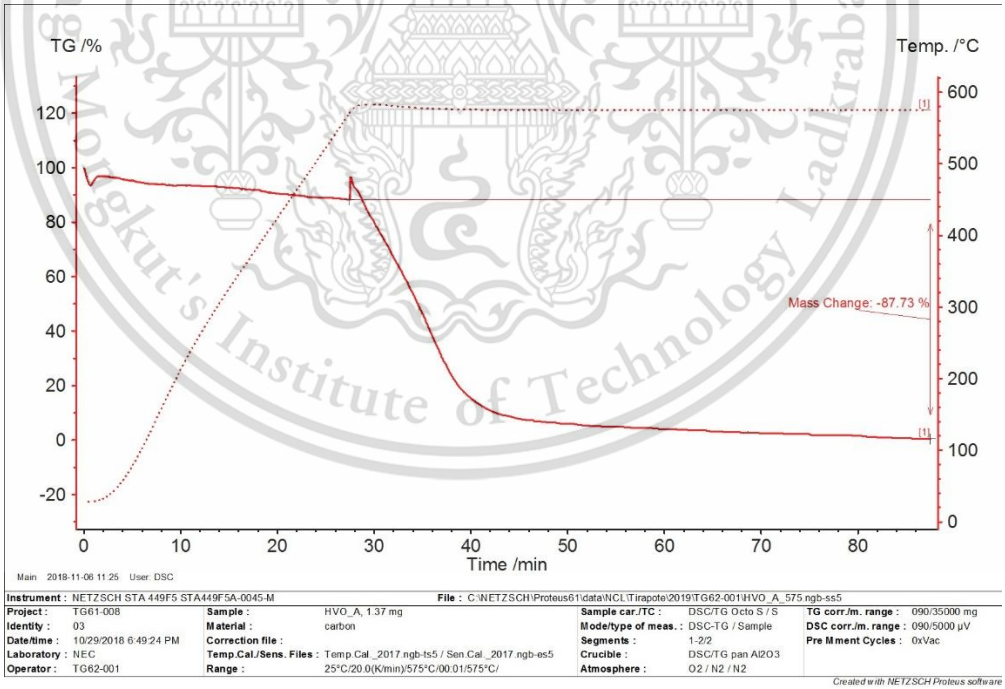

B-9: Thermogravimetric analysis report of HVO-L PM at isothermal 575°C with pure air atmospheric condition.

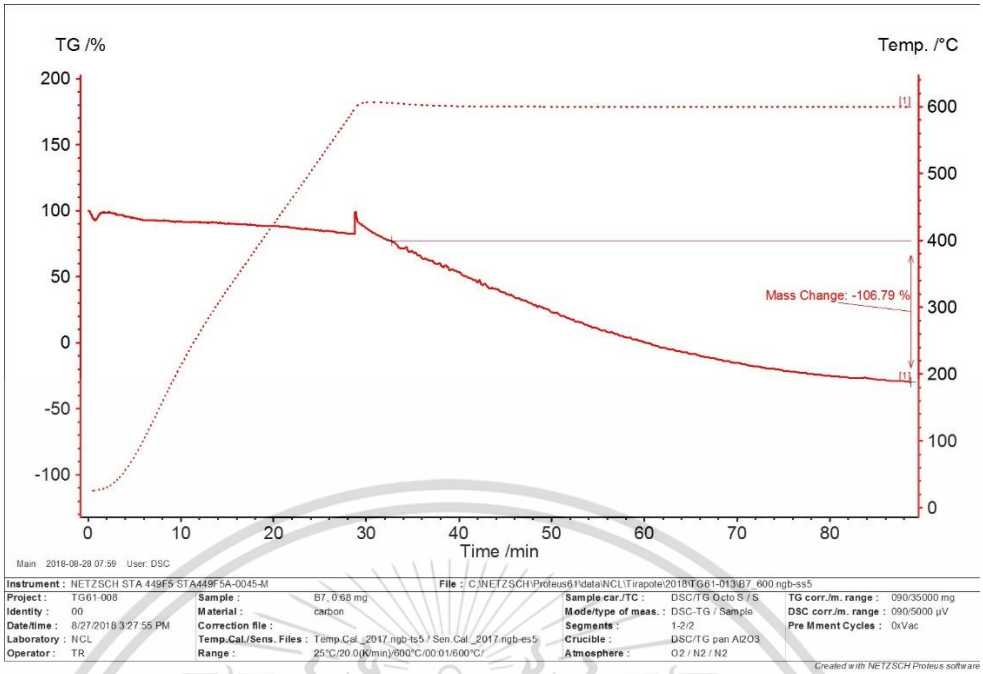

B-10: Thermogravimetric analysis report of Diesel PM at isothermal 600°C with pure air atmospheric condition.

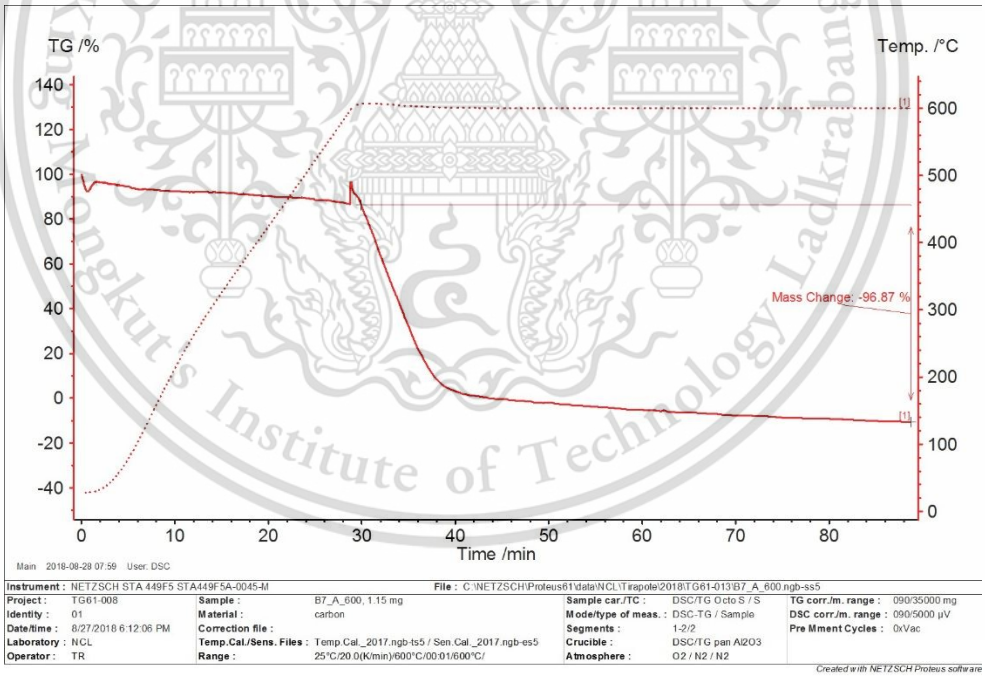

B-11: Thermogravimetric analysis report of Diesel-L PM at isothermal 600°C with pure air atmospheric condition.

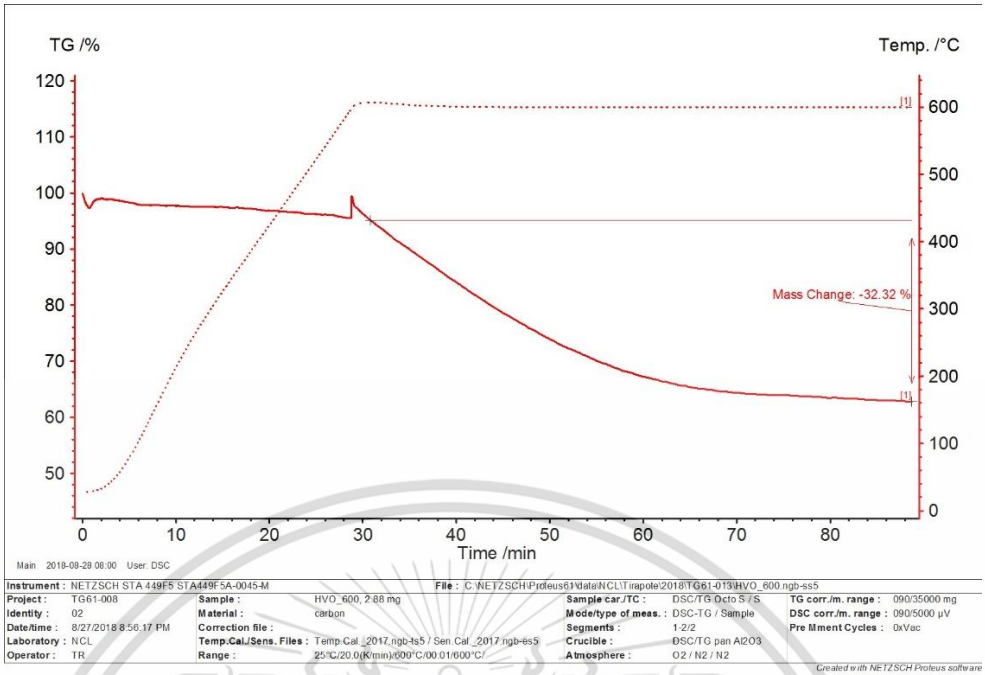

B-12: Thermogravimetric analysis report of HVO PM at isothermal 600°C with pure air atmospheric condition.

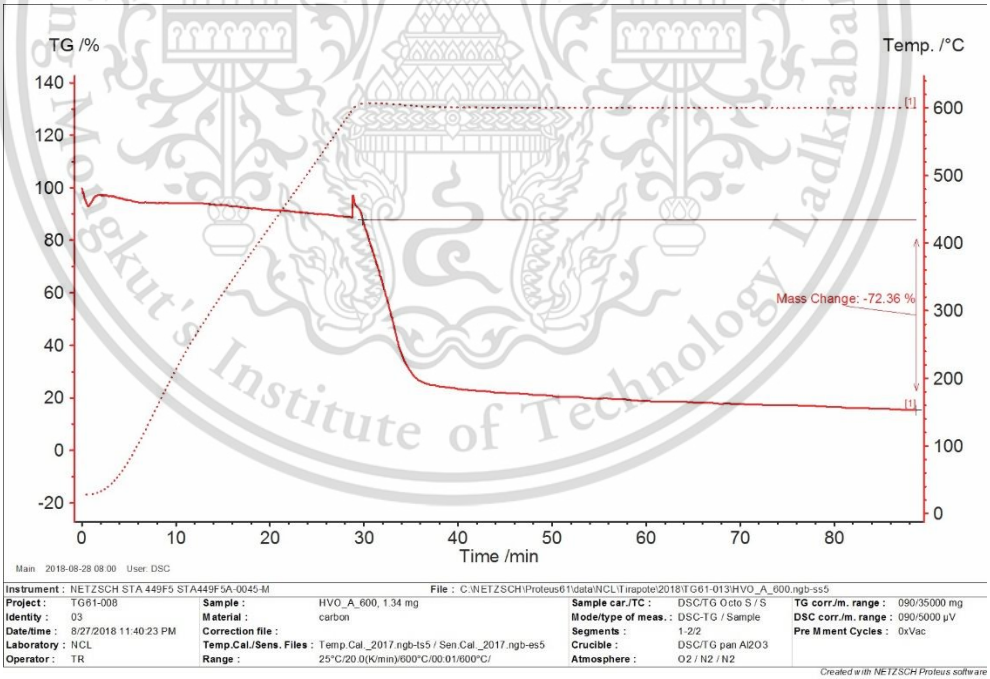

B-13: Thermogravimetric analysis report of HVO-L PM at isothermal 600°C with pure air atmospheric condition.

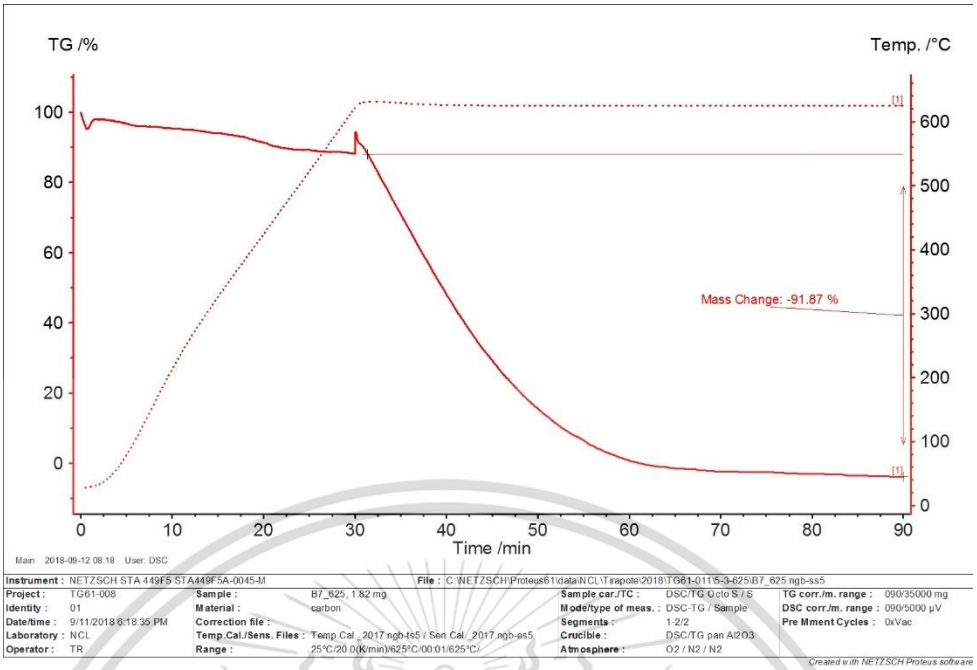

B-14: Thermogravimetric analysis report of Diesel PM at isothermal 625°C with pure air atmospheric condition.

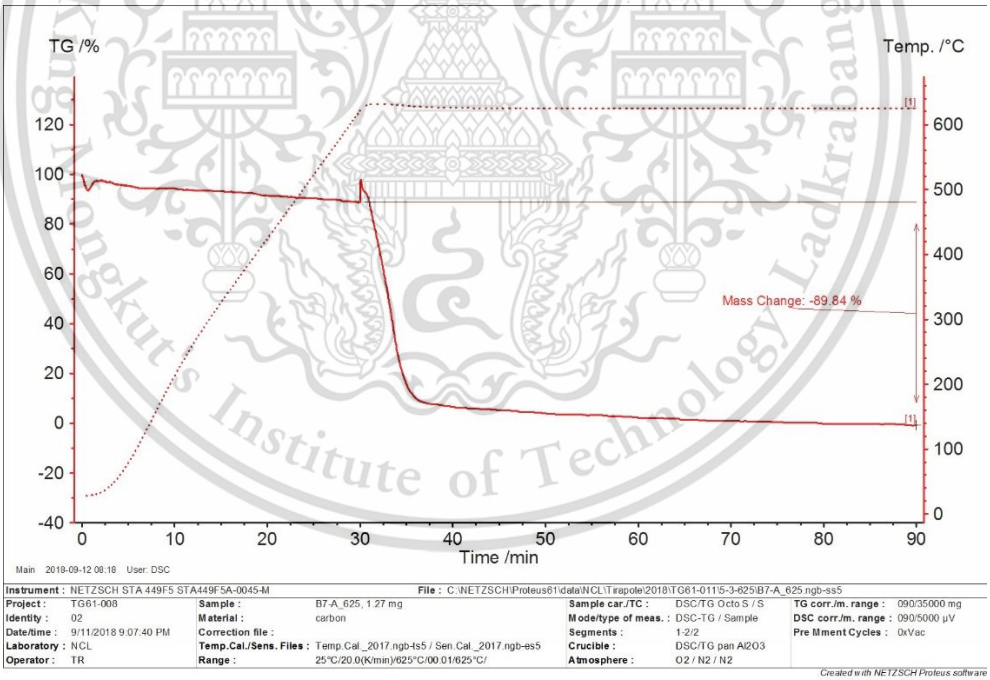

B-15: Thermogravimetric analysis report of Diesel-L PM at isothermal 625°C with pure air atmospheric condition.

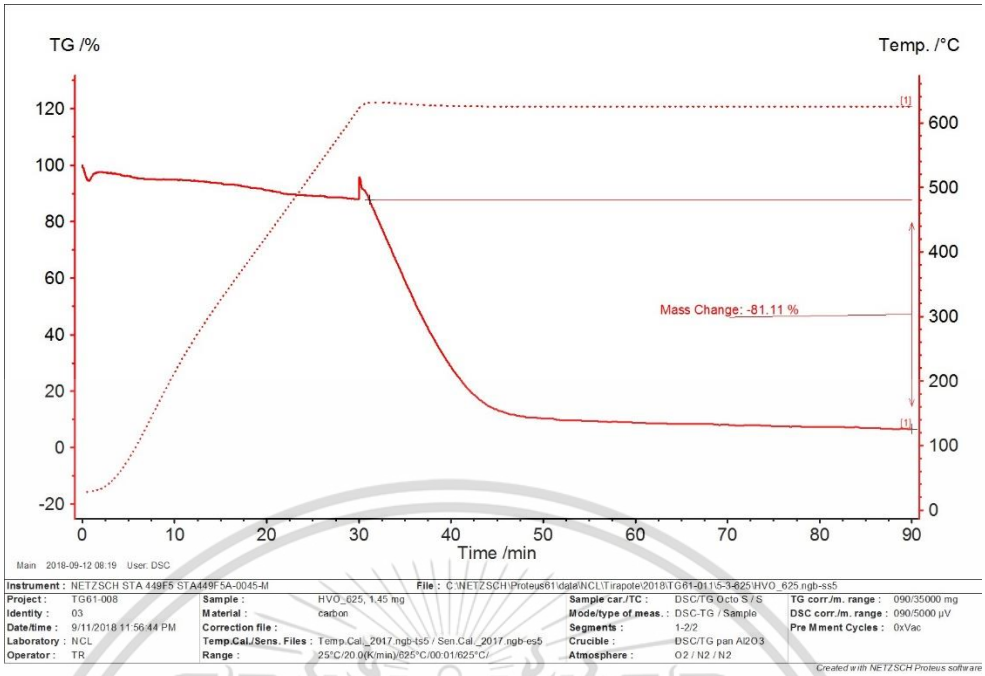

B-16: Thermogravimetric analysis report of HVO PM at isothermal 625°C with pure air atmospheric condition.

APPENDIX C :

PUBLICATIONS

Key Engineering Materials
ISSN: 1662-9795, Vol. 798, pp 412-418
doi:10.4028/www.scientific.net/KEM.798.412
© 2019 Trans Tech Publications, Switzerland

Submitted: 2018-09-29
Revised: 2019-01-10
Accepted: 2019-01-11
Online: 2019-04-08

Impact of Engine Oil's Additives on Particulate Matter's Micro- and Nanostructure Using Electron Microscopy Image Analysis

Phyozin Koko[1,a], Preechar Karin[1,b*], Sippakorn Rungsritanapaisan[1,c], Ruangdaj Tongsri[2,d] and Katsunori Hanamura[3,e]

[1]Automotive Engineering Program, International College, King Mongkut's Institute of Technology Ladkrabang, Bangkok 10520, Thailand

[2]National Metal and Materials Technology Center, National Science and Technology Development Agency, Pathumthani 12120, Thailand

[3]School of Engineering, Tokyo Institute of Technology, Tokyo 152-8552, Japan

[b*]preechar.ka@kmitl.ac.th

Keywords: Diesel Engine, Particulate Matter, Metal Oxide Ash, SEM-EDS, TEM

Abstract. According to increasingly stringent emission regulations on particle emissions from automotive vehicles, a diesel engine must be equipped with diesel particulate filter (DPF) to trap the particulate matters (PMs) which can be harmful to human health. Morphology and chemical composition of particulate matters were successfully studied using electron microscopy and electron dispersive x-ray spectroscopy (EDS) analysis. Microstructure of particulate matters derived from diesel blending lubricating oil were not significant different compared to diesel PM. Nanostructure of soot is a spherical shape composed of curve line crystallites and the particle sizes were in the range of 10 – 60 nm while the metal oxide ash is composed of lattice fringes. Chemical composition analysis of EDS result showed that metallic additives from lubricating oil cannot be burned during combustion and might be transformed into metal oxide ash.

1. Introduction

Diesel engine has higher thermal efficiency among internal combustion engines (ICEs) used in automobiles due to attaining higher compression ratio. However, diesel engines trail black smokes containing much amount of particulate matter (PM) resulting from incomplete combustion around single fuel droplets and are very harmful to human health such as lung cancer, asthma and so on. PM are composed primarily of unburned hydrocarbon, pure carbon (soot) and metal oxide ash as solid fractions. Each PM fraction is mainly dependent upon the chemical properties of fuel and lubricant, engine operating conditions, engine wear and exhaust after-treatment technologies [1 – 4].

One of the exhaust aftertreatment systems, diesel particulate filter (DPF) is an effective solution for reducing particle emission. DPF can trap up to (99%) of the PM emitted from the exhaust gas and a process which can oxidize the trapped soot into carbon dioxide is called regeneration process of DPF. Although regeneration process can burn the soot effectively, incombustible metal oxide ashes will be remained at the inlet channels of DPF and causing engine back pressure. These metal oxide ashes are mainly derived from lubricant additives, engine wear and a very few amounts of trace metals from the fuel [5, 6].

During combustion, lubricants can also participate inside engine cylinder and affect the composition of PM emission. Some literatures have already investigated about the impacts of lubricating oil contamination on particle emissions focusing on not only physical characterization but also chemical composition. Y. Wang et al., found that the anti-wear lubricant oil additives changed the nanostructure of emitted particles and led to particles with a more disordered nanostructure. Besides, oil-related particles have larger aggregate size than diesel particles [7 – 9].

P. Karin et al., investigated that the nanostructure of soot (Carbon) and ash (Calcium) by comparing the PM from engine and diesel lamp. The pattern of soot or carbon crystallites looks like a curve line where as the ash crystallite looks like a straight cross line pattern with round outlines. The average diameter of soot single primary nanoparticles emitted from engine are in the range of 10 – 60 nm. The chemical composition and morphology of lubricant derived ash have also been reported. The individual ash particles have round shapes and sizes of approximately 10 – 200 nm [10 – 12].

The objectives of this article are to investigate the physical and chemical characterization of diesel particulate matters which are influenced by the impact of engine oil's additives using electron microscopy and electron dispersive x-ray spectroscopy (EDS) analysis. Nanostructure of metal oxide ash would be briefly discussed which is still not briefly found out among previous literatures.

2. Experimental

Table 1 Engine specification

Items	Details
Engine type	1-cylinder, DI, CI engine
Bore x Stroke	(97 x 96) mm
Displacement	709 cm^3
Compression ratio	18:1
Power	9.2 kW @2400 RPM
Injection timing	19°CA bTDC

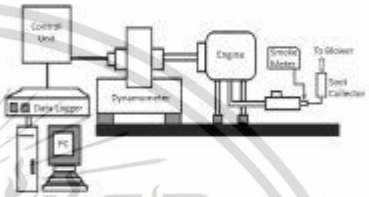

Fig. 1 Schematic diagram of engine setup

Table 2 Properties of diesel fuel

Fuel properties	Unit	Result
Chemical formula	-	$C_{14.5}H_{28}$
Auto ignition temperature	°C	288
Calorific value	kJ/kg	46,180
Heat of vaporization	kJ/kg	250
Density at 25 °C	kg/m^3	844.8
Viscosity at 40 °C	mm^2/s	3.0
Stoichiometric A/F ratio	-	14.7
Distillation temperature		
T10	°C	214.3
T50	°C	281.5
T70	°C	352.3

Table 3 Properties of lubricant

Test	Method	Unit	Result
Density @15°C	ASTM D4052-15	g/mL	0.8960
Density @30°C	ASTM D4052-15	g/mL	0.8866
Viscosity @40°C	ASTM D445-15a	cSt	154.8
Viscosity @100°C	ASTM D445-15a	cSt	15.05
Magnesium	ASTM D6481	%wt	0.1816
Zinc	ASTM D6481	%wt	0.0798
Phosphorous	ASTM D6481	%wt	0.0856
Pour point	ASTM D 6749-02	°C	-9
Viscosity index	ASTM D2270	-	97

A single cylinder natural aspurated direct injection compression engine (Kubota – RT140) was used to generate the particulate matter (PM). The engine specification are described in Table 1. Eddy current engine dynamometer was used to control the various engine speed and load conditions by the aid of Lab-view program. To measure the smoke intensity of the exhaust emission, opacity smoke meter (Okuda DSM – 240) was introduced between the exhaust muffler's outlet and the blower as described in figure 1. Paper filter was inserted into the smoke meter to measure the soot contamination percentage. A soot collector containing metal netting was used to collect the soot powder.

To conduct the experiment, conventional diesel was used as an ideal fuel and secondly, designed lubricant oil containing excess amount of Calcium (Ca) additives were blended directly into the diesel fuel. The blending condition is the amount of 10% by mass directly into the diesel fuel. The purpose of blending designed lubricant containing excess additives is to obtain more ash

formation among PM composition since these metal oxide ashes are mainly originated from engine oil's additives. Chemical properties of diesel fuel and blending lubricating oil are briefly described in Table 2 and 3. For the engine lubricating system, conventional lubricant 15W-40 API CI-4/SL synthetic engine oil was used.

3. Results and Discussion

3.1 Smoke Intensity

Opacity smoke meter determined the smoke intensities of diesel and diesel blending lube oil conditions as shown in figure 2. Diesel blending lubricant condition showed less smoke intensity compared to diesel condition especially in high engine load condition. Less smoke intensity means less soot contamination. Lubricating oils are basically formulated with metallic additives and acidic compositions. During engine combustion, the effect of excess metallic acidic composition from blending lubricating oil might promote more complete reaction of fuel and oxygen molecules.

3.2 Scanning Electron Microscopy (SEM)

Scanning electron microscopy (SEM) was used to investigate the agglomerate structure of particulate matters in micro- scales. Figure 3 (a) describes the agglomerate microstructure of particulate matter from diesel condition and figure 3 (b) shows the agglomerate microstructure of particulate matter derived from diesel blending lube oil condition respectively. According to the SEM images, the agglomerate structure of lubricant oil related particles have not shown significant different in micro- scales.

(a) Diesel black smoke (b) Diesel blending lube oil black smoke

Fig. 2 Smoke intensities in the engine's exhaust emission of (a) diesel and (b) diesel blending lube oil with high concentration of additives

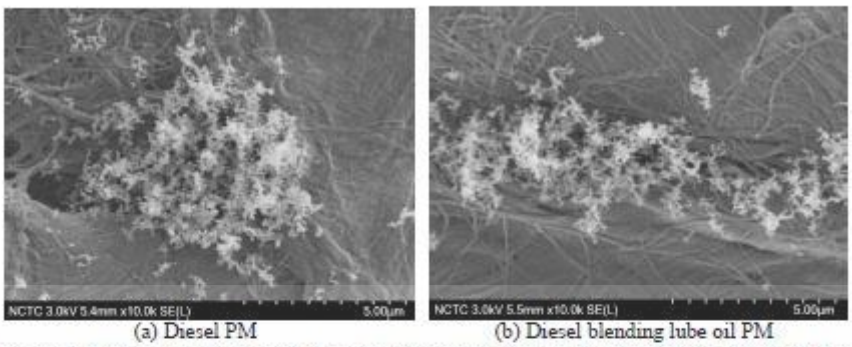

(a) Diesel PM (b) Diesel blending lube oil PM

Fig. 3 SEM images of agglomerate structure of (a) diesel PM and (b) diesel blending lube oil PM under 2000 rpm engine full load condition

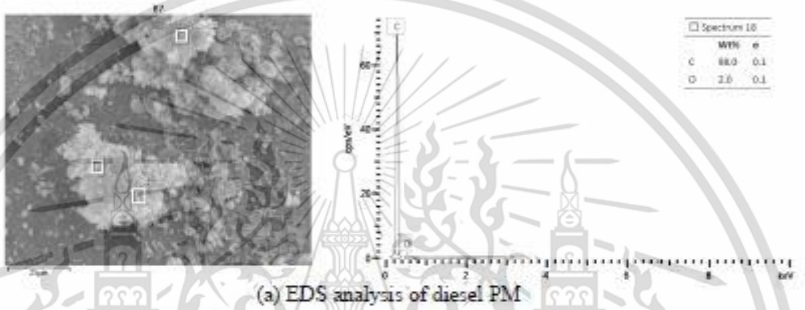

(a) EDS analysis of diesel PM

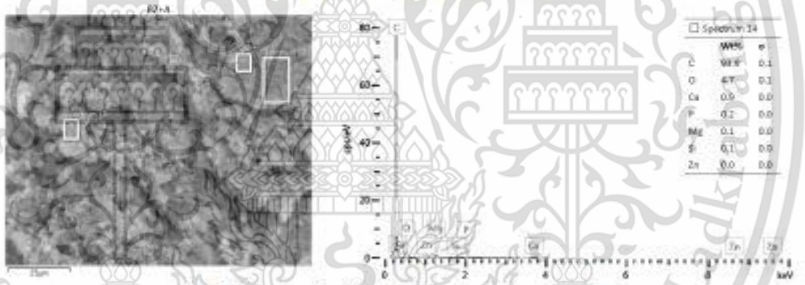

(b) EDS analysis of diesel blending lube oil PM

Fig. 4 Chemical composition of (a) diesel PM and (b) diesel blending lube oil PM showing unburned metallic additives from lubricating oil

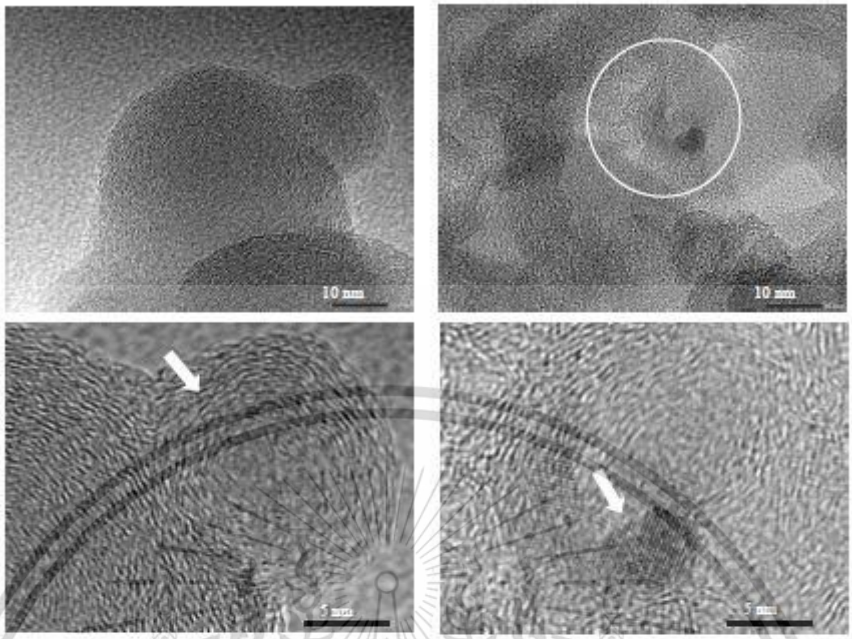

(a) Diesel PM (b) Diesel blending lube oil PM

Fig. 5 TEM images of (a) diesel soot nanostructure showing curve line crystallites and (b) nanostructure of metal oxide ash showing lattice fringes

3.3 Electron Dispersive X-ray Spectroscopy (SEM-EDS)

SEM-EDS analysis determined the chemical composition of PMs from diesel and diesel blending lube oil conditions as shown in figure 4 (a and b). Diesel PMs were mainly composed of chemical composition of Carbon (C) from soot. However, chemical composition of particulate matters from diesel blending lube oil conditions contain not only Carbon (C) but also unburned metallic elements such as Calcium (Ca), Phosphorous (P), Magnesium (Mg), Silicon (Si) and Zinc (Zn) which all are derived from lubricant additives as shown in figure 4 (b). Therefore, SEM-EDS results pointed out that metallic additives from engine lubricating oil cannot be burned during combustion and these metallic elements can be transformed into metal oxide ashes.

3.4 Transmission Electron Microscopy (TEM)

Transmission Electron Microscopy (TEM) was used to investigate the single primary nanostructures of diesel and diesel blending lube oil PMs as shown in figures 5 (a and b). Particulate matters were collected under 2400 rpm engine full load condition and 800k magnification was introduced to observe the nanostructure of primary particles. As described in figure 5 (a), nanostructure of diesel soot is a spherical shape composed of curve line crystallites and the particle sizes are in the range of 10 – 60 nm. Particles from diesel blending lube oil conditions were combined together with soot and metal oxide ash as briefly described in figure 5 (b). Unlike soot, nanostructure of metal oxide ash has shown small crystallites composed of lattice fringes.

4. Conclusion

Soot contamination of blending lubricant oil condition showed lower percentage than neat diesel condition especially in high engine load conditions. The effect of excess metallic acidic composition from blending lubricating oil might promote more complete reaction of fuel and oxygen molecules inside engine combustion chamber. As physical characterization, the agglomerate structures of diesel PM and diesel blending lube oil PM are not significant different in micro-scales. However, the single primary nanostructure of soot is a spherical shape composed of curve line crystallites and particle sizes are in the range of 10 – 60 nm while the nanostructure of metal oxide ash is composed of lattice fringes. Chemical composition of particulate matters from diesel blending lube oil condition showed that metallic additives from engine lubricating oil cannot be burned by engine combustion and these unburned metallic components might be transformed into metal oxide ash.

5. Acknowledgements

The author would like to acknowledge to International College, King Mongkut's Institute of Technology Ladkrabang (KMITL) for research funding and also Bangchak Corporation Public Company Limited (BCP) for supporting designed lubricant to accomplish this research.

References

[1] J. B. Heywood. (1998). Internal Combustion Engine Fundamentals, McGraw-Hill series in mechanical engineering, Singapore.

[2] Peter Eastwood. (2008). Particle Emission from Vehicles, John Wiley & Sons, Ltd, England.

[3] C.L. Myung and S. Park. (2012). Exhaust Nanoparticle Emissions from Internal Combustion Engines: A Review, International Journal of Automotive Technology, Vol. 13, No.1, pp.9-22.

[4] C. L. Myung, A. Ko and S. Park. (2014). Review on Characterization of Nano-particle Emissions and PM Morphology from Internal Combustion Engines: Part 1, International Journal of Automotive Technology, Vol. 15, No. 2, pp. 203-218.

[5] S. Mohankumar and P. Senthilkumar. (2017). Particulate Matter Formation and its Control Methodologies for Diesel Engine: A Comprehensive Review, Renewable and Sustainable Energy Reviews, Vol. 80, pp.1227-1238.

[6] K. Hanamura, P. Karin, L. Cui, P. Rubio, T. Tsuruta, T. Tanka and T. Suzuki. (2009). Micro- and Macroscopic Visualization of Particulate Matter Trapping and Regeneration Processes in Wall-flow Diesel Particulate Filters, International Journal of Engine Research, Vol. 10, pp. 305-321.

[7] P. Tornehed and U. Olofsson. (2011). Lubricant Ash Particles in Diesel Engine Exhaust: Literature Review and Modelling Study, Proceedings of the Institution of Mechanical Engineers, Journal of Automotive Engineering, Vol. 225, Part D, pp. 1055-1066.

[8] Y. Wang, X. Liang, G. Shu, L. Dong, X. Sun and H. Yu. (2015). Effects of an Anti-wear Oil Additive on the Size Distribution, Morphology, and Nanostructure of Diesel Exhaust Particles, Tribology International, Vol. 92, pp. 379-386.

[9] Y. Wang, X. Liang, G. Shu and L. Dong. (2015). Impact of Lubricating Oil on Morphology of Particles from a Diesel Engine, Energy Procedia, Vol.75, pp. 2388-2393.

[10] P. Karin, H. Oki, K. Hanamura and C. Charoenphonphanich. (2012). Nanostructures and Oxidation Kinetics of Diesel Particulate Matters, An International Journal of the Thai Society of Mechanical Engineers, Vol. 1, No.2, pp. 3-8.

[11] P. Karin, J. Boonsakda, K. Siricholathum, E. Saenkhumvong, C. Charoenphonphanich and K. Hanamura. (2017). Morphology and Oxidation Kinetics of CI Engine's Biodiesel Particulate Matters on Cordierite Diesel Particulate Filters using TGA, International Journal of Automotive Technology, Vol. 18, No. 1, pp. 31-40.

[12] A. Liati, P. Dimopoulos Eggenchwiler, D. Müller Gubler, Schreiber and M. Aguirre. (2012). Investigation of Diesel Ash Particulate Matter: A Scanning Electron Microscope and Transmission Electron Microscope Study, Atmospheric Environment, Vol. 49, pp. 391-402.

The 9th TSME International Conference on Mechanical Engineering
11-14 December 2018
Phuket, Thailand

AME0021

Influence of Metal Oxide Ashes on Soot Oxidation Kinetics and Nanostructure using Electron Microscopy and Thermogravimetric Analysis

P. Koko[1,*], P. Karin[1], E. Saenkhumvong[2], C. Charoenphonphanich[2], W. Phairote[2], N. Chollacoop[3] and K. Hanamura[4]

[1]Automotive Engineering Program, International College, King Mongkut's Institute of Technology Ladkrabang, Bangkok, 10520, Thailand
[2]Faculty of Engineering, King Mongkut's Institute of Technology Ladkrabang, Bangkok 10520, Thailand
[3]National Metal and Materials Technology Center, National Science and Technology Development Agency, Pathumthani 12120, Thailand
[4]Department of Mechanical Engineering, School of Engineering, Tokyo Institute of Technology, Tokyo 152-8550, Japan

* Corresponding Author. E-mail: phyozin.mech@gmail.com

Abstract. According to increasingly stringent regulations on particulate emission from automotive vehicles, diesel engine has to be equipped with Diesel Particulate Filter (DPF) to trap the Particulate Matter (PM) which are very harmful to human health. Diesel particulate matters are composed primarily of unburned hydrocarbon (soot) and metal oxide ashes as solid fraction. DPF can trap PM with higher filtration efficiency and the process which can burn the soot into carbon dioxide is called regeneration process. Although regeneration process can burn the soot effectively, incombustible ashes will be remained inside the DPF channel causing engine back pressure. These metal oxide ashes are mainly derived from lubricant additives, engine wear and trace metals from diesel fuel. In this article, different nanostructures of diesel soot and metal oxide ash derived by diesel blending lube oil condition were briefly compared using Transmission Electron Microscopy (TEM) image analysis. Electron Dispersive X-ray Spectroscopy (EDS) analysis was introduced to investigate the chemical composition of particulate matters. Thermogravimetric Analysis (TGA) was also conducted to compare the oxidation kinetics of pure diesel soot and the influence of metal oxide ash on soot oxidation kinetics. Contamination of metal oxide ashes promoted soot oxidation rate due to the presence of metallic additives from lube oil acting as a catalyst on soot oxidation kinetics.

Keywords: Diesel Particulate Matter, Metal Oxide Ash, TEM, TGA

1. Introduction

Particulate Matter (PM) emitted from diesel engines are very harmful to human health and must be removed due to stringent emission regulations. PM are mainly composed of solid fraction (soot and ash) and soluble organic fraction such as (sulfates and nitrates) organic compounds. Diesel Particulate Filter (DPF) is one of the most effective aftertreatment system which can perform higher PM trapping efficiency. There are honeycomb rectangular channels where the exhaust gas flows through its

porous walls. The trapped PMs must be burned out during vehicle running and a chemical oxidation process which can oxidize the trapped soot into carbon dioxide is called regeneration process. Although regeneration process can burn the soot effectively, the unburned metal oxide ashes will be remained along the inlet channels causing engine back pressure. These metal oxide ashes are originated mainly from lubricant additives and also a very few amount from engine wear and fuel trace metals [1 - 4].

Conventional lubricant additives such as anti-oxidants, rust and corrosion inhibitors, viscosity index modifiers, anti-wear (AW) agents, detergents and dispersants are well known additives which all are responsible to get better performance of engine lubricating oil. Among them, detergents help to prevent the high temperature deposits on the surface of metal walls and also it assists to neutralize acids that form in the lube oil. They are typically composed of calcium and magnesium as chemical metallic compounds. During engine combustion, lube oil can also participate and these metallic compounds leave as an ash deposit when the oil is burned [5, 6].

P. Karin et al., mentioned that nanostructure and oxidation kinetics of biodiesel PM compared to Diesel PM. A primary soot particle has two distinct parts: an inner core and an outer shell. The size of each crystallite and agglomeration might be strongly related to Brownian force of gas molecule, drag and shear forces of fluid dynamics, electrostatics forces of charge elements. Nanostructure of soot is composed of curve line crystallites while the ash nanostructure shows straight line structures [7, 8].

During engine combustion, the lubricants can also participate and the contamination of lube oil can vary the morphology and oxidation kinetics of particulate matters. Some literatures have already investigated not only physical characterization like morphology and particle size distribution but also chemical composition focusing on lube oil related particulate matters [9 - 11]. Y. Wang et al., found that the anti-wear lubricant oil additives changed the nanostructure of emitted particles and led to particles with a more disordered nanostructure. Moreover, oil-related particles have larger aggregate size than diesel particles [12].

In the previous literatures, oxidation kinetics of carbon black and engine's PMs were briefly compared. Engine's PMs are easier to oxidize than carbon black nanoparticles because of containing unburned hydrocarbon. Oxidation kinetics of PM is dependent upon both physical (shape of reactant substance) and chemical composition (oxygen, unburned hydrocarbon and others). The calculated apparent energy of diesel engine's PMs were in the range of 117-130 kJ/mol. H. Jung et al., also investigated that the influences of metals derived from lube oil on oxidation kinetics of soot particles by dosing 2% lube oil and determined apparent activation energy. By using Arrhenius equations, frequency factor of oil dosed PM were about twice as large as without dosing [13 - 15].

This research mainly compares nanostructure of diesel soot and metal oxide ash which are mainly derived from lubricant additives. The designed lube oil consisting excess amount of Calcium (Ca) additives was blended 10% directly into diesel fuel to obtain more ash formation among PM composition. Oxidation kinetics of diesel PM and diesel blending lube oil PM were also investigated to compare the influence of metal oxide ash on soot oxidation kinetics.

2. Experimental

Table 1: Engine Specification

Items	Details
Engine Type	1-cylinder, Direct Injection, CI engine
Bore x Stroke	(95 x 96) mm
Displacement	709 cm³
Compression ratio	18:1
Power	9.2 kW @2400 RPM
Injection Timing	19 °CA bTDC
Injection Pressure	22 MPa

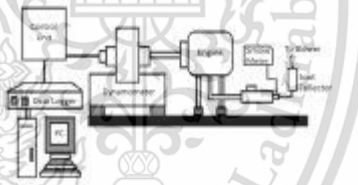

Fig. 1. Schematic diagram of engine setup

Table 2: Properties of fuel (Diesel)

Fuel Properties	Unit	Result
Chemical Formula	-	$C_{14.2}H_{28}$
Auto Ignition Temperature	°C	288
Calorific Value	kJ/kg	46180
Heat of Vaporization	kJ/kg	250
Viscosity	mm²/s	3.0
Stoichiometric A/F ratio	-	12.3
Density	kg/m³	844.8

Table 3: Properties of lubricant

Test	Method	Unit	Result
Density @15°C	ASTM D4052-15	g/mL	0.8960
Density @30°C	ASTM D4052-15	g/mL	0.8866
Viscosity @40°C	ASTM D445-15a	mm²/s	154.8
Viscosity @100°C	ASTM D445-15a	mm²/s	15.05
Magnesium	ASTM D6481	%wt	0.1816
Zinc	ASTM D6481	%wt	0.0798
Phosphorous	ASTM D6481	%wt	0.0856

A direct injection compression engine (Kubota – RT140) was used to generate the particulate matter. Engine specification are described in Table 1. Eddy Current Engine Dynamometer was used to control the desired engine speed and load conditions. Lab-View program controlled the engine dynamometer. A soot collector which contains metal netting inside was used to collect the PM. The schematic diagram of the engine setup are shown in figure 1. To conduct the experiment, commercial diesel containing ($C_{14.2}H_{28}$) was used as an ideal fuel and secondly, designed lube oil was blended 10% by mass directly into diesel fuel to obtain more ash formation among PM composition. This blending lubricant was supported by Bangchak Corporation and it contains excess amount of Calcium (Ca) additives since $CaSO_4$ is the most abundant sulfate compound found in diesel ashes inside used DPF. The fuel properties and blending lubricant oil properties are briefly described in Table 2 and 3. Density and viscosity of blending lubricants were tested under ASTM D4052-15 and ASTM D445-15a respectively. According to ASTM, viscosity is measured as kinematic viscosity and usually described in data sheets at 40°C and 100°C. For the engine lubrication system, conventional lubricating oil 15W-40 API CI-4/SL synthetic engine oil was used.

3. Results and Discussion

3.1 Morphology of ultrafine agglomerate particles

Transmission Electron Microscopy (TEM) image analysis was used to determine the ultrafine agglomerate primary particle nanostructures as shown in figure 2. Soot powders were collected under 2400 RPM engine full load condition since this engine condition is properable to generate the soot efficiently according to previous smoke intensity results. TEM image results showed that the agglomerate structure of ultrafine particles from diesel blending lube oil condition were not significant different compared to neat diesel engine's ultrafine particle. The primary particles from both conditions were grouped each other with similar agglomerate structures and results have not shown much differences.

3.2 Nanostructures of soot and metal oxide ash

Figure 3 compare TEM images of different nanostructures of soot (pure carbon) obtained from the neat diesel condition and metal oxide ash which is derived from diesel blending lube oil condition. The nanostructure of diesel soot primary particle is a spherical shape composed of curve line crystallites as described in figure 3 (a).

Different from soot, in figure 3 (b), metal oxide ash nanostructure is not a spherical shape composed of parallel straight line hatch patterns which shows similar nanostructures among metals. Due to the fact that blending lubricant oil contains metallic additives and these additives cannot be burned during engine combustion and finally it might be changed into metal oxide ashes. Therefore, particulate matters from diesel blending lubricant condition shows distinct straight lined patterns of ash collaborating with unburned hydrocarbon (soot).

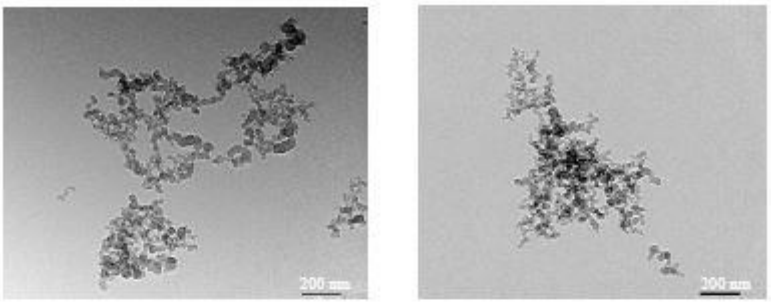

(a) PMs from neat diesel (b) PMs from diesel blending lube oil

Fig. 2 TEM images of ultrafine agglomerate particles from small engine (a) diesel and (b) diesel blending lubricating oil condition under 2400 RPM engine full load condition

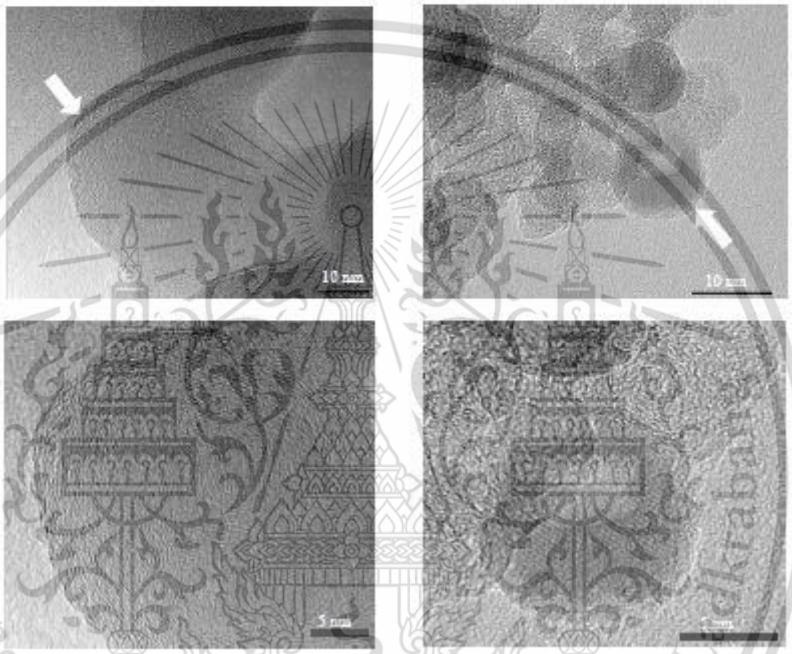

(a) Nanostructure of diesel soot (b) Nanostructure of metal oxide ash

Fig. 3 TEM images of nanostructure of (a) diesel soot and (b) metal oxide ash

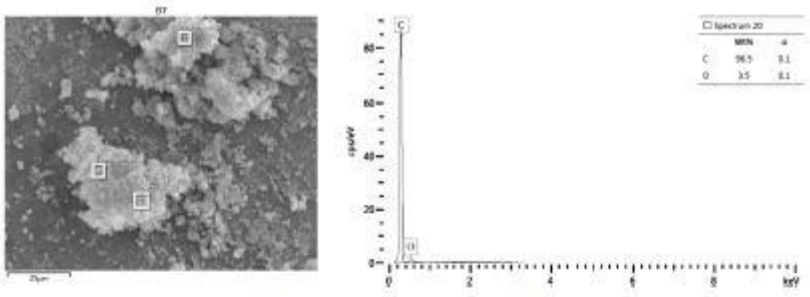

(a) Chemical composition of diesel PM

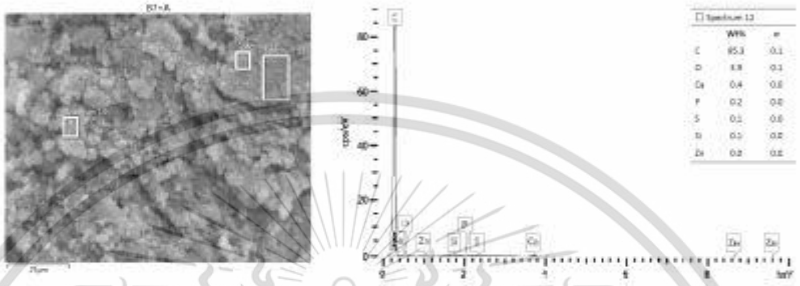

(b) Chemical composition of diesel blending lube oil PM

Fig. 4 Elemental analysis of (a) Diesel PM and (b) Diesel blending lube oil PM by using electron dispersive x-ray spectroscopy (SEM-EDS) showing unburned metallic lubricant additives derived from engine lubricating oil

3.3 Elemental composition of particulate matters

To investigate the chemical elemental composition of particulate matter, electron dispersive x-ray spectroscopy collaborating with SEM was introduced. X-ray spectrum detect the sample and distinguish the elements according to their particular atomic number. Regarding to the results of SEM-EDS as described in figure 4, particulate matters from neat diesel conditon shows only carbon (soot) and oxygen as elemental composition. However, particulate matters from diesel blending lube oil condition contain not only carbon and oxygen but also unburned metallic elements such as Calcium (Ca), Phosphorous (P), Sulfur (S), Silicon (Si) and Zinc (Zn) respectively. Among metallic additives, elemental composition amount of Ca expressed highest weight percentage due to the fact that the blending lubricant was designed with excess Ca additives. Therefore, EDS result pointed out that metallic additives from engine lubricating oil cannot be burned by engine combustion and these unburned metallic additives might be transformed into metal oxide ash which cannot be burned by regeneration process inside diesel particulate filter. On the other hand, these incombustible ashes might promote soot oxidation kinetics since ash are mainly originated from metallic additives of lube oil.

3.4 Oxidation kinetics of particulate matters

Thermogravimetric analysis (TGA) was conducted to investigate the influence of contamination of metal oxide ash on soot oxidation kinetics. Mass conversion results of diesel particles and diesel blending lube oil particles were compared under different operating temperatures (600 °C and 625 °C). Mass conversion rates can be calculated to describe the faster oxidation kinetics of diesel blending lube oil PMs. Isothermal method was used to maintain the operating temperature. Nitrogen was introduced before air is injected and the sample was oxidized until 90 minutes. Particles were treated with increasing temperature about (20 – 30) minutes by nitrogen atmosphere in order to occur vaporization process. After vaporization, air (oxygen and nitrogen) was start injected and the system was maintained under isothermal to initiate PM oxidation process. Chemical oxidation reaction of PM mass conversion results can be expressed by Eq.1 and the amount of mass conversion over time can be

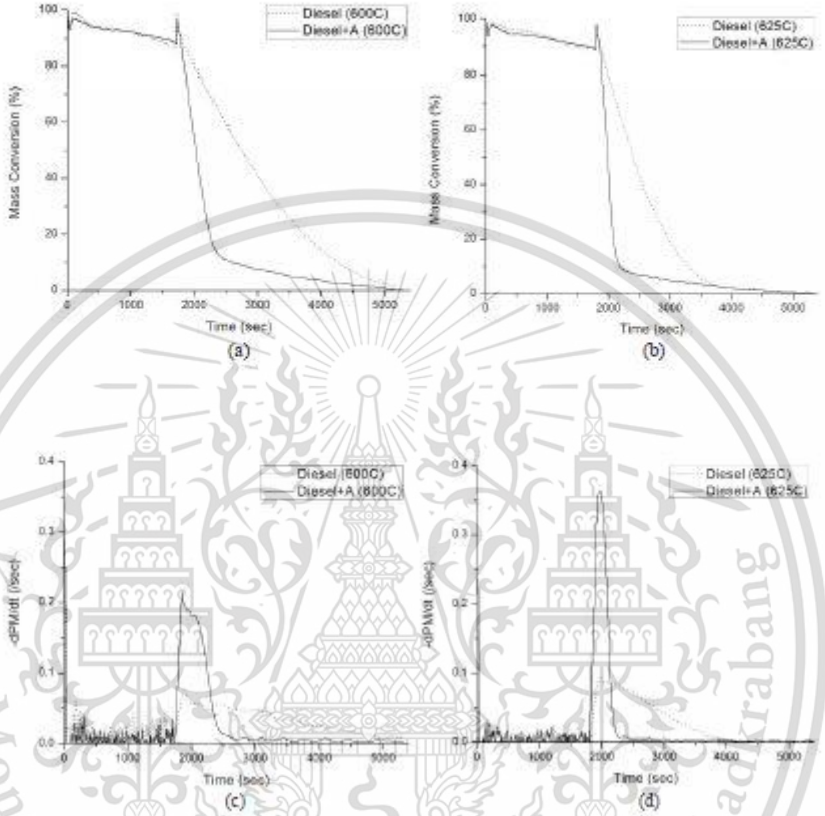

Fig. 4 Thermogravimetric analysis of mass conversion graphs of diesel PM and diesel blending lube oil PM at (a) 600°C and (b) 625°C, mass conversion rate of diesel PM and diesel blending lube oil PM at (c) 600°C and (d) 625°C

calculated as mass conversion rate by using Eq.2, where C is represented as PM mass, t is time, n and m are reaction order of PM and oxygen during oxidation process.

$$C + O_2 \rightarrow CO_2 \quad (1)$$

$$-\frac{d[C]}{dt} = k[C]^n[O_2]^m \quad (2)$$

Regarding to thermogravimetric analysis results as described in figure 5 (a and b), particles from diesel blending lube oil condition (represented as Diesel+A) were easier to oxidize than neat diesel's particles. The unburned lube oil metallic additives might be participated as an oxidative catalyst resulting faster oxidation kinetics under both operating temperatures 600°C and 625°C. As shown in figure 5 (c and d), mass conversion rates were also calculated to mention sharply for the higher mass conversion rate of diesel blending lube oil PMs.

4. Conclusion and Discussion

Morphology of ultrafine agglomerate particles, different primary particle nanostructures of lube oil derived metal oxide ashes compared to diesel soot and also influence of incombustible metal oxide ashes on soot oxidation kinetics were briefly discussed. The agglomerate structure of ultrafine particles from diesel blending lube oil condition has not shown significant difference compared to agglomerated ultrafine particles from neat diesel condition. Nanostructure of primary soot particle is a spherical shape composed of curve line crystallites while the metal oxide ash has not shown a spherical shape composed of parallel straight line hatch patterns. Nanostructure of metal oxide ash is similar to the nature of common metals' nanostructures since these metal oxide ashes are also derived from unburned metallic additives of engine lubricating oil.

According to the chemical characterization results, PM from neat diesel condition composed mainly of carbon and oxygen as elemental composition while PM from diesel blending lube oil condition contained not only carbon and oxygen but also unburned metallic additives from engine lubricating oil. Particulate matters from diesel blending lube oil condition were easier to oxidize than PMs from neat diesel condition. Metallic additives from engine lubricating oil cannot be burned by engine combustion and it might be changed into metal oxide ash. These metal oxide ashes promote oxidation kinetics resulting faster mass conversion rate. Moreover, although accumulated metal oxide ashes tend to reduce effective filtration length of diesel particulate filters, on the other hand, these incombustible ashes might assist to promote the soot oxidation kinetics during regeneration process of diesel particulate filter.

5. Acknowledgement

The author would like to acknowledge to International College, King Mongkut's Institute of Technology Ladkrabang (KMITL) for research funding and also Bangchak Corporation (BCP) for supporting designed lubricating oil to accomplish this research.

6. References

[1] Peter Eastwood (2008). Particle Emission from Vehicles, John Wiley & Sons, Ltd. England.

[2] Myung, C. L. and Park, S. (2012). Exhaust Nanoparticle Emissions from Internal Combustion Engines: A Review, International Journal of Automotive Technology, Vol. 13, No.1, pp.9-22.

[3] Mohankumar, S. and Senthilkumar, P. (2017). Particulate Matter Formation and its Control Methodologies for Diesel Engine: A Comprehensive Review, Renewable and Sustainable Energy Reviews, Vol. 80, pp.1227-1238.

[4] Myung, C. L. Ko, A. and Park, S. (2014). Review on Characterization of Nano-particle Emissions and PM Morphology from Internal Combustion Engines: Part 1, International Journal of Automotive Technology, Vol. 15, No. 2, pp. 203-218.

[5] Leslie R. Rudnick (2008), Lubricant Additives Chemistry and Applications, Taylor & Franscis Group, London, New York.

[6] Tornehed, P. and Olofsson, U. (2011). Lubricant Ash Particles in Diesel Engine Exhaust: Literature Review and Modelling Study, Proceedings of the Institution of Mechanical Engineers, Journal of Automotive Engineering, Vol. 225, Part D, pp. 1055-1066.

[7] Karin, P. Oki, H. Hanamura, K. and Charoenphonphanich, C. (2012). Nanostructures and Oxidation Kinetics of Diesel Particulate Matters, Journal of Research and Applications in Mechanical Engineering, Vol. 1, No.2, pp. 3-8.

[8] Liati, A. Dimopoulos Eggenchwiler, P. Müller Gubler, Schreiber, D. Aguirre, M. (2012). Investigation of Diesel Ash Particulate Matter: A Scanning Electron Microscope and Transmission Electron Microscope Study, Atmospheric Environment, Vol. 49, pp. 391-402.

[9] Vouitsis, E. (2007). Effect of Lube Oil on the Physicochemical Characteristics of Particulate Matter Emitted from a Euro 4 Light Duty Diesel Vehicle, SAE Technical Paper 2007-24-0110.

[10] Karin, P. Supanamok, C. Hanamura, K. (2016). Impact of Soot on Metal Wear Characteristics using Laser Diffraction Spectroscopy, Journal of Research and Applications in Mechanical Engineering, Vol. 4, No.2, pp. 126-134.

[11] Tan, P. (2017). Effect of Lubricant Sulphur on the Morphology and Elemental Composition of Diesel Exhaust Particles, Journal of Environmental Sciences, pp. 354-362.

[12] Wang, Y. Liang, X. Shu, G. Dong, L. Sun, X. Yu, H. Wang, Y. (2015). Effects of an Anti-wear Oil Additive on the Size Distribution, Morphology, and Nanostructure of Diesel Exhaust Particles, Tribology International, Vol. 92, pp. 379-386.

[13] Karin, P. (2015). Oxidation Kinetics of Small CI Engine's Biodiesel Particulate Matter, International Journal of Automotive Technology, Vol. 16, No.2, pp. 211-219.

[14] Karin, P. (2017). Morphology and Oxidation Kinetics of CI Engine's Biodiesel Particulate Matters on Cordierite Diesel Particulate Filters using TGA, International Journal of Automotive Technology, Vol. 18, No.1, pp. 31-40.

[15] Jung, H. 2003. The Influence of Engine Lubricating Oil on Diesel Nanoparticle Emissions and Kinetics of Oxidation, SAE Technical Paper 2003-01-3179.

JSAE 20199226
SAE 2019-YY-YYYY

Impact of Engine Oil Additives on Nanostructure and Oxidation Kinetics of Diesel and Synthetic Biodiesel Particulate Matters using Electron Microscopy

Phyozin Koko, Preechar Karin, Chinda Charoenphonphanich
King Mongkut's Institute of Technology Ladkrabang

Nuwong Chollacoop
National Science and Technology Development Agency

Katsunori Hanamura
Tokyo Institute of Technology

ABSTRACT

Physicochemical characteristics of particulate matters which are influenced by engine oil additives from engine combustion of diesel and synthetic biodiesel: hydrotreated vegetable oil (HVO) were successfully investigated using electron microscopy, electron dispersive x-ray spectroscopy and thermogravimetric analysis. The agglomerate structure of diesel PM, HVO PM and diesel blending lubricant PM are similar in micro- scales. However, nanostructure of soot is a spherical shape composed of curve line crystallites while the metal oxide ash nanostructure is composed of parallel straight line hatch patterns. The oxidation kinetics of fuel blending lubricant PMs are higher than neat fuel PMs due to catalytic effect of incombustible metal additives from engine lubricating oil.

INTRODUCTION

Among internal combustion engines used in automotive vehicles, diesel engine has higher thermal efficiency due to its higher compression ratio. On the other hand, diesel engines trail black smokes containing much amount of particulate matter (PM) which are derived from incomplete combustion around single fuel droplets during spraying the fuel inside the engine cylinder. Diesel particulate matters are harmful to human health and must be removed owing to increasingly stringent emission regulations. PM are mainly composed of solid fraction (soot and ash) and soluble organic fraction (sulfates and nitrates organic compounds). Each PM morphology and chemical composition are commonly varied by the engine operating conditions, fuel properties and types of lubricating oil [1, 2]. As an after-treatment emission control system, diesel particulate filters (DPF) can be used to trap the particulate matters effectively. Inside DPF, honeycomb shape rectangular channels made up of silicon carbide (SiC) or Cordierite ceramic materials. Exhaust gas containing (PM, CO and HC) enter into the DPF's inlet channel and passing through the channel wall and exit to the atmosphere through the outlet channel. When the exhaust gas passing through the channel wall, PM must be trapped at the wall surface. The trapped PM must be burned out by the chemical oxidation process called DPF regeneration process. Although regeneration process can burn the soot efficiently, incombustible metal oxide ashes will be remained along the inlet channel over time and causing engine back pressure [3, 4].

Many literatures have been reported about morphology and quantity of particulate matters from the engine combustion of diesel and various alternative fuels. The quantity of particulate emission is increased by higher engine load conditions. Besides, the number of particles is decreased in biodiesel combustion due to presence of oxygenated molecules. The sizes of single primary nanoparticles are in the range of (10 – 60) nm [5 – 7]. Regarding to decrease the consumption of fossil diesel and reduce the particulate emission, a synthetic biodiesel: hydrotreated vegetable oil (HVO) is presented as a second generation of biodiesel which is the absence

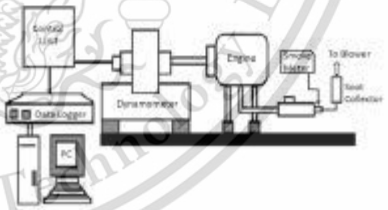

Fig. 1. Schematic diagram of engine setup

of oxygenated molecules. Combustion behaviors, exhaust gases and particulate emissions of HVO fuel are much better due to its higher cetane number and heating value compared to conventional diesel [8 – 11]. During engine combustion inside the cylinder, lubricant oil can also participate in the combustion process. Engine lubricating oil are basically formulated with base oil and metal additives.

Table 1. Engine specifications

Items	Details
Engine Type	1-cylinder, Direct Injection, CI engine
Bore x Stroke	(97 x 96) mm
Displacement	709 cm^3
Compression ratio	18:1
Power	9.2 kW @2400 RPM
Injection Timing	19°CA bTDC
Injection Pressure	22 MPa

Table 2. Properties of test fuels

Properties	Diesel	HVO
Chemical formula	$C_{14.11}H_{26.23}$	$C_{14.22}H_{29.96}$
Density @30°C (g/cm^3)	0.824	0.778
Kinematic viscosity @40°C (mm^2/s)	3.24	2.64
Carbon content (%)	85.73	84.24
Hydrogen content (%)	13.22	15.05
Oxygen content (%)	0.00	0.00
Cetane index	60.43	76.89
Distillation T10 (°C)	207.7	227.4
Distillation T50 (°C)	287.9	279.2
Distillation T90 (°C)	352.3	293.2
Auto ignition temperature (°C)	288	288

Table 3. Properties of blending lubricant

Test	Units	Result
Density @15°C	g/mL	0.896
Density @30°C	g/mL	0.8866
Viscosity @40°C	mm²/s	154.8
Viscosity @100°C	mm^2/s	15.05
Calcium	PPM	1942
Phosphorous	PPM	757
Zinc	PPM	845
Silicon	PPM	5.6

According to the contamination of lubricant in engine combustion, not only morphology and size distribution but also chemical composition of particulate matters can be affected [12 – 17]. Oxidation kinetics of each PMs are dependent upon shape of reactant substance, chemical composition and operating atmosphere. The impact of metallic elements which are originated from dosed lube oil were also investigated and determined activation energy by using Arrhenius equations [18, 19].

This research investigates on physical and chemical characterization of particulate matters which are influenced by lubricant additives. Morphologies and different nanostructures of soot and metal oxide ash were mainly compared which are still a few numbers of research in current literatures. Thermogravimetric analysis (TGA) of neat fuel PMs and fuel blending lube oil PMs were also investigated to describe the impact of metal oxide ash on soot oxidation kinetics.

METHODOLOGY

ENGINE SETUP

A single cylinder direct injection compression ignition (CI) engine was used to generate the PM. Specifications of engine are shown in Table 1. Eddy current engine dynamometer was used to control the desired engine speed and load conditions by using lab-view program. Opacity smoke meter (Okuda DSM – 240) was used to measure the soot contamination from the exhaust gas by passing through the filter paper under each various engine speed and load conditions. A soot collector with metal netting was installed at the outlet of exhaust muffler to collect the PM powder. The schematic diagram of engine setup is described in figure 1.

TEST FUELS

Conventional diesel and hydrotreated vegetable oil (HVO) were used as ideal fuels. Designed lubricating oil including excess amount of additives supported by Bangchak Corporation (BCP) was blended by the amount of (10%) by mass directly into the diesel and HVO fuels respectively. Chemical properties of test fuels and blending lubricating oil properties are shown in Table 2 and 3 respectively. Blending lube oil is the designed lubricant which is supported by Bangchak Corporation (BCP) containing excess amount of Calcium as a composition of 1942 parts-per-million (PPM). The purpose of blending lubricating oil with excess additives directly into the fuels is to investigate the physicochemical characteristics of metal oxide ash by promoting the composition of ash in particulate matters since these metal oxide ashes are mainly originated from engine oil additives. For the lubricating system, conventional engine oil 15W – 40 API CI-4/SL synthetic engine oil was used.

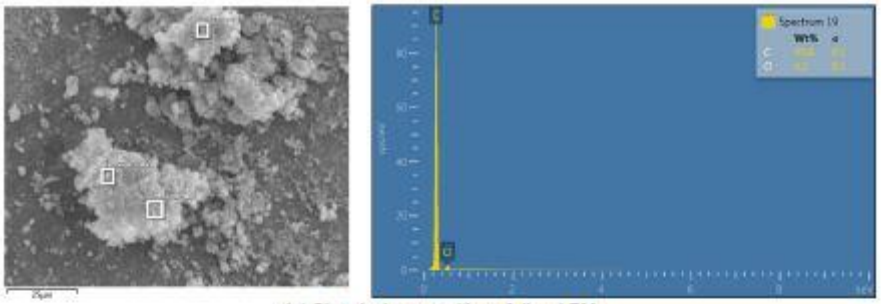

(a) Chemical composition of diesel PM

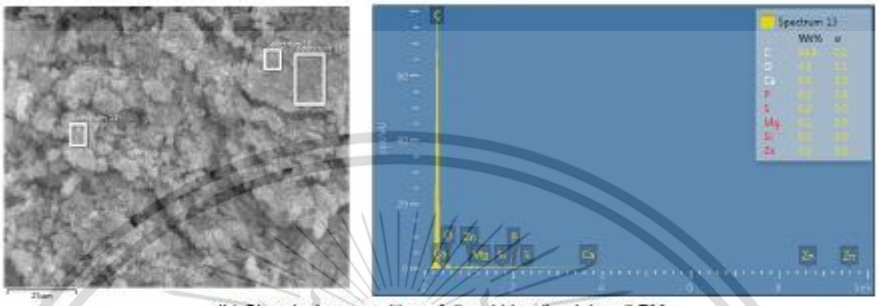

(b) Chemical composition of diesel blending lube oil PM

Fig. 2 Chemical composition of (a) diesel PM (b) diesel-L PM trapped by paper filter using SEM-EDS

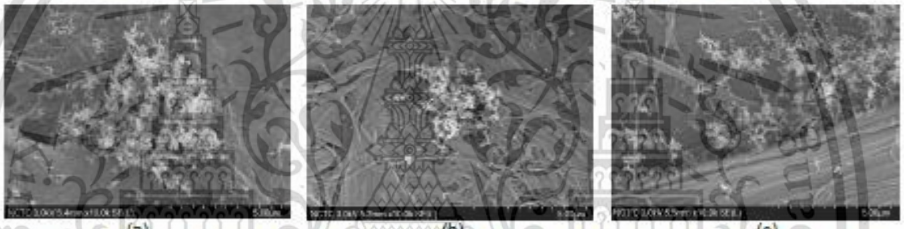

(a) (b) (c)

Fig. 3 SEM images of agglomerate structure of particulate matters (PM 2.5) and (PM 10) from the engine combustion of (a) diesel (b) HVO (c) diesel-L under 2000 rpm engine full load condition

THERMOGRAVIMETRIC ANALYSIS

A TGA instrument (NETZSCH STA 449F5) was used to investigate the oxidation kinetics of particulate matters. PM powder sample is placed inside the aluminum oxide crucible pan and the sample weight is about 2 milligrams for each condition. PM powders were oxidized isothermally and maintained the operating temperature at 575°C under pure air and pure oxygen atmospheres. Samples were heated until reaching desired operating temperature (575°C) about 30 minutes with nitrogen atmosphere to vaporize water and volatile organic matters. Then, oxygen was uniformly injected to initiate the oxidation process for an hour. Oxidation mass conversion data were collected between each 3 seconds using top loading balance system.

RESULTS AND DISCUSSION

ELECTRON MICROSCOPY AND ELECTRON DISPERSIVE X-RAY SPECTROSCOPY

Diesel PM and diesel blending lube oil PM trapped by paper filter were investigated using electron dispersive x-ray spectroscopy (SEM-EDS). As shown in figures 2, diesel PM is mainly composed of carbon while diesel blending lube oil PMs contain not only carbon but also additional metallic elements such as Calcium (Ca), Phosphorous (P), Sulfur (S), Magnesium (Mg), Silicon (Si) and Zinc (Zn) which all are derived from lubricant additives. Therefore, SEM-EDS results confirmed that the metallic additives from engine lubricating oil cannot be burned out by engine combustion.

Trapped soot on the paper filter were observed under scanning electron microscope and (10k) magnification was introduced to compare the agglomerate microstructures of particulate matter. According to SEM image described in figures 3, the agglomerate structures of HVO PM and diesel blending lube oil PM have not shown significant different compared to diesel PM in microscales. Transmission Electron Microscopy (TEM) was conducted to investigate the ultrafine agglomerate particles. Soot powders were collected by soot collector and the engine was operated at 2400 rpm under full engine load condition. Figures 4 show the ultrafine agglomerate structure of diesel PMs, HVO PMs and diesel blending lube oil PMs. Single primary particles were connected each other with similar morphologies to become agglomerate particles. Regarding to electron microscopy, morphology and agglomerate structures of particulate matters from diesel, HVO and diesel blending lube oil conditions are similar. Figures 5 compare the nanostructures of single primary particulate matters. The nanostructure of soot from both diesel and HVO fuel described in figure 5 (a and b) are spherical shapes composed of curve line crystallites. PMs derived from fuel blending lubricant condition are briefly described in figures 5 (c and d).

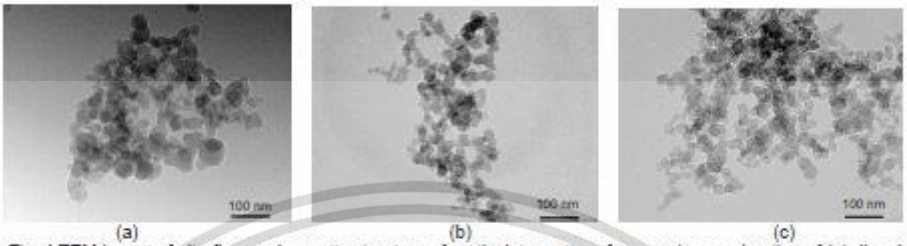

Fig. 4 TEM image of ultrafine agglomerate structure of particulate matters from engine combustion of (a) diesel (b) HVO (c) diesel-L under 2400 rpm engine full load condition

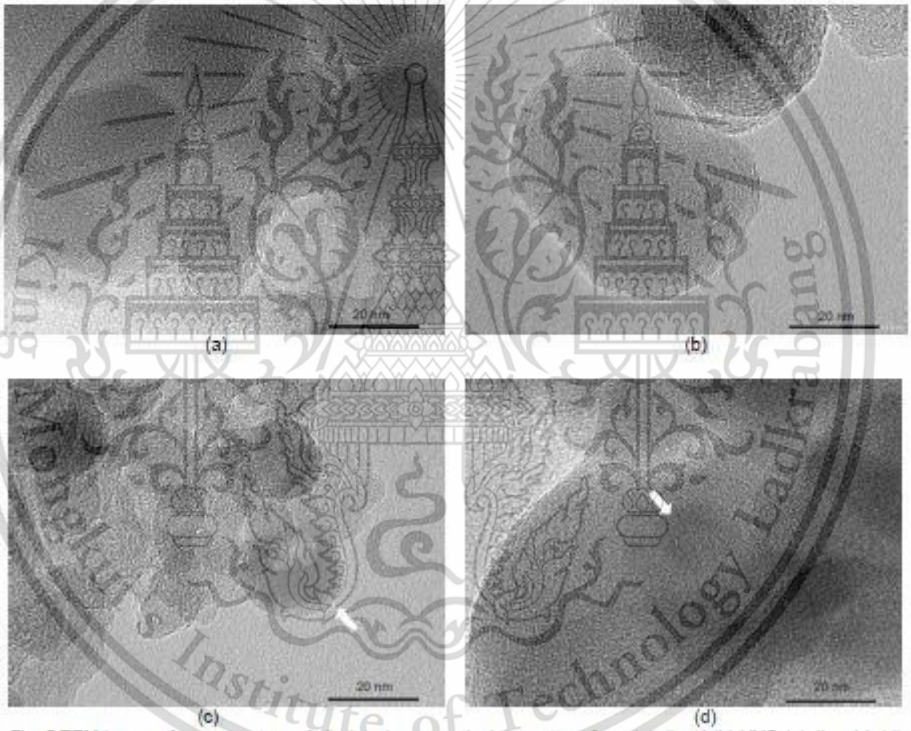

Fig. 5 TEM image of nanostructure of single primary particulate matters from (a) diesel (b) HVO (c) diesel-L (d) HVO-L under 2400 rpm engine full load condition

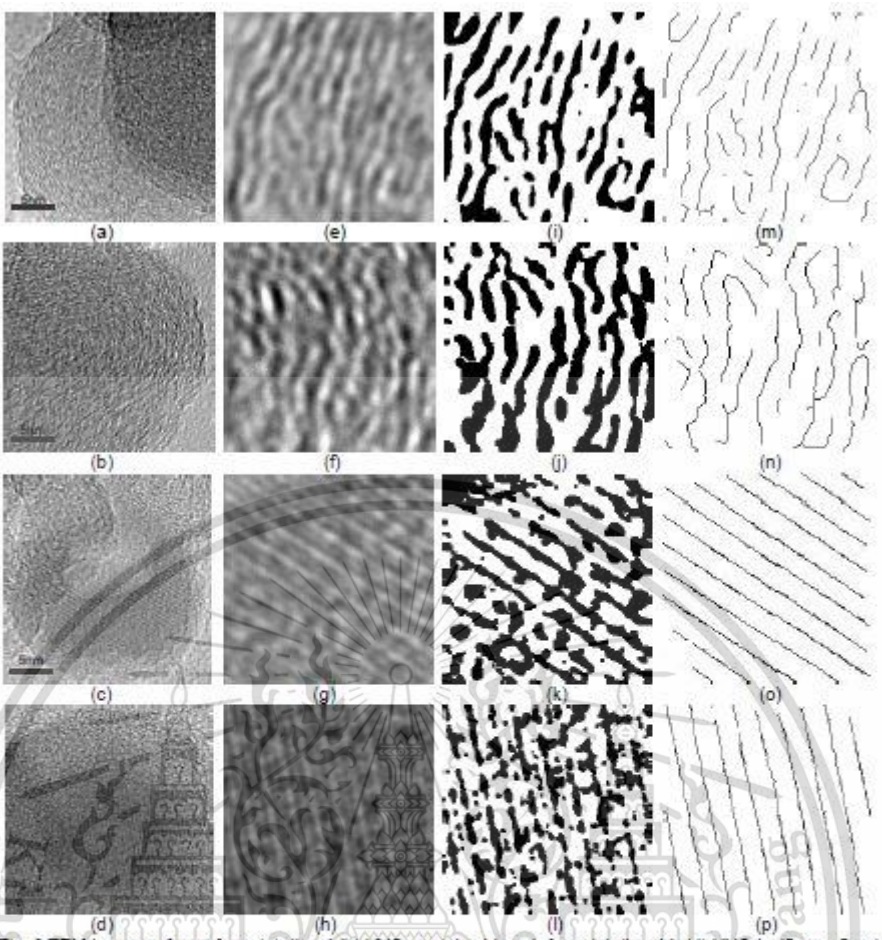

Fig. 6 TEM images of soot from (a) diesel (b) HVO, metal oxide ash from (c) diesel-L (d) HVO-L, (5nm x 5nm) cropped images of soot from (e) diesel (f) HVO, metal oxide ash from (g) diesel-L (h) HVO-L, black and white binary images of soot from (i) diesel (j) HVO, metal oxide ash from (k) diesel-L (l) HVO-L, skeletonized images of spot from (m) diesel (n) HVO, metal oxide ash from (o) diesel-L and (p) HVO-L

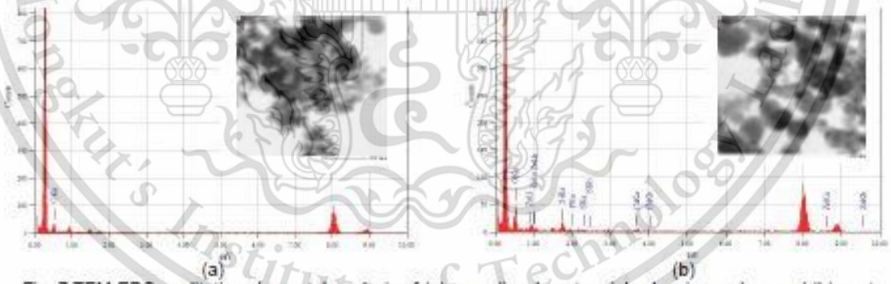

Fig. 7 TEM-EDS qualitative elemental analysis of (a) pure diesel soot mainly showing carbon and (b) soot mixed with metal oxide ash showing carbon and incombustible metallic additives

Table 4. Quantitative elemental analysis of PM nanoparticles using TEM-EDS

	Composition (%)	
Element	Diesel	Diesel-L
C	99.208	97.243
O	0.792	1.386
Si	-	1.32
P	-	0.001
S	-	0.021
Ca	-	0.036
Zn	-	0.003

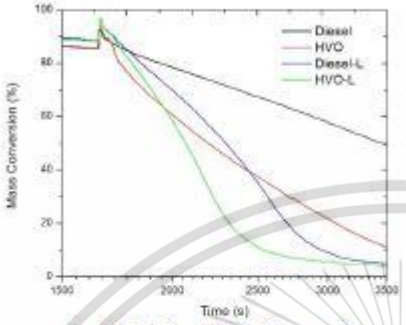

Fig. 8 Oxidation of PM with pure air

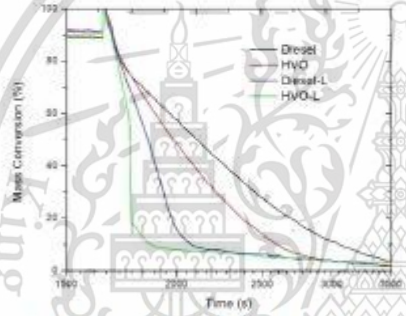

Fig. 9 Oxidation of PM with pure oxygen

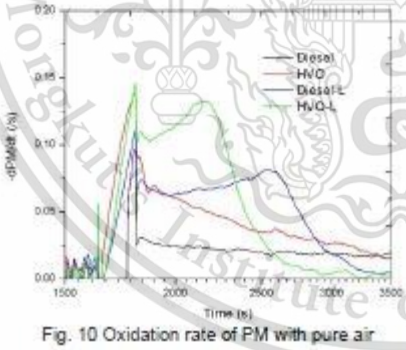

Fig. 10 Oxidation rate of PM with pure air

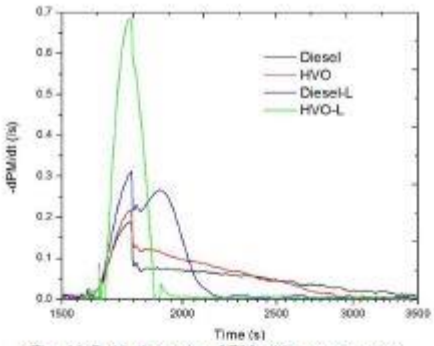

Fig. 11 Oxidation rate of PM with pure oxygen

Due to blending lube oil into fuel, metal oxide ash showing parallel straight-line hatch patterns with round outlines are combined with soot. These metal oxide ashes are mainly derived from metal additives of engine lubricating oil. The diameters of single primary nanostructure of metal oxide ashes are in the range of 10-30 nm while single soot nanostructure is in the range of 10-60 nm. To investigate the different crystallite structure of soot and metal oxide ash, TEM images were cropped into (5nm x 5nm) scales and changed into black and white images and finally into skeletonized images by the aid of ImageJ software as shown in figures 6. The skeletonized images of soot are composed of curve line carbon fringe crystallites while the ash shows parallel straight-line hatch patterns. Inter-planer spacing of both soot and metal oxide ash crystallites are approximately 0.35 nm. The elemental composition of particulate matters from neat diesel condition and diesel blending lubricant condition were analyzed using TEM-EDS. Regarding to the qualitative analysis of EDS, the electron beam is exerted onto the particles and determined the elements according to x-ray energies. As described in figures 7 (a), pure diesel soot is composed mainly of carbon. However, particles from blending lube oil condition as in figure 7 (b) contain not only carbon but also unburned metallic additive elements. Regarding to thermogravimetric analysis of PM oxidation, soluble organic fraction (less than 10% of total sample) were heated and vaporized with nitrogen atmosphere before the oxidation process occurs. From CHNS/O analysis, chemical composition percentage of carbon, oxygen and hydrogen were (92.87%, 5.62% and 1.51%) respectively. Quantitative elemental analysis of PM nanoparticles was also conducted to analyze the elemental composition of nanoparticles using TEM-EDS. Elemental composition percentage for both diesel and diesel blending lube oil PMs are described in table 4. According to TEM-EDS quantitative elemental analysis, diesel PM mainly contain carbon while diesel blending lube oil (Diesel-L) PM contains higher Calcium (Ca) composition compared to other unburned metal additives elements such as Phosphorous (P), Zinc (Zn) and Sulfur (S) due to blending the designed lube oil with excess Ca additives.

OXIDATION KINETICS OF PARTICULATE MATTERS

Figure 8 and 9 briefly describe the oxidation kinetics of diesel PM, HVO PM, diesel blending lube oil PM and HVO blending lube oil PM (indicating as Diesel, HVO, Diesel-L and HVO-L). During oxidation, oxygen was start injected uniformly when the sample was heated using nitrogen atmosphere until reaching desired temperature (i.e. 575°C). Different oxidation kinetics of PM mass conversion can be observed according to different atmosphere conditions. PMs from pure oxygen atmosphere show higher oxidation rate compared to pure air atmosphere in which injected oxygen compart as one of the most important parameters during oxidation. HVO PMs were easier to oxidize than diesel PM in both pure air and oxygen atmospheres. Different fuel properties might generate PM with different chemical composition, morphology and nanostructure which is strongly affect on oxidation kinetics. Unlike conventional diesel fuel, PM derived from paraffinic properties of HVO fuel might be easier to oxidize. In fact, HVO fuel contains no aromatics, lower fuel density and higher cetane number. PMs from both fuel blending lube oil conditions were faster oxidation kinetics than PMs from neat fuel conditions. Electron microscopy analysis proved that PMs from fuel blending lube oil condition contain metal oxide ash which are derived from unburned metal additives of lubricating oil. The impact of contamination of incombustible metal oxide ashes might promote oxidation rate acting as catalysts on soot oxidation kinetics. Faster oxidation rate of ash catalytic PM from fuel blending lube oil conditions under pure oxygen and pure air atmospheres can be interpreted by mass conversion rate as shown in figures 10 and 11.

CONCLUSIONS

Physicochemical characterization of engine oil additives contamination on particulate emissions such as morphology, nanostructure, chemical composition and oxidation kinetics were briefly discussed. According to electron microscopy, the agglomerate micro- structures and ultrafine particles of diesel PM, HVO PM and diesel blending lube oil PM are not significant different. Skeletonized images were clearly described that the nanostructure of soot from diesel and HVO are spherical shapes composed of curve line crystallites while the metal oxide ashes are composed of parallel straight-line hatch patterns. Chemical elemental analysis from SEM-EDS and TEM-EDS confirmed that the metal additives from the lubricant cannot be burned by engine combustion and might be transformed into metal oxide ashes. Regarding to thermogravimetric analysis, soot oxidation rate was increased due to the contamination of metal oxide ashes acting as catalyst on soot oxidation kinetics.

ACKNOWLEDGEMENTS

The author would like to greatly acknowledge to Thailand Research Fund (TRF) for research funding and Bangchak Corporation (BCP) for supporting designed lubricant to accomplish this research.

REFERENCES

[1] J. B. Heywood. (1998). Internal Combustion Engine Fundamentals, McGraw-Hill series in mechanical engineering, Singapore.

[2] Peter Eastwood. (2008). Particle Emission from Vehicles, John Wiley & Sons, Ltd, England.

[3] C. L. Myung and S. Park (2012). Exhaust Nanoparticle Emissions from Internal Combustion Engines: A Review, International Journal of Automotive Technology, Vol. 13, No.1, pp.9-22.

[4] C. L. Myung, A. Ko and S. Park. (2014). Review on Characterization of Nano-particle Emissions and PM Morphology from Internal Combustion Engines: P-1, International Journal of Automotive Technology, Vol. 15, No. 2, pp. 203-218.

[5] P. Karin, J. Boonsakda, K. Siricholathum, E. Saenkhumvong, C. Charoenphonphanich and K. Hanamura. (2017). Morphology and Oxidation Kinetics of CI Engine's Biodiesel Particulate Matters on Cordierite Diesel Particulate Filters using TGA, International Journal of Automotive Technology, Vol. 18, No. 1, pp. 31-40.

[6] P. Karin, P. Watanawongskorn, J. Boonsakda, E. Saenkhumvong, S. Rungsritanapaisan, S. Srivarocha, C. Charoenphonphanich, N. Chollacoop, K. Hanamura. (2017). Impact of Biodiesel on Small CI Engine Combustion Behavior and Particle Emission Characteristics, SAE Technical Papers, 2017-32-0094.

[7] P. Karin, C. Supanamok, K. Hanamura. (2008). Impact of Soot on Metal Wear Characteristics using Laser Diffraction Spectroscopy, Journal of Research and Applications in Mechanical Engineering, Vol. 4, No.2, pp. 126-134.

[8] N. Soo-Young. (2014). Application of Hydrotreated Vegetable Oil from Triglyceride Based Biomass to CI Engines – A review, Fuel, Vol. 115, pp. 88-96.

[9] S. Marasri, P. Ewphun, P. Srichai, S. Saeo, V. Tan Chau, C. Charoenphonphanich, P. Karin, M. Tongroon, H. Kosaka. (2017). Experimental Investigation on Spray combustion Characteristis of Hydrotreated Vegetable Oil (HVO)-Diesel Blends in Constant Volume Combustion Chamber (CVCC), JSAE Technical Papers, 20175375.

[10] S. Rungsritanapaisan, P. Ewphun, P. Karin, S. Sato, H. Kosaka, N. Chollacoop. (2018). Characterization of Hydro-treated Vegetable Oil Combustion Behavior and Particle Emission Nanostructure, JSAE Technical Papers, 20185030.

[11] H. Aatola, M. Larmi, T. Sarjovaara, S. Mikkonen. (2008). Hydrotreated Vegetable Oil (HVO) as a

Renewable Diesel Fuel: Trade-off between NOx, Particulate Emission and Fuel Consumption of a Heavy-Duty Engine, SAE Technical Papers, 2008-01-2500.

[12] Leslie R. Rudnick. (2008), Lubricant Additives Chemistry and Applications, Taylor & Franscis Group, London, New York.

[13] Y. Wang, X. Liang, G. Shu, L. Dong, X. Sun, H. Yu. (2015). Effects of an Anti-wear Oil Additive on the Size Distribution, Morphology, and Nanostructure of Diesel Exhaust Particles, Tribology International, Vol. 92, pp. 379-386.

[14] Y. Wang, X. Liang, G. Shu and L. Dong. (2015). Impact of Lubricating Oil on Morphology of Particles from a Diesel Engine, Energy Procedia, Vol.75, pp. 2388-2393.

[15] A. Liati, P. Dimopoulos Eggenchwiler, D. Müller Gubler, Schreiber, M. Aguirre. (2012). Investigation of Diesel Ash Particulate Matter: A Scanning Electron Microscope and Transmission Electron Microscope Study, Atmospheric Environment, Vol. 49, pp. 391-402.

[16] P. Karin, H. Oki, K. Hanamura, C. Charoenphonphanich. (2012). Nanostructures and Oxidation Kinetics of Diesel Particulate Matters, Journal of Research and Applications in Mechanical Engineering, Vol. 1, No.2, pp. 3-8.

[17] Y. Wang, X. Liang, X. Wang. (2014). Effect of Lubricating Oil Additive Package on the Characterization of Diesel Particles, Applied Energy, Vol. 136, pp. 682-691.

[18] P. Karin (2015). Oxidation Kinetics of Small CI Engine's Biodiesel Particulate Matter, International Journal of Automotive Technology, Vol. 16, No.2, pp. 211-219.

[19] H. Jung (2003). The Influence of Engine Lubricating Oil on Diesel Nanoparticle Emissions and Kinetics of Oxidation, SAE Technical Paper 2003-01-3179.

CONTACT

Preechar Karin, D.Eng.

King Mongkut's Institute of Technology Ladkrabang, Bangkok 10520, Thailand.

Email: kkpreech@staff.kmitl.ac.th, preechar.ka@kmitl.ac.th

ABBREVIATIONS

ASTM: American Society for Testing and Materials

Diesel-L: Diesel blending lubricating oil

EDS: Electron Dispersive X-ray Spectroscopy

HVO: Hydrotreated Vegetable Oil

HVO-L: HVO blending lubricating oil

SEM: Scanning Electron Microscopy

TEM: Transmission Electron Microscopy

TGA: Thermogravimetric analysis

JSAE Paper Number: 20199226

APPENDIX D :

Revised Questions and Answers

Questions by Prof. Dr. Katsunori Hanamura

Q1. How to confirm the reaction mechanism? How to measure adsorption and desorption of oxygen vacancy by using this idea? Why and what kind of catalytic impact (physical/chemical) might be possible?
(Same question with Dr. Ruangdaj Tongsri)

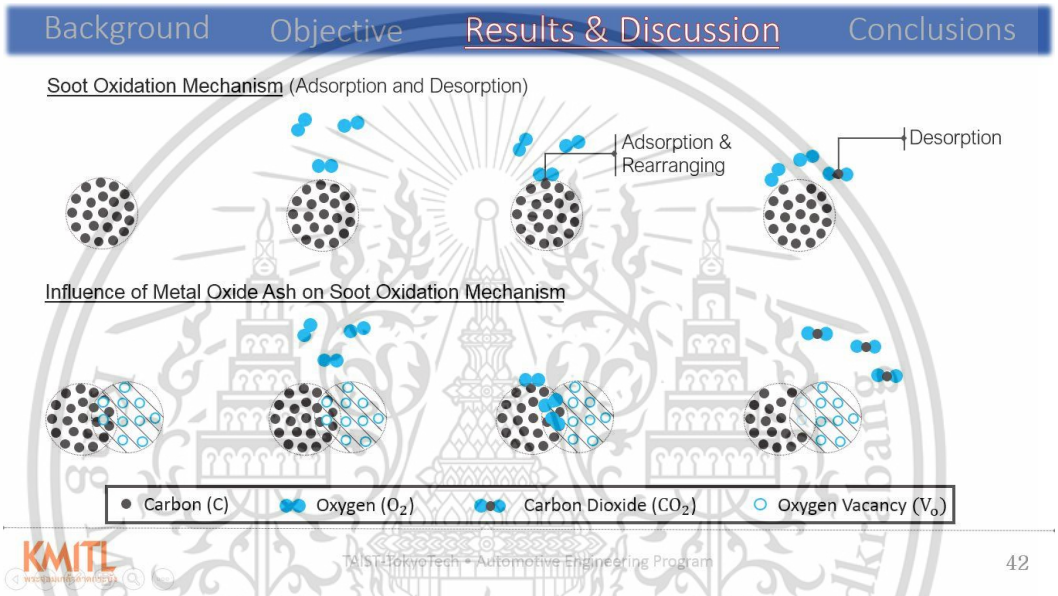

Revised answer

By using only the information of TEM image, specific explanation for the reaction mechanism may not be enough. Therefore, the articles about this mechanism would be removed in thesis book and replaced by some possible catalytic mechanisms of metal oxides from literature which is reviewed by J. Uchisawa et al. [1] as described in figure 1.

In this literature, the author reviewed among catalytic reactions on various metal oxides by summarizing with (3) common mechanisms. In mechanism (1), active oxygen is released from the lattice by redox reaction of CeO_2 and carbon from soot. Regarding to activity series, carbon (C) is more active than cerium (Ce). Therefore, oxides from CeO_2 can be diffused into carbon as active oxygen. In mechanism (2), oxygen molecules from supply gas are dissociative adsorbed on metal oxide surface, move onto the soot surface and reacts with soot. In mechanism (3), active oxygen species (O_2^-) are formed on surface oxygen vacancy sites generated by the reduction of

CeO_2 and the vacancies can accept the oxygen molecules from supplied gas then oxidize the soot. Moreover, the phenomena of oxygen vacancy from mechanism (3) is mainly based on solid-gas reaction of Mars-Van Krevelen mechanism.

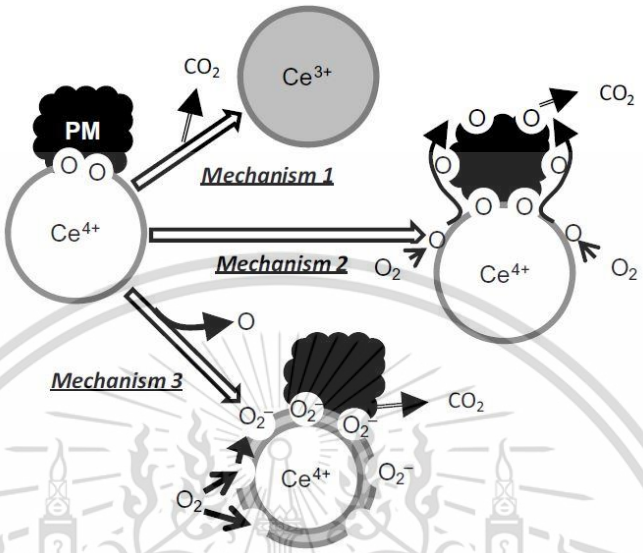

Fig. 1 Three possible catalytic effect of metal oxide on soot oxidation [1].

Q2. How much sulfur composition is included in designed lubricating oil?

Revised answer

The composition of sulfur (%Wt.) is added in designed lubricant properties as shown in table 1.

Table 1. Chemical properties of designed lubricating oil

Test	Units	Result
Density @30°C	g/mL	0.8866
Viscosity @40°C	mm^2/s	154.8
Viscosity index	-	97
Sulfur	%Wt.	0.411
Magnesium	PPM	1190
Calcium	PPM	1942
Phosphorous	PPM	757
Zinc	PPM	846
Silicon	PPM	5.6

Q3. What is the reason for lower activation energy of HVO PM compared to diesel PM?

Revised answer

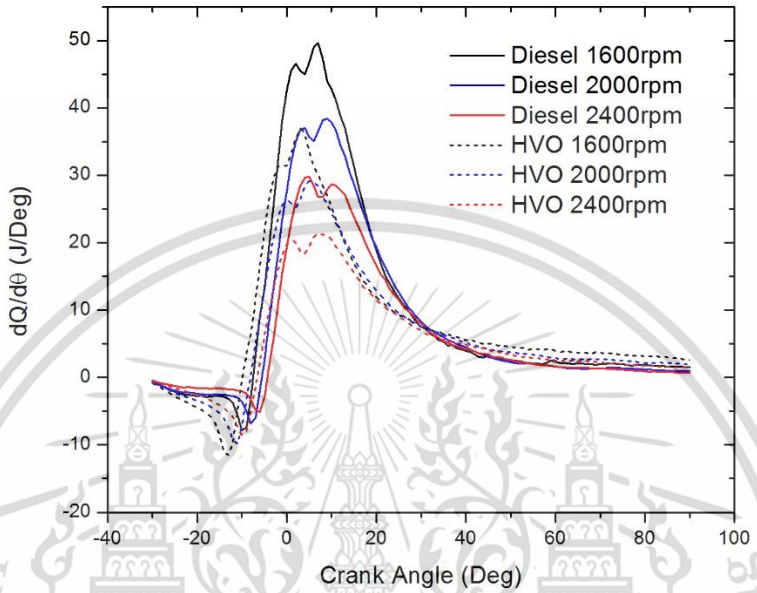

Fig. 2 Heat release rates of diesel and HVO fuel combustion

According to fuel distillation tests of diesel and HVO, HVO fuel is composed of lower fuel molecules than diesel fuel. As shown in figure 2, HVO fuel combustion has lower combustion temperature than diesel fuel combustion due to lower fuel molecules of HVO which might be leading to better fuel atomization and greater fuel vaporization. Furthermore, HVO PMs that are derived from lower combustion temperature might be easier to oxidize than diesel PMs because the particles derived from higher combustion temperature might become more dense than that of lower combustion temperature.

Different fuel properties might generate PMs with different chemical composition, morphology and nanostructure which is strongly related to soot oxidation kinetics. Unlike conventional diesel fuel, PM derived from paraffinic properties of HVO fuel might be easier to oxidize. Therefore, the oxidation kinetics of HVO PMs were faster than diesel PMs and apparent activation of diesel PMs and HVO PM were 155 kJ/mol and 141 kJ/mol respectively.

Suggestions by Prof. Dr. Katsunori Hanamura

1. To explain clearly about that the experiment is accelerated ash experiment in order to investigate the physical and chemical characteristics of metal oxide ash which are mainly derived from engine oil additives.

2. To mention clearly about the collected PM were passed through diesel oxidation catalyst (DOC) or not.

3. If possible, please describe the composition of sulfur from designed lubricant.

References

[1] Uchisawa, J. et al. (2015). Soot Oxidation in Particulate Filter Regeneration. Handbook of Advanced Methods and Process in Oxidation Catalysts. pp. 25 – 50.

Questions by Dr. Ruangdaj Tongsri

Q4. How to confirm the experimental result of soot oxidation kinetics with and without ash?

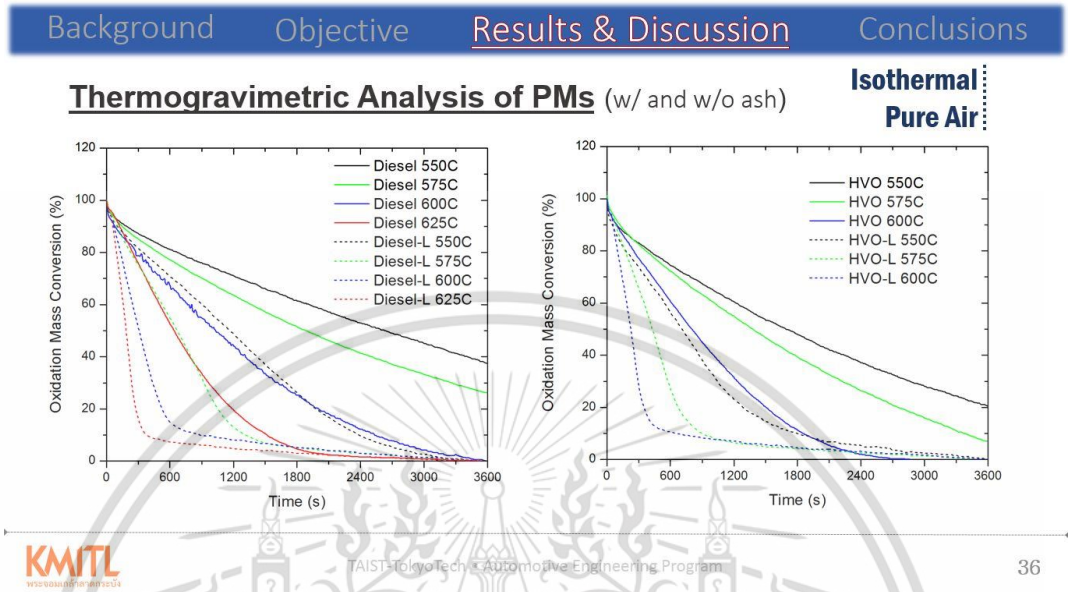

Revised answer

Soot oxidation kinetics, dPM/dt is dependent upon operating temperature, physical and chemical impacts as discussed in equation 1. Physical impact is the size of particulate matter and it is also termed as pre-exponential factor (Ln A). As physical size (Ln A) is increased, oxidation rate would be increased since larger surface area can be reacted with gas molecules. On the other hand, the amount of oxygen either from test sample or injected oxygen molecules during TGA experiment would become chemical impact. The more oxygen is composed, higher soot oxidation kinetics would be achieved.

$$\ln\left[\frac{-1}{[PM]^n}\frac{dPM}{dt}\right] = \frac{-E_a}{RT} + \ln A + m\ln[O_2] \quad (1)$$

TEM image and TEM-EDS results confirmed that diesel blending lube oil PM (indicating as Diesel-L) were composed of metal oxide ashes which are mainly originated from unburned engine oil additives. These ashes are capable to adsorb more injected oxygen molecules from the supply gas due to their catalytic properties of metal oxides as discussed in figure 1. Therefore, faster oxidation mass conversion result in

the case of Diesel-L condition (i.e. with ash condition) might be more influenced by chemical impact.

Questions by Asst. Prof. Dr. Chinda Charoenphonphanich

Q5. What is the purpose of comparison between interlayer spacing of soot and lattice spacing of metal oxide ash?

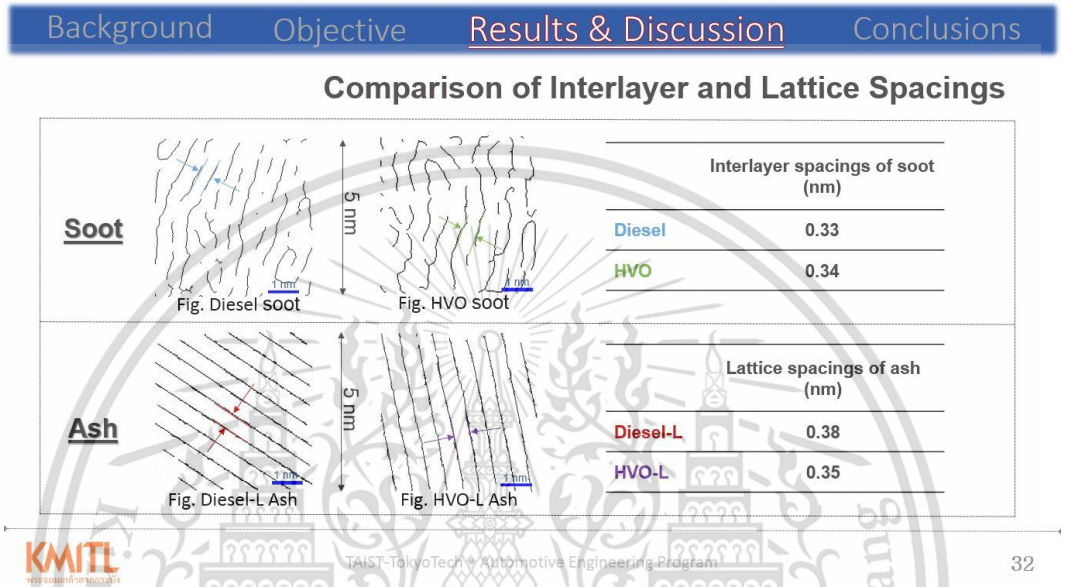

Revised answer

Analysis of soot interlayer spacing between each curve-lined carbon fringes in nanometer scales would be useful to estimate the density (g/cm^3) of the soot. The information of estimated soot density would be applicable to be considered in soot oxidation kinetics, soot trapping mechanism for diesel particulate filter and mechanism of engine wear due to soot contamination inside engine oil. Fringe length distribution, number of fringes per unit volume and interlayer spacing between each fringes are important parameters to determine the density of the soot.

In metal oxide materials, the information of lattice spacing (also called lattice parameter or lattice constant) are represented as physical dimension to describe the structural compatibility. Different materials have different lattice spacings and are mostly in the range of 0.3 nm to 0.7 nm.

Questions by Dr. Nuwong Chollacoop

Q6. Is there significant physical impact (Ln A) on PM when the ash is contaminated with?

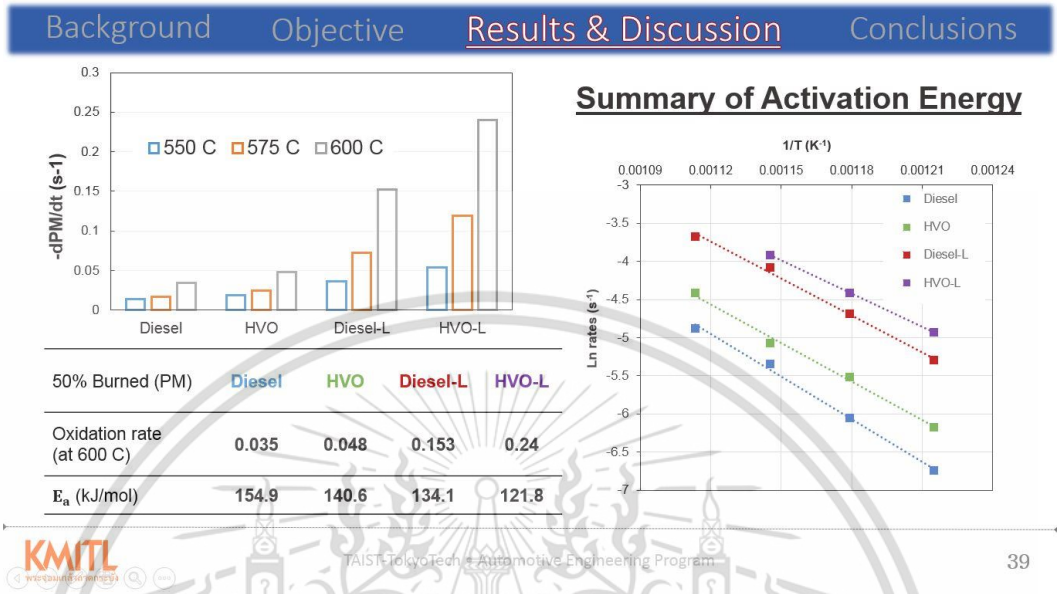

Revised answer

According to Arrhenius plot in figure 3, physical impact values (also termed as pre-exponential factor or Ln A) would be found out in table 1. Pre-exponential factors of diesel PM and diesel blending lube oil PM were 15.9 and 14.3. Besides, pre-exponential factors of HVO PM verses HVO blending lube oil PM were 14.4 and 12.9 respectively. Smaller physical sizes (i.e. Ln A) could be found out when metal oxide ashes are combined together with soot. Because spherical soot can be covered by ashes and this effect might reduce the possible reactive surfaces of the soot.

Table 1. Summary of oxidation rate, Ea and Ln A

50% Burned (PM)	Diesel	HVO	Diesel-L	HVO-L
Oxidation rate (at 600 C)	0.035	0.048	0.153	0.24
E_a (kJ/mol)	154.9	140.6	134.1	121.8
Ln A	15.9	14.4	14.3	12.9

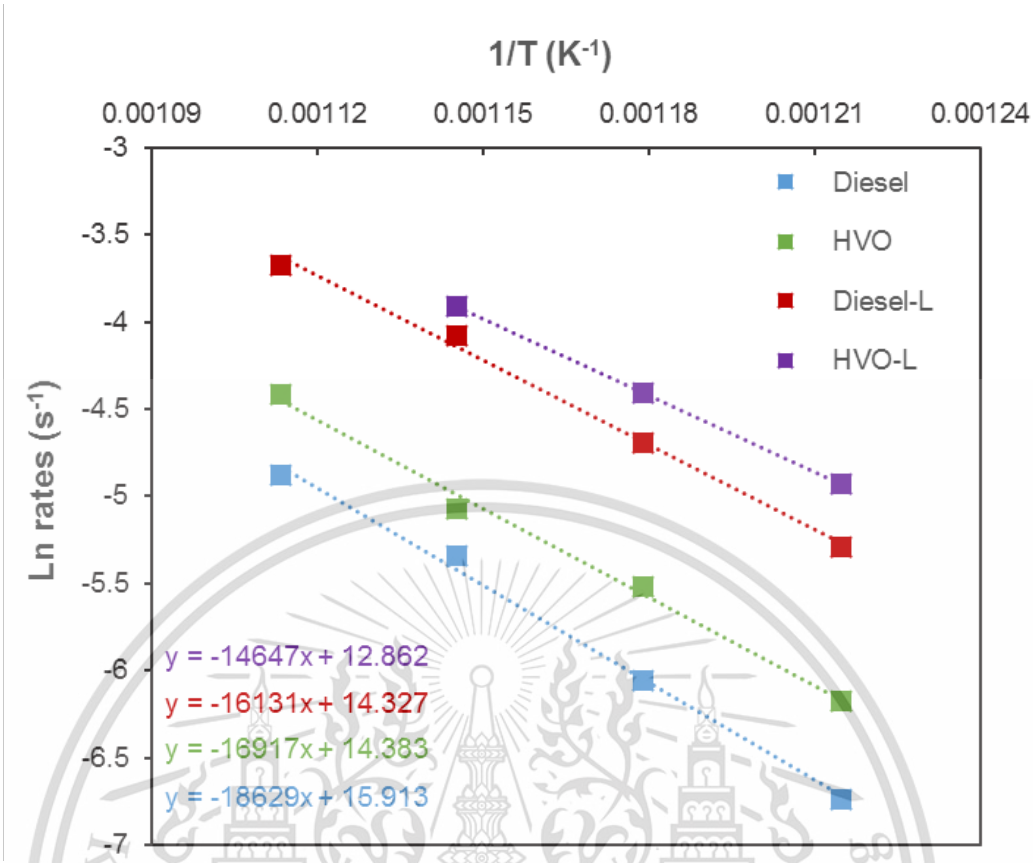

Fig. 3 Arrhenius plot of PMs

Suggestions by Dr. Nuwong Chollacoop

1. Slightly lower engine performance of HVO fuel combustion could be related to the compressible impact of HVO with lower fuel density on mechanical pump of small diesel engine.

AUTHOR BIOGRAPHY

Author: Mr. Phyo Zin Ko Ko

Date of Birth: 03/03/1994

Nationality: Myanmar

Place of Birth: Yangon, Myanmar

Email: phyozin.mech@gmail.com

Education:

- June 2019

  Master of Engineering, Automotive Engineering

  International College, King Mongkut's Institute of Technology Ladkrabang

- February 2015

  Bachelor of Engineering, Mechanical Engineering

  West Yangon Technological University

Conference Participation and Publications:

1) P. Koko, P. Karin, S. Rungsritanapaisan, R. Tongsri and K. Hanamura, "Impact of Engine Oil's Additives on Particulate Matter's Micro- and Nanostructure using Electron Microscopy Image Analysis", The 10thInternational Conference on Materials Science and Technology, 6-7 September 2018, Bangkok Thailand, and Key Engineering Materials (KEM), Trans Tech Publications, 2019.
   DOI: scientific.net/KEM.798.412

2) P. Koko, P. Karin, E. Saenkhumvong, C. Charoenphonphanich, W. Phairote, N. Chollacoop and K. Hanamura, "Influence of Metal Oxide Ashes on Soot Oxidation Kinetics and Nanostructure using Electron Microscopy and Thermogravimetric Analysis", The 9th TSME International Conference on Mechanical Engineering, AME0021, Institute of Physics (IOP), 11-14 December 2018, Phuket, Thailand.
   DOI: IOP Conf. Series: Materials Science and Engineering 501 (2019) 012016

3) P. Koko, P. Karin, N. Chollacoop and K. Hanamura, "Impact of Engine Oil Additives on Nanostructure and Oxidation Kinetics of Diesel and Synthetic Biodiesel Particulate Matters using Electron Microscopy", SAE International, SAE Technical Paper, PFL2019.
   JSAE Paper Number: 20199226